



THE HONG KONG
POLYTECHNIC UNIVERSITY

香港理工大學

Pao Yue-kong Library

包玉剛圖書館

Copyright Undertaking

This thesis is protected by copyright, with all rights reserved.

By reading and using the thesis, the reader understands and agrees to the following terms:

1. The reader will abide by the rules and legal ordinances governing copyright regarding the use of the thesis.
2. The reader will use the thesis for the purpose of research or private study only and not for distribution or further reproduction or any other purpose.
3. The reader agrees to indemnify and hold the University harmless from and against any loss, damage, cost, liability or expenses arising from copyright infringement or unauthorized usage.

IMPORTANT

If you have reasons to believe that any materials in this thesis are deemed not suitable to be distributed in this form, or a copyright owner having difficulty with the material being included in our database, please contact lbsys@polyu.edu.hk providing details. The Library will look into your claim and consider taking remedial action upon receipt of the written requests.

DECENTRALIZED STRUCTURAL DAMAGE DETECTION
METHODS UNDER EARTHQUAKE AND AMBIENT
EXCITATIONS

PINGHE NI

PhD

The Hong Kong Polytechnic University

2018

The Hong Kong Polytechnic University
Department of Civil and Environmental Engineering

**DECENTRALIZED STRUCTURAL DAMAGE
DETECTION METHODS UNDER EARTHQUAKE AND
AMBIENT EXCITATIONS**

PINGHE NI

A Thesis Submitted in partial fulfilment of the requirements for the Degree
of **Doctor of Philosophy**

June 2018

CERTIFICATE OF ORIGINALITY

I hereby declare that this thesis is my own work and that, to the best of my knowledge and belief, it reproduces no material previously published or written, nor material that has been accepted for the award of any other degree or diploma, except where due acknowledgement has been made in the text.

_____ (Signed)

Pinghe NI (Name of student)

To my family

ABSTRACT

The structural health monitoring (SHM) technology has been developed and applied to numerous large-scale structures. Structural damage identification using the vibration data of the SHM systems has gained much attention during the past three decades. However, condition assessment and damage detection of large-scale structures are still challenging due to the slow convergence in the inverse problem with a large number of unknowns and limitation in computational resources.

This thesis aims to develop a decentralized damage detection framework for large-scale structures, which would be used to evaluate the structural condition under seismic loading and ambient excitations. The study contributes to following aspects.

First, a parallel, decentralized damage detection method is developed for large-scale structures. A large-scale structure is divided into several smaller zones according to its finite element configuration. Each zone is dynamically tested with the sensors in the zone. The dynamic responses in the zone are then used to update the corresponding structural parameters in that zone based on the assumption that the structural damage has more significant effects on the responses of the zone than other zones. The structural parameters in each zone are updated using the Newton Successive Over-Relaxation method. Parallel computing is used in the model updating process.

The decentralized damage detection under seismic and ambient excitations is then studied. Under the earthquake excitation, the nonlinear behaviors of the structure are studied and two kinds of nonlinear models are addressed. One is the simplified mass-spring-dashpot model, and the other is the nonlinear finite element model. In the case of the simplified nonlinear model, an output only decentralized damage detection method is developed, in which the nonlinear structural parameters and the unknown input force are identified iteratively. In the case of a large-scale structure modelled by nonlinear finite elements, a decentralized nonlinear finite element model updating is developed and the parameters of the nonlinear constitutive material laws (such as compressive strength of concrete, the yield stress of reinforcement, etc.) are identified.

Structural damage detection under ambient excitations is then addressed, in which the ambient excitations are considered as white noise processes. Two damage detection methods are proposed based on correlation functions. In the first method, a two-stage model updating technique is developed to identify the structural damage with the correlation function. In the second method, the correlation function is treated as the free vibration response based on the natural excitation technique. The proposed decentralized technique is used to determine the structural damage. The measured correlation functions are divided into several subsets according to its finite element configuration. Each subset of correlation functions is used to identify the corresponding structural parameters in the zone.

Besides the theoretical development, numerical and experimental investigations are conducted to verify the effectiveness of the proposed methods.

PUBLICATIONS

Journal papers

1. **Ni, P.**, Xia, Y., Law, S.-S. and Zhu, S. (2014). Structural Damage Detection Using Auto/Cross-Correlation Functions under Multiple Unknown Excitations. *International Journal of Structural Stability and Dynamics* 14(05): 1440006.
2. Law, S.S., **Ni, P.H.** and Li, J. (2014). Parallel Decentralized Damage Detection of a Structure with Subsets of Parameters. *AIAA Journal* 52(3): 650-656.
3. **Ni, P.**, Xia, Y., Li, J. and Hao, H. (2018). Improved Decentralized Structural Identification with Output-Only Measurements. *Measurement* 122: 597-610.
4. **Ni, P.H.** and Law, S.S. (2016). Hybrid Computational Strategy for Structural Damage Detection with Short-Term Monitoring Data. *Mechanical Systems and Signal Processing* 70-71: 650-663.
5. Kaur, N., Li, L., Bhalla, S., Xia, Y., **Ni, P.** and Adhikari, S. (2017). Integration and Evaluation of Multiple Piezo Configurations for Optimal Health Monitoring of Reinforced Concrete Structures. *Journal of Intelligent Material Systems and Structures* 28(19): 2717-2736.
6. Li, J., Hao, H., Fan, G., **Ni, P.**, Wang, X., Wu, C., Lee, J.M. and Jung, K.H. (2017). Numerical and Experimental Verifications on Damping Identification with Model Updating and Vibration Monitoring Data. *Smart Structures and Systems*, 20(2): 127-137.
7. **Ni, P.**, Li, J., Hao, H. and Xia, Y. (2018). Stochastic Dynamic Analysis of Marine

Risers Considering Gaussian System Uncertainties. *Journal of Sound and Vibration* 416: 224-243.

8. **Ni, P.**, Li, J., Hao, H., Xia, Y., Wang, X., Lee, J.M. and Jung, K.H. (2018). Time-Varying System Identification Using Variational Mode Decomposition. *Structural Control and Health Monitoring*, e2175.

Conference papers

1. **Ni, P.** and Xia, Y., Decentralized damage detection under ambient excitations with random decrement functions, *Proceedings of the 9th International Workshop on Structural Health Monitoring*, 1-3 September 2015, Stanford, California, USA.
2. **Ni, P.** and Xia, Y., Decentralized damage detection for nonlinear structures, *Proceedings of the 24th Australian Conference on the Mechanics of Structures and Materials*, 6-9 December 2016, Perth, Australia.

ACKNOWLEDGEMENTS

I would like to express my sincere appreciation to my supervisor, Professor Yong Xia, for his extensive discussion, valuable academic guidance and encouragement as well as providing me with the unique opportunity to study in the Hong Kong Polytechnic University. I have been impressed by his profound insights into academic problems, meticulous attitudes to research, always try-to-be-perfect attitude and high responsibility to students.

I also would like to express my heartfelt thanks to Professor Hong Hao at Guangzhou University, Professor Siuseong Law at Chongqing University, and Dr. Jun Li at Curtin University for their professional and useful suggestions, kindly discussion, and constructive comments on my research.

My grateful thanks are also extended The Hong Kong Polytechnic University for providing me with a PhD studentship as well as other necessary financial supports and excellent research facilities. I am thankful to the technical staffs at the Structural Dynamics Laboratory for their useful suggestions and kindly help in my experimental studies.

Over the past few years, I benefited from the generosity of our group members, classmates, and friends, in particular, Dr. P. Zhang, Dr. J.Z. Su, Dr. W.L. Luo, Dr. Q. Xia, Miss. R.R. Hou, Miss. L.F. Li, Mr. W. L. Wu, Dr. C.D. Zhang, Dr. C.X. Qiu, Dr. W.Y. He, Dr. X.Y.

Ye, Dr. X.H. Zhang, Dr. Z. Li, Dr. G. Lin, Dr. C., Zhang, Mr C, Li, Mr, X.Y. Fan, Miss H.H. Dong, and Dr. L.Q. Huang. They helped me both in my research and daily life.

As a final word, I would like to express my gratitude and thanks to my family members and friends for their love, endless support, and encouragement

CONTENTS

CERTIFICATE OF ORIGINALITY	i
ABSTRACT.....	iii
PUBLICATIONS	v
ACKNOWLEDGEMENTS	vii
CONTENTS	ix
LIST OF FIGURES	xv
LIST OF TABLES	xix
LIST OF SYMBOLS	xxi
LIST OF ABBREVIATIONS	xxvii
CHAPTER 1 INTRODUCTION.....	1
1.1 Background	1
1.2 Research Objectives	3
1.3 Thesis Organization.....	4
CHAPTER 2 LITERATURE REVIEW.....	7
2.1 Damage Detection Methods for Civil Structures	7
2.1.1 Global damage detection methods.....	8
2.1.2 Substructural damage detection methods	12
2.1.3 Decentralized damage detection methods	16
2.2 Nonlinear Damage Detection Methods under Earthquake loading.....	18
2.2.1 Nonlinear dynamic analysis models	18

2.2.2 Nonlinear damage detection methods	21
2.3 Damage Detection Methods under Ambient loading	25
2.3.1 Modal parameter identification methods	25
2.3.2 Structural damage detection methods	28
2.3.3 Correlation function-based damage detection methods	31
2.4 Summary.....	33
CHAPTER 3 DECENTRALIZED STRUCTURAL DAMAGE DETECTION	35
3.1 Introduction	35
3.2 Force Identification.....	36
3.2.1 Equation of motion	36
3.2.2 Unit impulse response (UIR) function in wavelet domain	37
3.2.3 Force identification in wavelet domain.....	39
3.3 Damage Detection with Unknown Input Force	40
3.3.1 Sensitivities of dynamic responses	41
3.3.2 Sensitivity-based model updating	42
3.3.3 Damage detection from several sets of responses.....	43
3.3.4 Parallel computing	48
3.4 Numerical Study	50
3.4.1 Damage detection without measurement noise.....	52
3.4.2 Damage scenario with measurement noise	56
3.4.3 Damage detection with unknown damping ratios.....	60
3.4.4 Modelling error effect and computation effort	63
3.5 Summary.....	66

CHAPTER 4 DECENTRALIZED DAMAGE DETECTION OF NONLINEAR STRUCTURES USING OUTPUT MEASUREMENT ONLY.....	67
4.1 Introduction	67
4.2 Theoretical Development	69
4.2.1 Equation of motion	69
4.2.2 Force identification based on Kalman filter technique.....	70
4.2.3 Damage detection from subset responses	72
4.2.4 Computational procedure of the proposed approach.....	74
4.3 Numerical Studies	76
4.3.1 Model updating of a 6-DOFs nonlinear structure.....	76
4.3.2 Damage detection of a linear plane truss structure	81
4.4 Experimental Verification	90
4.4.1 Experimental setup and initial model updating	92
4.4.2 Decentralized damage detection	97
4.5 Summary	100
CHAPTER 5 NONLINEAR FINITE ELEMENT MODEL UPDATING WITH THE DECENTRALIZED APPROACH.....	101
5.1 Introduction	101
5.2 Methodology	102
5.2.1 Nonlinear finite element analysis procedure	102
5.2.2 Decentralized identification of nonlinear material parameters.....	104
5.2.3 Dynamic response sensitivity considering material nonlinearity	107
5.2.4 Implementation procedure of the model updating technique	110
5.3 Numerical Examples	111

5.3.1 A reinforced concrete frame	111
5.3.2 A steel frame	120
5.4 Summary.....	128
CHAPTER 6 CORRELATION FUNCTION BASED DAMAGE DETECTION	129
6.1 Introduction	129
6.2 Correlation Function of Vibration Response.....	131
6.2.1 Correlation function of response under single white noise excitation	131
6.2.2 Correlation function of response under unit impulse excitation	132
6.2.3 Correlation function of response under multiple excitations.....	134
6.3 Damage Detection Using Correlation Function	136
6.4 Numerical Study	139
6.4.1 Structural stiffness identification	140
6.4.2 Effect of measurement noise.....	142
6.4.3 Effect of measurement point.....	144
6.5 Experimental Study	145
6.5.1 Experimental setup.....	147
6.5.2 Modal testing and model updating in the undamaged state	147
6.5.3 Damage detection.....	150
6.6 Summary.....	151
CHAPTER 7 DECENTRALIZED DAMAGE DETECTION WITH AMBIENT LOADING VIA CORRELATION FUNCTION.....	153
7.1 Introduction	153
7.2 Representation of the Correlation Function of Vibration Response via NExT..	154
7.2.1 Natural excitation technique (NExT).....	154

7.2.2 Equivalent initial free vibration responses	156
7.3 Decentralized Damage Detection with Correlation Functions.....	159
7.4 Numerical Study.....	163
7.4.1 Initial value identification.....	165
7.4.2 Damage detection without noise.....	167
7.4.3 Damage detection with noise.....	169
7.4.4 Damage detection under non-standard white noise excitation	171
7.5 Experimental Study	174
7.6 Summary	177
CHAPTER 8 CONCLUSIONS AND FUTURE RESEARCH	179
8.1 Conclusions	179
8.2 Recommendations for Further Research	182
REFERENCES.....	185

LIST OF FIGURES

Figure 1.1 Overview of the structure of the thesis.....	5
Figure 3.1 Framework of the parallel computation	49
Figure 3.2 Computation for each zone.....	50
Figure 3.3 Truss structure	51
Figure 3.4 Location of sensors and excitation	52
Figure 3.5 Evolution of the identified results without measurement noise	55
Figure 3.6 Relative error with iteration.	55
Figure 3.7 Comparison of the identified input force without noise.....	56
Figure 3.8 Identified stiffness reduction factor.....	59
Figure 3.9 Comparison of the identified input force with measurement noise.....	60
Figure 3.10 Fourier transform of the vertical acceleration of Node 10	62
Figure 3.11 The identified results with unknown damping ratios	63
Figure 3.12 Identified result including model error and without measurement noise	65
Figure 3.13 Identified result including model error and measurement noise	65
Figure 4.1 The nonlinear shear building model	77
Figure 4.2 Identified system parameters with iterations.....	79
Figure 4.3 Identified ground motion using noise-free responses.....	79
Figure 4.4 Identified system parameters with noise effect	80

Figure 4.5 Identified ground motion with noise effect	81
Figure 4.6 A linear planar truss structure model.....	81
Figure 4.7 The sensor placement of the truss model.....	82
Figure 4.8 Identified and true ground motions without measurement noise	86
Figure 4.9 Damage identification results without noise effect	87
Figure 4.10 Damage identification results with different noise levels	89
Figure 4.11 Identified and true forces with different noise levels in the measurements	90
Figure 4.12 Laboratory steel frame model.....	91
Figure 4.13 Dimensions of the steel frame model (unit: mm, not to scale).....	92
Figure 4.14 Initial model updating.....	94
Figure 4.15 Identified force in the undamaged state.....	94
Figure 4.16 Mode shapes of the frame before and after updating	96
Figure 4.17 Introduced damages of the frame model	97
Figure 4.18 Damage identification results of the frame.....	99
Figure 4.19 Identified force of the frame in the damage cases	99
Figure 5.1 Computational framework of nonlinear dynamic analysis.....	104
Figure 5.2 Dimensions of the reinforcement concrete structure	112
Figure 5.3 Material models	113
Figure 5.4 Materials defined in the cross section.....	114
Figure 5.5 Finite element model of the frame structure.....	115
Figure 5.6 Comparison of the computation time of global method and decentralized method.....	117
Figure 5.7 Identified results of reinforcement concrete structure	118

Figure 5.8 Identified material parameter of reinforcement concrete structure using noisy measurement data	120
Figure 5.9 Dimension of the steel structure	122
Figure 5.10 Finite element of the steel structure	123
Figure 5.11 Normalized identified results of steel structure	125
Figure 5.12 Comparison of computational time of steel structure with global method and decentralized method	126
Figure 5.13 Normalized identification results with different level of earthquake loading	127
Figure 5.14 The sensitivity acceleration response at the top floor with respect to f_{y,B_6} at the top floor	127
Figure 6.1 Cantilever beam	140
Figure 6.2 Evolution of identification results of the cantilever beam	141
Figure 6.3 Model updating results without measurement noise	142
Figure 6.4 Model updating results with different noise levels	143
Figure 6.5 Comparison between the correlation functions $R_{4,6}$	144
Figure 6.6 Identification error from different sensor locations	145
Figure 6.7 Laboratory tested steel frame model	146
Figure 6.8 Dimensions of the frame (unit: mm)	146
Figure 6.9 Auto- and cross-correlation functions	148
Figure 6.10 Damage of the frame	149
Figure 6.11 Iteration of damage identification results	151
Figure 7.1 Flow chart of proposed damage detection method	163
Figure 7.2 Truss structure	164
Figure 7.3 Sensor and force locations	165

Figure 7.4 Initial values of correlation function	167
Figure 7.5 Identified structural parameters with different durations of measurement data	168
Figure 7.6 Final identified results with measurement noise	170
Figure 7.7 Non-standard white noise excitation	172
Figure 7.8 Identified results under non-standard white noise excitations.....	173
Figure 7.9 Time history of correlation function in damage Case 1	175
Figure 7.10 Damage identification results	176

LIST OF TABLES

Table 3.1 The identification error (%)	59
Table 3.2 The identified modal frequencies and damping ratios.....	63
Table 3.3 Computational time in model updating	66
Table 4.1 Identification results with different sampling rates and covariance matrices.....	84
Table 4.2 Measured and analytical natural frequencies of the frame in the undamaged state	95
Table 5.1 Material parameters of the reinforcement concrete structure	114
Table 5.2 Material parameters of the steel structure.....	123
Table 6.1 Frequencies of the structure in the undamaged state	149
Table 6.2 Identified flexural stiffness of columns in the undamaged and damage state ...	150
Table 7.1 Modal data of the structure in damage Cases 1 and 2	177

LIST OF SYMBOLS

Symbol	Description
M	mass matrix
C	damping matrix
K	stiffness matrix
θ	unknown parameter vector
$x(t)$	displacement
$\dot{x}(t)$	velocity
$\ddot{x}(t)$	acceleration
$h(t)$	unit impulse response function of displacement
$\dot{h}(t)$	unit impulse response function of velocity
$\ddot{h}(t)$	unit impulse response function of acceleration
ne	total number of elements in the structure
S	sensitivity matrix
E_p	percentage noise level
N_{noise}	white noise vector
$\sigma(\ddot{x})$	standard deviation of the actual acceleration response
K_i	stiffness matrix of the i -th element in the intact state
K^d	global stiffness matrix in the damaged state

α_i damage index of i -th element

Chapter Three

B force location matrix

$f(t)$ force vector

ψ wavelet basis function

h^{DWT} wavelet coefficients of the impulse response function

f^{DWT} wavelet coefficients of the external excitation

a_1, a_2 damping coefficients

ζ_i damping ratio of i -th mode

ω_i i -th circular frequency

$\ddot{\mathbf{x}}_{mea}$ measured acceleration responses

$\ddot{\mathbf{x}}_{cal}$ calculated acceleration responses

Chapter Four

F_c dissipating force vector

F_s stiffness force vector

$\mathbf{v}(t)$ measurement noise vector

R_{ij} covariance variance matrix of the measurement noises.

K_k^e Kalman gain matrix

$X(t)$ state vector

\hat{X}_{k+1} estimation of X_{k+1}

$\tilde{\mathbf{X}}_{k+1}$ state prediction of \mathbf{X}_{k+1}

$\ddot{x}_g(t)$ ground motion acceleration

Chapter Five

\mathbf{K}_r resisting force vector

$b_1 \sim b_8$ constant integration coefficients.

$\mathbf{K}^{ele,i}$ resisting force vector of the i -th element

$\boldsymbol{\sigma}^{sec}$ section stress vector

$\boldsymbol{\varepsilon}^{sec}$ section strain.

σ^{fib} fiber stress

ε^{fib} fiber strain.

f_c compressive strength of confined concrete

ε_c concrete strain at maximum strength of confined concrete

E_c initial tangent stiffness of confined concrete

f_{uc} compressive strength of unconfined concrete

ε_{uc} concrete strain at maximum strength of unconfined concrete

E_{uc} initial tangent stiffness of unconfined concrete

f_y initial yield stress of steel

E_s Young's modulus of steel

b strain-hardening ratio of steel

Chapter Six

\ddot{h}_i unit impulse response function of acceleration at i

R_{ij}	correlation function of the accelerations at the i -th and j -th DOFs
ε	impulse duration
φ	difference step
$f_i(t)$	i -th excitation force
\mathbf{B}_i	mapping vector corresponding to excitation $f_i(t)$
nf	number of excitations
\mathbf{R}_{mea}	measured correlation functions from measured data
\mathbf{R}_{cal}	calculated correlation functions from the finite element model.

Chapter Seven

$\ddot{\mathbf{x}}_{ref}(t)$	reference response vector
R_{AB}	correlation function of A and B
S_{AB}	discrete cross-spectral density function of A and B
k	discrete frequency index
N	total number of time steps
\mathbf{C}_a	mapping matrix of acceleration output
\mathbf{C}_v	mapping matrix of velocity output
\mathbf{C}_d	mapping matrix of displacement output
\mathbf{A}_d	discrete state matrix
\mathbf{Z}	state vector of the equivalent free vibration system
\mathbf{Z}_i	discrete state vector of the equivalent free vibration system
$\mathbf{z}(t)$	displacements vector of equivalent free vibration system
$\dot{\mathbf{z}}(t)$	displacements vector of equivalent free vibration system

$\ddot{\mathbf{z}}(t)$	acceleration vector of equivalent free vibration system
\mathbf{H}	system Markov parameters
$\mathbf{Y}_{mea, i}$	correlation function measured from the i -zone

LIST OF ABBREVIATIONS

AMV	Auto Correlation Function at Maximum Point Value Vector
CMIF	Complex Mode Indicator Function
CMS	Component Mode Synthesis
DOF	Degrees of Freedom
ERA	Eigensystem Realization Algorithm
FDD	Frequency Domain Decomposition
FRF	Frequency Response Function
NExT	Natural Excitation Technique
OMA	Operational Modal Analysis
OMAX	Operational Modal Analysis with Exogenous Forces
RDT	Random Decrement Technique
SHM	Structural Health Monitoring
SOR	Successive-Over-Relaxation
SSI	Stochastic Subspace Identification

CHAPTER 1

INTRODUCTION

1.1 Background

Structural damage and failure cause a huge loss of properties and human lives every year. In order to detect the structural damage at an early stage, many large-scale structures have been installed with a structural health monitoring (SHM) system, for example, Guangzhou New Television Tower (Ni *et al.*, 2009), Tsing Ma Bridge (Ko and Ni, 2005), and Shanghai Tower (Su *et al.*, 2013). During the last decades, Monitoring and condition assessment of large-scale civil infrastructure, such as dams, long-span bridge, radio masts/towers, have become more and more popular worldwide.

Structural damage identification has attracted considerable attentions since the 1990s. Damage is usually considered as a reduction in the stiffness parameters, which may cause the adverse effects in the vibration characteristics of the structure (Doebling *et al.*, 1998). A large number of methods have been developed to identify the damage occurrence, location and severity of structures. A comprehensive review of vibration

based damage detection can be found by Doebling *et al.* (1998). Damage detection methods can be categorized according to their characteristics, e.g. frequency domain and time domain methods, model-based and model free methods. Frequency domain methods use the frequencies, mode shapes, flexibility matrix and modal strain energy to identify the structural damage, while time domain methods use the time history data (e.g. acceleration, velocity, displacement and strain data) directly. Model free methods are based on the measurement data only, also referred to as data-driven methods, while model-based methods need the finite element model of the structure. As the finite element model is able to simulate damage numerically, the model-based methods quantify the damage in general. Although a lot of methods have been developed, most of these methods are only suitable for small scale structures, which can only identify a small number of unknown structural parameters.

For large-scale structures, model updating is still a challenging because there are a large number of unknown structural parameters to be identified. The increasing number of degrees of freedom (DOFs) and the unknown structural parameters make the model updating more complicated and time consuming. For example, Xia *et al.* (2008) updated a real bridge model, consisting of more than 900 elements and 5000 DOFs, which took more than 400 hours. In another study, Li *et al.* (2013) proposed a damage detection method for bridge structures considering the interaction effect of the bridge-vehicle system. The computational time for each iteration was more than 6 hours and the entire damage identification process took more than one week. The low computational performance of existing methods discourages the use for large-scale structures and calls for efficient damage detection and model updating techniques.

This study aims at developing a more efficient damage detection method for large-scale structures, which would be used to evaluate the structural conditions under natural hazards (e.g., seismic events) and continually assess structural conditions under operational conditions. The loading characteristics and structural behaviors under the two situations are different.

- When the structure is under the operational conditions, the loading may not exceed the designed capacity, and the structural behavior is generally at the linear stage. Moreover, cracks may occur and the opening and closing of the cracks may causes nonlinearity (Chen *et al.*, 2006). These nonlinearities should be considered in damage detection under earthquake loading.
- When the structure is under earthquake loading, the force locations are known. The earthquake loading can be measured from accelerometer or seismometer. However, the ambient loading (e.g., wind loading, traffic loading) are difficult to measure. The output only methods are then highly desired for damage detection under ambient loading. To the best knowledge of the author, most of time domain output only methods require that the number of sensors is more than the number of forces. In a practical SHM system, this requirement may be difficult to meet because it could be challenging to install large number of sensors. The new methods should be developed to overcome the limitation.

1.2 Research Objectives

Recognizing the challenging problems in damage detection under earthquake and ambient loadings, the main objectives of the PhD study are as follows:

1. Improve the computational performance of structural identification for large-scale structures through a decentralized method with parallel computing;
2. Develop linear and nonlinear damage identification methods for large-scale structures under seismic loading via the decentralized approach;
3. Develop a correlation function-based damage detection method for large-scale structures under ambient condition, which does not require the number of sensors is more than that of unknown forces.

1.3 Thesis Organization

The thesis consists of eight chapters, as illustrated in Figure 1.1. Details as follows.

Chapter 1 introduces the research background, objectives, and structure of the thesis.

In Chapter 2, the literature on relevant topics will be reviewed, which includes the general damage detection methods, the state-of-the-art of damage detection methods for civil structures, nonlinear damage detection methods under earthquake loading, and damage detection methods under ambient loading.

A parallel decentralized damage detection method is proposed for condition evaluation in Chapter 3. A large-scale structure is divided into a limited number of smaller zones according to its finite element configuration. Each zone is dynamically tested in sequence with its own set of sensors. Then each subset of parameters is updated with its

own measurements using the Newton-SOR method. Parallel computing is used in the model updating process.

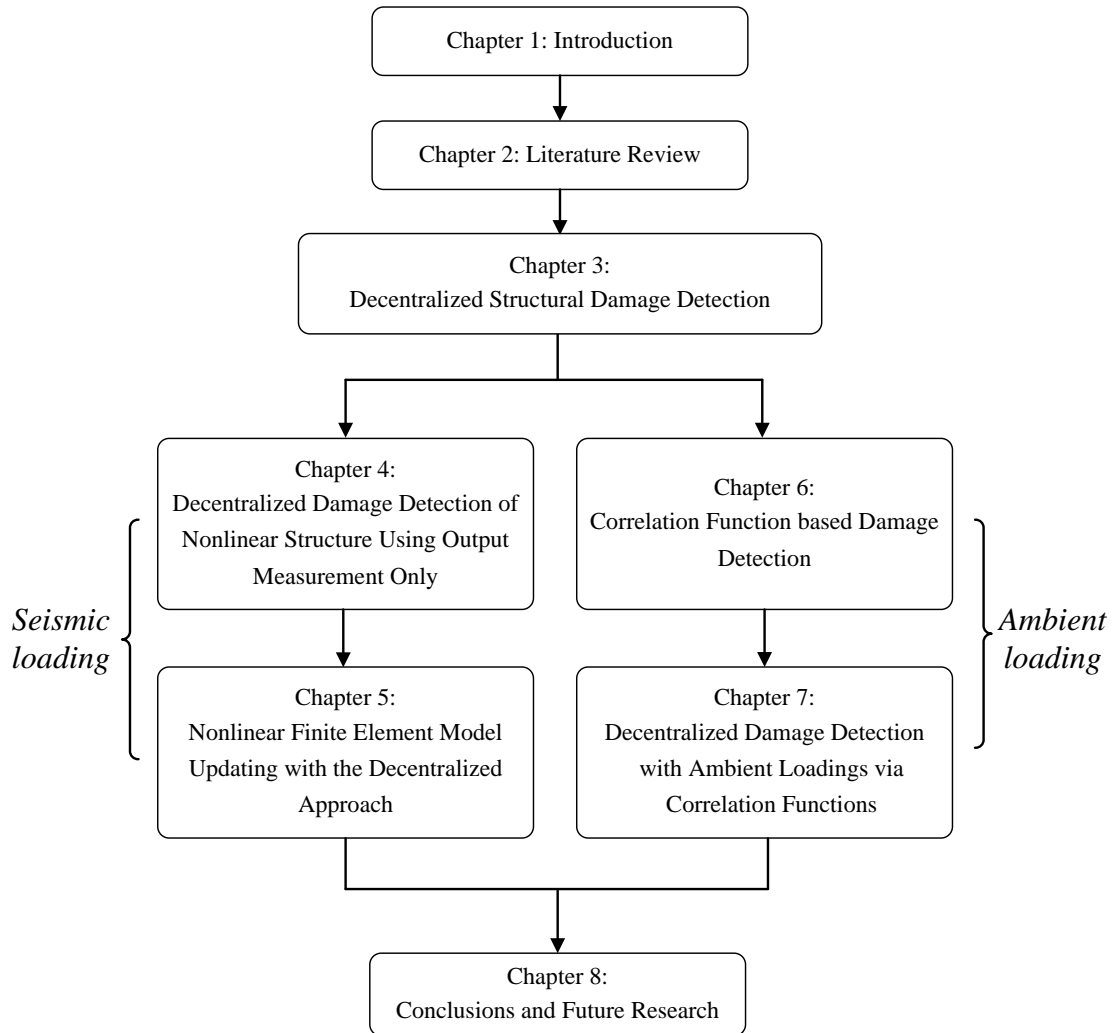


Figure 1.1 Overview of the structure of the thesis

The subsequent two chapters present decentralized structural damage identification methods under seismic loadings. In particular, Chapter 4 addresses linear and simplified nonlinear structures. The external excitation forces and structural parameters are

identified using the Kalman filter technique and Newton-SOR method, respectively. Chapter 5 addresses nonlinear reinforced concrete and steel structures. The nonlinear dynamic responses of the structure are computed based on nonlinear finite element models, and the sensitivity of dynamic responses with respect to material parameters is obtained from the direct differentiation method. The parameters of the constitutive model of concrete and steel are identified with the decentralized method.

The correlation function-based damage identification methods with ambient vibration responses are developed in Chapters 6 and 7. In Chapter 6, the formula of correlation function under multiple ambient white noise or impact excitations are derived. The structural damage is identified with the sensitivity method. A decentralized method is developed in Chapter 7. The natural excitation technique (NExT) is used and the correlation functions are treated as free decay vibration responses. This method overcomes the limitations of most time domain methods, which require the information of force location and the number of sensors larger than the number of force.

Finally, the main findings of this thesis are concluded in Chapter 8. Some recommendations for future work are also provided.

CHAPTER 2

LITERATURE REVIEW

Condition assessment of civil structures has attracted much attention since the 1990s, and numerous studies have been proposed. This thesis aims to develop novel damage detection methods for large-scale structures considering seismic loading and ambient loading. This chapter reviews the current development of relevant topics, which includes damage detection methods for civil structures, damage detection under earthquake loading, and damage detection under ambient excitations.

2.1 Damage Detection Methods for Civil Structures

The interesting to identify structural damage has gained much attention since the 1990s (Pandey *et al.*, 1991; Pandey and Biswas, 1994; Salawu, 1997). The damage detection methods for civil structures can be categorized into global, substructural, and decentralized damage detection methods.

2.1.1 Global damage detection methods

In earlier studies, researchers focused on the problem of damage detection in small civil structures. Many studies have investigated on the identification of structural damages. The finite element model usually consists of several structural elements, and the number of unknown structural parameters is small. Several widely used global damage detection methods are reviewed in the following section.

Least-squares method is one of the earliest time domain damage detection methods (Wang and Haldar, 1994). The equation of motion of a linear system can be rewritten as an algebraic equation with unknown stiffness and damping coefficients. The structural parameter can then be identified from the algebraic equation with the least-square method and measurement response. The idea and implementation of this method is simple. However, this method requires full measurement from displacement, velocity, and acceleration. Wang and Haldar (1997) extended this method for structural damage detection with limited observations. The unavailable measurements were estimated by the extended Kalman filter method with a weighted global iteration. The stiffness and damping parameters were identified with the least-squares method. A recursive least-squares estimation approach was proposed for online damage detection (Yang *et al.*, 2007b). The analytical recursive solutions were derived from the least-squares method. An adaptive tracking technique was implemented to track the damage events.

The limitation of the least-squares method is that the full measurement of displacement, velocity, and acceleration is required for damage detection. When the displacement and

velocity measurements are unavailable, the responses can be used to computed from numerical integration of acceleration responses. However, a double numerical integration may cause a significant numerical drift in the displacement response. To address this problem, damage detection methods with extended Kalman filter technique were proposed. Hoshiya and Saito (1984) proposed the first study on system identification problems. The stiffness parameters of the two DOFs shear type were identified. Yang *et al.* (2006b) presented an adaptive damage detection method with the extended Kalman filter approach to detect the structural parameters and damage events. Zhou *et al.* (2008) presented experimental studies to verify the capability of the adaptive extended Kalman filter approach. The Kalman filter technique gains much attention for structural damage detection, and many studies have proposed this method (Chatzi and Smyth, 2009; Xie and Feng, 2012; Azam *et al.*, 2015; Guo *et al.*, 2018).

Yang *et al.* (2009a) developed a damage detection method, using the analytical recursive solution of the quadratic sum-squares error method. The unknown structural parameters and unknown excitations were estimated directly by minimizing the error between the measured output data and the theoretical values. Wu *et al.* (2012) investigated the accuracy of the quadratic sum-squares error method for structural damage detection. A two-story reinforcement concrete structure with stiffness degradation was conducted in the experimental studies. The quadratic sum-squares error method required a large number of acceleration measurements for structural damage detection. To overcome this problem, Xia (2011) combined the model reduction technique with the quadratic sum-square error method for the experimental study of steel frame structure with joint damage.

Sensitivity-based model updating methods consider the unknown structural parameters as an implicit function of dynamic characteristics. The unknown parameter can be identified by minimizing the difference between the measured dynamic characteristics and the analytical part. The dynamic characteristics can be the time history of vibration responses, frequencies, and mode shapes. The structural damage can be detected by comparing the changes in the structural parameter before and after damage. Farhat and Hemez (1993) utilized the sensitivity method to update a beam and a truss. The mass and stiffness matrices were identified from the measured mode shapes with an iterative procedure. Bakir *et al.* (2007) updated the finite element model of a reinforced concrete structure with eigenfrequencies and mode shapes. The structural parameters were identified with the trust region algorithm. Lu and Law (2007a) derived the dynamic response sensitivity with respect to unknown structural parameters, and the dynamic response sensitivity was obtained from the Newmark method. Tikhonov regularization technique was proposed in model updating to reduce the ill-posed problem. Zhang *et al.* (2009) represented the unknown input force with Chebyshev polynomial approximation. The dynamic response sensitivity with respect to unknown structural parameters and coefficients of Chebyshev polynomial expansions were derived. The unknown structural parameters and input force were identified sequentially with the two-stage procedure. Zhu *et al.* (2014) derived the dynamic response sensitivity with respect to the element stiffness factor with the state space method. The structural damage was identified with a sensitivity-based method using transmissibility concept. However, the conventional sensitivity-based damage detection methods may not work for large damage. To address this problem, Lu and Wang (2017) proposed an enhanced

sensitivity method for structural damage detection. The trust-region restriction was applied to improve the identified results.

Computational intelligence methods are a group of approaches inspired from the laws of nature and biology. Computational intelligence methods, such as genetic algorithm (Chou and Ghaboussi, 2001; Hao and Xia, 2002; Perry *et al.*, 2006), artificial bee colony algorithm (Kang *et al.*, 2009; Sun *et al.*, 2013; Ding *et al.*, 2018), and particle swarm optimization (Kang *et al.*, 2012; Seyedpoor, 2012; Wei *et al.*, 2018) are proposed for structural damage detection in recent years. The advantage of these methods is that they do not require the derivation of sensitivity matrix for damage detection because, in some cases, the sensitivity matrix is unavailable. The structural damage can be detected by minimizing the error between the measured vibration characteristics and the analytical section with the computational intelligence methods. The vibration characteristics can include time history of acceleration responses (Perry *et al.*, 2006; Sun *et al.*, 2013), static measurements of displacements (Chou and Ghaboussi, 2001), modal strain energy (Seyedpoor, 2012), frequencies, and mode shapes (Hao and Xia, 2002; Kang *et al.*, 2012). However, the nature-inspired methods consume large amount of computational time to obtain the results. In addition, it can easily obtain the local minimum solution when the structural model is complex.

The above-mentioned methods are suitable for damage detection in simple structures, which involve only several unknown structural elements and DOFs. In a complex structure, the computation workload is usually heavy because a large number of structural parameters need to be updated. In addition, a large number of sensors are

installed in the SHM system of the large-scale structure. A huge number of data is difficult to process at once. Thus, effects have been performed to improve the performance of condition assessment in the large-scale structure.

2.1.2 Substructural damage detection methods

Substructural analysis and identification approaches have been proven effective and efficient methods for large-scale structures.

The first notable method is the component mode synthesis (CMS) technique, which is frequently used in dynamics analysis of large-scale structures. A given structure is decomposed into several components/substructures, and each one can be analyzed independently. The frequencies and mode shapes of the global structure can be constructed from the modal data of each component (Farhat and Geradin, 1994). The CMS method is applied to model the update of large-scale structures (Arruda and Santos, 1993; Liu *et al.*, 2014). Papadimitriou and Papadioti (2013) used Craig–Bampton CMS method to update the finite element model of bridge. The computational time was reduced from one month to several minutes. Yu *et al.* (2016) proposed a sensitivity-based damage detection approach with CMS method. The eigensensitivity of the entire structure with respect to the element parameter was assembled from the corresponding section of each substructure. The computational time for the calculation of eigenvalue and eigensensitivity was reduced. One limitation of this method is that minor damage cannot be detected accurately because the changes in dynamic properties are infinitesimal.

The changes in flexibility may reflect the structural parameter damage. Alvin and Park (1999) proposed a damage detection method based on substructural flexibility matrix. They developed a method to extract the substructure flexibility matrix from global modal parameters. The damages were determined by the difference of substructure flexibility matrix between the healthy and damaged conditions. Another similar study was proposed by Weng *et al.* (2013). The damage in a substructure may change the mode shapes of only the substructure, whereas the mode shapes of other substructures may remain unchanged. The damage locations were then detected from the changes in the substructural flexibility matrix. The eigenvalues and eigenvectors of the substructural flexibility matrix were used as indicators for damage detection.

Damage detection methods with the frequency response function (FRF) of a substructure were also proposed. Park and Park (2005) detected the substructural damage using the force balance equation. The damage severity and location were identified from the reduced dynamic stiffness matrix and measured frequency response function. Sjövall and Abrahamsson (2008) proposed a method to extract the FRF of a substructural system. A frequency domain force identification method was initially developed, and the unknown subsystem FRF was extracted by the least-squares estimate. The proposed method could extract the unknown subsystem FRF when a sufficient number of experimental tests on the global system were carried out. Similarly, Lin *et al.* (2012) used substructure-based frequency response function to detect the damage location of a 1/4-scale six-story steel structure. The substructure-based FRFs of the shear-type structure were analytically derived.

The time domain substructural damage detection methods are also reported. The global structure is divided into several substructures, and each substructure is applied with additional force, considering the coupling effect of the other substructures. Koh *et al.* (1991) used extended Kalman filter and a global iteration scheme to estimate the structural parameters from vibration data. In the identification process, the substructural members with and without overlap were considered. Numerical studies with different types of structures were conducted to verify the performance of the proposed method. Compared with the global identification method, the substructural-based method consumed less computation time. Lei *et al.* (2012a) developed a Kalman filter-based method to identify the structural parameter of a linear structure. Two methods were developed to identify the unknown interface forces. One was treated interconnection force as additional unknown input. However, the measurement at the interfaces should be available. Another method used was the extended state vector to estimate the interconnection force. However, the extended state vector of the adjacent substructures should be known. This method was also proposed for nonlinear system identification (Lei & He, 2013).

One critical issue of the time domain substructure identification methods is estimating the interface force. If the interface force can be estimated, then each substructure can be assessed independently. Koh *et al.* (2003) utilized the quasi-static displacement and relative displacement of the structure to represent the interface force on the substructure. The damping force and inertia effect were ignored. However, the accelerations at interface DOFs were required. Another method to evaluate the interface force was

proposed by Trinh and Koh (2012). The interface forces were reconstructed from the displacement, velocity, and acceleration at the interface DOFs. The interface velocity and displacement, which were usually unknown, were obtained from the numerical integration of measured interface acceleration. Law and Yong (2011) proposed a substructure condition assessment method. The interface force was estimated from state space, whereas the structural parameters were updated with sensitivity method.

Some researchers utilized structural interface forces for condition assessment. Koh and Shankar (2003) proposed the substructural damage detection method with genetic algorithms. The interface forces of the structures were reconstructed by using frequencies and mode shapes with the concept of receptance. Then, the structural damage and severity can be detected by minimizing the difference between the measured interface and the analytical forces. Law *et al.* (2010) derived the dynamic response sensitivity of the coupling forces with respect to the unknown structural parameter using the state space method. The structural damage was identified with the damped least-squares method.

Studies to eliminate the interface force for the substructural damage detection were also explored. Li and Law (2012b) developed a substructural condition assessment method with the concept of transmissibility. The dynamic responses at one set of the structure were reconstructed from another set of vibration responses. The wavelet domain and frequency domain methods for dynamic signal reconstruction were investigated (Li and Law, 2012a; Li *et al.*, 2012). The structural damage of the target substructure was

estimated by minimizing the error between the measured and reconstructed vibration responses.

2.1.3 Decentralized damage detection methods

Decentralized methods have been proposed for modal identification, vibration control, and damage detection in large-scale structures. Decentralized methods are used in SHM in combination with wireless smart sensor networks (WSSNs). Traditional signal processing methods need to collect all sensor data from a signal location. However, power consumption increases with increasing size of WSSNs. The long-distance signal transmission causes unreliable sensor communication. To acquire and process a large number of dynamic data at once, the central sensor should possess a high computational capability. When decentralized methods are embedded in WSSNs, they can be used to acquire and process their own data because each smart wireless sensor has a low level of computational capability. The final data transmission and computational workload in the central section are reduced. Jo *et al.* (2011) developed a decentralized modal identification method by combining natural excitation technique and stochastic modal identification. The method was applied in Imote2 WSS platform. The efficacy of the decentralized modal identification method was verified by experimental studies of a steel truss bridge. Kim and Lynch (2011) proposed a decentralized computational framework for system parameter estimation. The Markov parameters were estimated at each wireless sensor and then sent to the base station to assemble global structural properties. Sim *et al.* (2011) developed a new aggregation approach with decentralized random decrement technique. The proposed data aggregation approach reduces data

communication in system identification but maintains the same accuracy in the results. Nagayama *et al.* (2009) utilized smart sensors to realize autonomous structural condition assessment. Decentralized damage detection algorithm was applied to a 3D truss structure to evaluate its performance.

Decentralized methods are considered a promising solution in a large SHM system. The large system is divided into several subsystems, and each subsystem makes a decision by its own sensors and actuator. If one subsystem fails to function, then the other subsystems can still work effectively, and the robustness of the system is improved. Each subsystem only needs to make a decision by its own sensors and actuator; thus, the workload for signal processing and decision making is reduced, and finally, the time delay of the system is reduced.

Decentralized algorithms were also proposed for structural damage detection. Wu *et al.* (2002) proposed a decentralized approach for damage detection by using neural networks. The dynamic outputs (e.g., displacement, velocity, and restoring force) were used as input to train the neural networks. The errors between the measured and predicted restoring force were used as a damage index to detect the damage location. Jayawardhana *et al.* (2013) developed a correlation function-based and a time series-based decentralized method for condition assessment of a reinforced concrete slab. Both methods can detect the damage location using only the output. The results show that the correlation function-based method is more effective, whereas the time series-based method is more reliable in the damage detection. Gao *et al.* (2006) used the distributed computing strategy to identify damage in a planar truss structure, in which a flexibility-

based method was embedded in the wireless sensors. Yun *et al.* (2011) proposed a decentralized damage identification method and embedded on the Imote2 sensor. The Imote2 sensor was used to calculate the wavelet coefficients of acceleration responses, and a base station was used to calculate wavelet entropy indices. Structural damage can be detected from the wavelet entropy indices.

2.2 Nonlinear Damage Detection Methods under Earthquake loading

Post-earthquake condition assessment of large-scale structures has gained considerable attention in recent years. The dynamic behavior of civil structures (e.g. opening and closing of cracks) under extreme loadings is typically nonlinear, thereby leading to the hysteretic performance of the structures. Therefore, the nonlinear hysteretic restoring force should be considered during the post-earthquake condition assessment. In this section, the nonlinear dynamic analysis models are reviewed first, followed by the nonlinear damage detection technique.

2.2.1 Nonlinear dynamic analysis models

The models for the nonlinear response analysis of structures can be divided into three categories, as follows: global models, microscopic finite element models, and discrete finite element models (Taucer *et al.*, 1991).

Most of the existing studies used the first type of models to simulate the nonlinear vibration responses for structural damage detection. These models, such as mass-spring-

damper models and shear-building models, are based on simplified assumptions and are insufficient to predict the vibration characteristics/responses of actual structures. The restoring force of the system was represented by a polynomial function of displacement and velocity. For example, Toussi and Yao (1983) used a polynomial function to represent the hysteretic behavior of a 10-story reinforced concrete structure under earthquake loading. The nonlinear force-deformation relationship due to the strength deterioration, energy dissipation, and permanent deformation was considered. Benedettini *et al.* (1995) proposed the orthogonal and nonorthogonal polynomial functions to approximate the restoring force. A nonparametric estimation technique was proposed to identify the nonlinear system parameters. The dynamic restoring force of a base isolation system subjected to strong ground motion is usually considered nonlinear. Furukawa *et al.* (2005) used a trilinear hysteretic multiple shear spring model to represent the nonlinear restoring force of a base-isolation system. The hysteretic restoring force is frequently used to simulate the non-linear behavior of civil structures under extreme loadings (Baber and Wen, 1981; Sireteanu *et al.*, 2010). Ma *et al.* (2006) developed a generalized Bouc–Wen model to represent the structural strength degradation, stiffness degradation, and pinching characteristics of the structure. The differential evolution approach was proposed to evaluate the system parameters of the hysteresis model. Kunnath *et al.* (1997) used a modified Bouc-Wen model to simulate the behavior of prestressed concrete elements and beam-column joints. The control parameters of the hysteretic model were determined by the modified Gauss-Newton method. Foliente (1995) proposed a modified Bouc-Wen Baber-Noori model to represent the hysteretic behavior of wood joints.

The second type is the microscopic finite element model, which has been widely used in the forward analysis. Each structural member (e.g. beam, column) is discretized into thousands of solid finite elements in the computation, causing the entire structure to obtain thousands of solid finite elements. Bi and Hao (2013) used a 3D finite element model to simulate the dynamic behavior of bridge structure under seismic loading. The pounding damages between girders and abutment were investigated. The bridge consists of more than 500000 nodes, and the dynamic analysis of this model was conducted for more than one week. The microscopic finite element models have been successfully used to simulate the behavior of bond-slip of the reinforcement bar (Naaman and Najm, 1991), crack extension phenomena (Moës *et al.*, 1999), concrete deterioration (Coronelli and Gambarova, 2004), and FRP-concrete debonding (Lu *et al.*, 2005). However, due to the high computational workloads in the forward problem analysis, this model is rarely used in the inverse problem analysis.

The discrete finite element models can also be used to simulate the complex nonlinear behavior of structures (e.g., bond-slip of reinforcement), but not suffer such a heavy computational workload. Each element is subdivided into longitudinal fibers, which follow the uniaxial stress–strain relation of the particular material. This model is considered a compromise between the global model and microscopic finite element model (Taucer *et al.*, 1991). This model has been proposed for dynamic analysis of large-scale structures, performance-based seismic design, and structural reliability evaluation. Lu *et al.* (2015) used multi-layer shell elements to simulate the collapse of super-tall buildings. The numerical results using the discrete finite element model matched effectively with the experimental results. Val *et al.* (1997) evaluated the

reliability of a reinforced concrete structure with the discrete finite element model. The influence of random parameters on structural reliability is evaluated with sensitivity analysis. The discrete finite element models gain much attention because they can better simulate the structural nonlinear behavior. Some damage detection methods are reported and reviewed in the next section.

2.2.2 Nonlinear damage detection methods

Identifying parameters in a hysteretic system (e.g., stiffness and strength degradations) is considered a challenging problem in the engineering field. Most existing methods are proposed to identify the parameters using the global nonlinear models. For example, Yang *et al.* (2014) used an adaptive quadratic sum-square error estimate method to identify the time-varying parameters of nonlinear structures. The hysteretic behavior due to the stiffness degradations and pinching effect was simulated with the Duffing model. Numerical and experimental studies showed that the unknown ground motion and system parameters can be identified.

Bayesian inference methods are proposed to identify the structural parameter and their confidence bounds. It is considered an efficient method because the results provide the probability density functions of each identified parameter. Some studies on Bayesian-based damage detection approach were proposed. Yuen and Beck (2003) presented a Bayesian approach for nonlinear parameter identification with incomplete measurements. The nonlinear parameters and their probability density function were updated by the spectral density of output responses. Li *et al.* (2004) presented a method

to estimate the parameters of hysteretic systems, considering pinching effect in wood buildings and reinforced concrete structures. The proposed method was based on the Bayesian state estimation and bootstrap filter. The simulation results showed that the Bayesian method was more advantageous in handling nonlinear system identification with high-level measurement noise than the least-squares methods. Worden and Hensman (2012) proposed a Bayesian inference method to identify the parameter of a Duffing oscillator. A deviance information criterion was proposed for model selection, and the Markov Chain Monte Carlo method was proposed for the parameter identification.

The least-squares methods and Kalman filtering technique are two widely used methods for nonlinear system identification. The least-squares methods for nonlinear system identification are reviewed in the following section. Lin *et al.* (2001) presented a recursive least-squares algorithm to identify the parameters in Bouc–Wen model. The variable trace approach was proposed to update the adaptation gain matrix and the parameter variation given that the progressive damage could be captured. Yang and Lin (2004) used the least-squares estimation to identify the parameters of non-linear hysteretic structures. An adaptive tracking technique was proposed to track the damage event. The simulation results showed that the abrupt and slow degradations of hysteretic parameters were accurately identified. Xu *et al.* (2012) used power series polynomial model to represent the nonlinear restoring force. The least-squares technique was proposed to identify the coefficient of the polynomial functions. The advantage of the proposed method is that it does not need any assumption and prior knowledge of the system. This method was subsequently extended to identify the nonlinear restoring

force and unknown dynamic loadings in a nonlinear MDOF chain-like structural system (He *et al.*, 2012). Experimental studies on a four-story steel frame structure equipped with two actively-controlled MR dampers were conducted to verify the accuracy of the proposed method.

Ching *et al.* (2006) compared the performance of the extended Kalman filter and the particle filter for nonlinear system identification. The results showed that the particle filter was more advantageous than the extended Kalman filter in tracking the moderately and highly nonlinear behavior. Wu and Smyth (2007b) used unscented Kalman filter and extended Kalman filter for real-time nonlinear structural system identification. The results showed that the unscented Kalman filter was less sensitive to measurement noise. Chatzi and Smyth (2009) used unscented Kalman filter and particle filter methods to identify the system parameters of a three-DOFs system. The Bouc–Wen hysteretic model was used to simulate the hysteretic behavior, whereas displacement and acceleration measurements were performed for parameter identification. Lei and Wu (2011) proposed an identification method with limited input and output measurements. The identification algorithm was based on the sequential use of the classical Kalman estimator for the structural responses and the recursive least squares estimation for the nonlinear restoring force. Ghorbani and Cha (2018) presented a cubature Kalman filter-based method to improve the identification performance of the large-scale structures. The results showed that the new proposed method was better than the traditional unscented Kalman filter approach when the high-level noise was considered in the measurement noise. Guo *et al.* (2018) proposed a force identification method for hysteretic nonlinear structures. The seismic loading was estimated from the unscented

Kalman filter. The effect of measurement noise, model error, and environmental disturbances was also studied.

Nonlinear finite element analysis can better simulate the dynamic behavior of the structure under earthquake loading. Nonlinear model updating technique was proposed to calibrate the nonlinear numerical model of the actual structure. Ebrahimian *et al.* (2015) proposed a novel method for material parameter identification. The nonlinear dynamic response of the structure was simulated with the nonlinear finite element method framework. The extended Kalman filter was proposed to update the parameters in the concrete and reinforcement, whereas the dynamic response sensitivities were obtained using the direct differentiation method. The numerical example on model updating of a reinforced concrete was studied to verify the proposed method. Astroza *et al.* (2014) identified the material parameters of a distributed plasticity finite element model. The nonlinear stochastic filtering technique was proposed to update the frame-type structure. Similar studies also reported the use of batch Bayesian approach (Ebrahimian *et al.*, 2017). These methods require seismic input information. Some studies were proposed to identify the material parameter and the seismic input (Astroza *et al.*, 2017; Ebrahimian *et al.*, 2018). Asgarieh *et al.* (2014) calibrated the nonlinear finite element model of a masonry infilled frame structure. The hysteretic material models were used to simulate the nonlinear behavior at the element level. Li *et al.* (2017b) performed an experimental investigation on model updating of a seismic isolated bridge. The parameters of the isolators were calibrated from the experimental test data. The results showed that the predicted responses from the updated bridge model were in good agreement with the measured ones.

2.3 Damage Detection Methods under Ambient loading

Without considering extreme loadings, the civil infrastructure is generally subjected to ambient excitation. Structural identification methods with ambient vibration tests are preferred over forced vibration ones because the artificial excitation of large structures with low natural frequencies is quite difficult and expensive (Bahlous *et al.*, 2009). In the ambient vibration test, the structure is subjected to a variety of excitations (e.g., traffic loading, wind loading, and temperature loading). These excitations are immeasurable and are considered broadband in the frequency domain. The spectral characteristics of the ambient vibration response contain the dynamic properties of the structure; thus, structural damage can be detected from the ambient vibration response. Some studies have been conducted to extract the vibration characteristics and identify the structural damages. In this section, modal parameter identification methods are initially reviewed, and followed by damage detection methods, particularly correlation function-based damage detection methods.

2.3.1 Modal parameter identification methods

The conventional methods utilize impulse response function or frequency response function to extract the modal parameters. For example, Sun *et al.* (2017) proposed a model parameter identification method in the Bayesian probabilistic framework. The impulse response functions were obtained by deconvolving the measurement accelerations with respect to the recorded ground motion. However, the measurement of the input force of the structure is unknown. Carrying out field tests in large engineering

structures with artificial excitation is challenging. The output-only method is desirable, and some approaches have been proposed.

Peeters and De Roeck (2001) reviewed stochastic system identification methods for civil structures under operational conditions. The input-output based methods and output-only based modal parameter estimation methods were appropriately discussed. The results showed that the classical input-output modal parameter identification methods can be modified into the output-only method. For example, FRF-based methods can be converted to spectrum-based methods. Ren and Peng (2005) updated a large span bridge with ambient vibration measurement. The dynamic characteristics of the bridge were extracted from peak picking method and stochastic subspace identification (SSI) method. The results showed that the ambient vibration signals can be used to identify the frequencies and mode shapes of the bridge. Deraemaeker *et al.* (2008) proposed the output-only identification method, considering the environmental effect on the vibration characteristics. The SSI approach and peak value from the Fourier transform of modal filters were used for feature extraction.

The operational modal analysis (OMA) techniques gain much attention because these methods can extract the frequencies and mode shapes without interrupting the daily use of the structure. Reynders *et al.* (2010) proposed a hybrid vibration test, namely, operational modal analysis with exogenous forces (OMAX) technique, for modal parameter identification. Exogenous inputs were applied to the structure under operational conditions. The experimental results of a three-span bridge showed that the OMAX technique could achieve better results than the OMA technique. Brownjohn

(2003) identified the frequencies of a tower structure and a smaller office block with Natural Excitation Technique (NExT) and Eigensystem Realization Algorithm (ERA). The results showed that the frequencies were underestimated, and the design is conservative. Yuen and Kuok (2010) studied the effect of seasonal variation on the vibration characteristics of the reinforced concrete building. Bayesian spectral density approach with ambient vibration responses was used to quantify the variation of modal frequencies and modal shapes. Siringoringo and Fujino (2008) developed two system identification methods for a suspension bridge using ambient vibration response. One method was based on Random Decrement Technique (RDT) and Ibrahim time domain approach. The other method was based on NExT combined with ERA. The modal parameters were identified with ambient response. Gul and Catbas (2008) used Complex Mode Indicator Functions (CMIFs) for system identification. The random decrement technique was used to generate the input for the CMIF method. The natural frequencies, mode shapes, and damping ratios of a long-span bridge were identified.

Among these studies, the NExT and RDT are two widely used signal pre-processing methods for ambient vibration responses. These two methods are based on the assumption that the input excitation is broadband and stationary. When sufficient long-time histories of continuous data are collected, the correlation function/random decrement function can be written as a summation of free decay vibration signals. Each vibration signal has a damped natural frequency and damping ratio, which is equal to the corresponding structural mode. The correlation function/random decrement function can reflect the properties of the structure, thereby indicating that structural damages can be detected using this information.

2.3.2 Structural damage detection methods

The time domain damage detection methods cannot be easily applied to civil structures because the input excitation force is unknown in the ambient conditions. For this reason, frequency domain methods can be used for structural parameter identification methods. Most of the studies extracted modal parameters and then used the frequency domain information (e.g., frequencies, mode shape, and flexibility matrix) to identify the structural parameters.

Teughels and De Roeck (2004) proposed a sensitivity-based method for damage detection of a concrete bridge. The frequencies and mode shapes were extracted from SSI method with ambient vibration responses. The Gauss-Newton method was used to update the Young's and the shear modulus of the actual bridge with the modal parameters.

Lee and Yun (2006) presented a conventional back-propagation neural network-based damage detection method for steel girder bridges. The modal parameters obtained from frequency domain decomposition (FDD) technique were used as input feature vectors to train the neural networks. A modal strain energy-based damage indicator was also proposed to detect the potentially damaged elements. Only the identified potential elements were considered in the neural networks for further damage identification. Michel *et al.* (2008) also used the FDD technique to estimate the modal parameters of a nine-story reinforced concrete dwelling. The stiffness parameters of the reinforced concrete structure were evaluated using the extracted frequencies and mode shapes.

Sohn and Law (1997) developed a damage detection method based on the Bayesian probabilistic framework. The most probable damage location and severities were identified with a few fundamental modes. The measurement noise was also considered. A two-stage Bayesian-based identification method was proposed by Yuen *et al.* (2004). The approach was used to identify the modal properties and structural parameters, sequentially. The model error and measurement noise were considered.

Miguel *et al.* (2012) extracted the modal parameters θ from SSI technique. The structural damage in a cantilever beam was identified by using the evolutionary harmony search algorithm with the extracted modal parameters. Amani *et al.* (2007) detected the structural damage location and intensity from changes of damping and stiffness matrices. The structure was constructed from the natural frequencies and modal properties. Experimental studies on a reinforced concrete beam and multi-story frame structure under ambient excitations were conducted to verify the accuracy of the proposed method.

Caicedo *et al.* (2004) proposed a damage detection method based on the modal identification and least-squares method. The model parameters were extracted from ambient vibration responses using NExT and ERA. The stiffness parameters of the structure were identified by the least-squares approach with the extracted model parameters. Yin *et al.* (2009) developed a substructural based method to detect the damage in a three-dimensional transmission tower. The frequency domain vibration characteristics of the tower were extracted by a combination of the NExT and ERA

methods. After obtaining the frequencies and mode shapes, the substructural damage was identified with dynamic model reduction.

Jaishi and Ren (2005) presented a comparative study on vibration characteristics for structural damage detection. The field test results from an actual bridge under ambient excitations were conducted for experimental study. The different vibration characteristics, such as frequencies, mode shape, flexibility matrix, and their combinations, were selected as objective functions for model updating.

These methods utilized frequency domain information (e.g., frequencies and mode shapes) for structural damage detection. However, these methods have some common problems. For example, the low-frequency modes are less sensitive to structural damage, whereas the high-frequency modes cannot be easily estimated in the ambient condition because large amount of energy is required to excite the high-frequency component of a structure. Structural damage is usually considered a local phenomenon, and the local response is used to better capture the local damage. The second problem is identifying errors in the frequencies and mode shapes. The measurement data always contain environment noise, thereby resulting in errors in the results of modal parameter extraction. The errors in the first stage affect the second stage of damage identification, and this problem cannot be ignored. The third problem is that frequency domain methods need a large number of measurement points to identify the structural parameters. When the structure is complicated and the number of unknown structural parameters is large, evaluating the condition of this structure is difficult.

2.3.3 Correlation function-based damage detection methods

The conventional time domain methods cannot easily identify the structural parameters under ambient conditions because these methods require larger number of sensors than the number of excitation forces. In the ambient conditions, the input location and the number of excitation are unknown, causing much difficult identification. The correlation function can be written as a summation of free decay vibration signals. Each signal is equal to the corresponding structural mode. Some researchers found that the structural damage can be detected with the correlation function, which may be a new solution for condition assessment under operational conditions. The correlation function-based damage detection methods are reviewed in the following section.

Yang *et al.* (2007c) utilized the amplitude vector of correlation functions for structural damage detection. Experimental experiments on a composite beam and an aircraft panel were performed to verify that the proposed index can detect and locate the structural damages. Wang *et al.* (2010) utilized the inner product vector of correlation functions for structural damage detection. Experimental studies on a shear frame structure, a composite beam, and an aircraft stiffened panel were carried out to verify the accuracy and effectiveness of the developed method. Zhang and Schmidt (2014) proposed a damage index, namely, Auto Correlation Function at Maximum Point Value Vector (AMV) for damage detection. The structural damage location can be detected from the changes of the normalized AMV. Sensitivity analysis of the AMV damage index was also studied (Zhang and Schmidt, 2015). These correlation-based methods can detect structural damages. However, the damage severity and location cannot be identified.

Law *et al.* (2012) proposed a damage detection method based on the covariance of covariance (CoC) matrix. The CoC matrix was obtained from the correlation function of acceleration response. The sensitivity matrix of CoC with respect to a local stiffness change was derived. A two-dimensional truss was used to verify the accuracy and effectiveness of the proposed damage detection method. The results showed that the CoC was more sensitive to the structural damage than frequencies and mode shapes. The CoC-based method requires many sensors for structural condition assessment in a complex structure. Li *et al.* (2017a) used the covariance of strain responses to identify the stiffness degradation in a seven-story planar frame structure and a circular arch structure.

The damage detection methods with the time history of correlation function are also explored. Ni *et al.* (2014) presented a correlation function-based method for structural condition assessment with multiple ambient excitations. The correlation functions were formed by two components. One component was a nonlinear function of structural parameters, and the other was a constant value, which depends on the energy of the excitation. The two components were updated sequentially using an iterative method. The numerical and experimental examples were studied to verify the effectiveness of the technique. Lei *et al.* (2017) utilized the correlation functions to detect the damage in a four-story building structure and a cantilever beam. The extended Kalman filter was used to identify the stiffness parameters. The stationary and non-stationary ambient excitations were considered.

2.4 Summary

This chapter presents the background on condition assessment methods for civil structures and related topics. Decentralized damage detection methods are considered alternative methods for damage detection in the large-scale civil structures. When the vibration responses under earthquake loading are used for damage detection, the nonlinear behavior in the civil structures should be considered. The nonlinear behavior of structures can be simulated with the global model or nonlinear finite element model. The correlation function-based methods show more advantages in damage detection under ambient excitations, because the time history and location excitation force are unknown. The correlation function-based method for damage detection will be explored in this thesis and extension studies with the proposed decentralized method for damage detection in large-scale civil structures will also be investigated.

CHAPTER 3

DECENTRALIZED STRUCTURAL DAMAGE

DETECTION

3.1 Introduction

Many damage detection methods have been proposed for a structure with unknown input to meet the general practical requirement in field measurement (Li and Chen, 2003; Carden and Fanning, 2004; Yang *et al.*, 2006a; Lu and Law, 2007b; Yang *et al.*, 2007a; Huang *et al.*, 2010). However, all existing methods for damage detection down to element level are suitable for a small to medium-size structure, and they are difficult to be applied to a large-scale structure with many structural components. The main reasons are that the large amount of data need to be collected and analysed and a lot of unknown parameters are to be identified. When iteration based method is used for damage detection, each iteration of identification with large number of data from the SHM system takes a long duration and the identification is computationally inefficient. The capital cost on sensor installation, problems with power supply and power

consumption by the sensors, and data processing capability of hardware are several of the many adverse factors for a high-density sensor configuration. A new method for damage detection from only a few number of sensors should be explored.

In this chapter, a decentralized damage detection method for large-scale structures is proposed. The large-scale structure is divided into a number of smaller zones according to its finite element configuration. Vibration tests are conducted in each zone in sequence with the sensors in the zone. After all the response sets are obtained, the external excitations in each test are identified in the wavelet domain. The structural parameters of the whole structure are divided into several subsets and they are updated using the Newton-SOR method. Both the external excitations and the physical structural parameters will be closer to their true value in further iterations of model updating. The iteration continues until a prescribed convergence condition is satisfied. This decentralized damage detection method is implemented in a multi-core central processing unit with parallel processing. Each subset of parameters is updated in separate core of the processing unit using the Parallel Computing Toolbox in MATLAB. Simulation results with a plane frame structure show that both unknown structural parameters and unknown excitation force can be identified. The parallel computing achieves a reduction of approximately 37% computation time compared to that from computation in sequence.

3.2 Force Identification

3.2.1 Equation of motion

The equation of motion of an N -DOFs damped structural system under external excitations can be written as

$$\mathbf{M}\ddot{\mathbf{x}}(t) + \mathbf{C}\dot{\mathbf{x}}(t) + \mathbf{K}\mathbf{x}(t) = \mathbf{B}\mathbf{f}(t) \quad (3.1)$$

where \mathbf{x} , $\dot{\mathbf{x}}$, and $\ddot{\mathbf{x}}$ are vectors of displacements, velocity and acceleration responses of the structure, respectively; \mathbf{M} , \mathbf{C} and \mathbf{K} are the mass, damping, and stiffness matrices of the structure, respectively. $\mathbf{f}(t)$ is the external excitation force vector, and \mathbf{B} is the force location matrix associated with vector $\mathbf{f}(t)$. As suggested by Clough and Penzien (1975), Rayleigh damping is used in this study. The coefficients of the mass and stiffness are obtained from the first two natural frequencies and the damping ratio for the first two modes is assumed as 2%. The dynamic responses of the structure are calculated from Newmark method with coefficients $\beta = 0.25$ and $\gamma = 0.5$.

3.2.2 Unit impulse response (UIR) function in wavelet domain

UIR is the response function of the system under the input of a unit pulse at a specific location. It is an intrinsic function of the structural system. The wavelet domain UIR function of a structure at a specific DOF has been derived analytically from the general system equation of motion (Law and Li, 2007) and it will be introduced briefly in the following section.

The equation of motion of an N -DOFs damped structural system under the unit impulse excitation can be written as

$$\mathbf{M}\ddot{\mathbf{x}}(t) + \mathbf{C}\dot{\mathbf{x}}(t) + \mathbf{K}\mathbf{x}(t) = \mathbf{B}\delta(t) \quad (3.2)$$

where $\delta(t)$ is the Dirac delta function. The impulse response function can be represented as a free vibration state under some specific initial conditions. Assuming that the system is in static equilibrium initially, the UIR function can be computed from the equation of motion using the Newmark method:

$$\begin{cases} \mathbf{M}\ddot{\mathbf{h}}(t) + \mathbf{C}\dot{\mathbf{h}}(t) + \mathbf{K}\mathbf{h}(t) = \mathbf{0} \\ \mathbf{h}(0) = \mathbf{0}, \quad \dot{\mathbf{h}}(0) = \mathbf{M}^{-1}\mathbf{B} \end{cases} \quad (3.3)$$

where \mathbf{h} , $\dot{\mathbf{h}}$, and $\ddot{\mathbf{h}}$ are the unit impulse displacement, velocity and acceleration vectors, respectively.

When the structural system is under general excitation $\mathbf{f}(t)$ with zero initial conditions, the acceleration response $\ddot{\mathbf{x}}_s(t_n)$ at sensor location s at time instant t_n is

$$\ddot{\mathbf{x}}_s(t_n) = \int_0^{t_n} \ddot{\mathbf{h}}_s(t_n - \tau) \mathbf{f}(\tau) d\tau \quad (3.4)$$

where $\ddot{\mathbf{h}}_s$ is the UIR function at sensor location s . Eq. (3.4) represents the input-output relationship of the dynamic structural system under the input force $\mathbf{f}(t)$ at a specific location. Vectors $\ddot{\mathbf{h}}_s(t_n - \tau)$ and $\mathbf{f}(\tau)$ can be expanded in terms of the discrete wavelet transform as (Peppin, 1994),

$$\ddot{\mathbf{h}}_s(t_n - \tau) = h_{s,0}^{DWT} + \sum_j \sum_k h_{s,2^j+k}^{DWT} \psi(2^j \tau - k) \quad (3.5)$$

$$\mathbf{f}(\tau) = f_0^{DWT} + \sum_j \sum_k f_{2^j+k}^{DWT} \psi(2^j \tau - k) \quad (3.6)$$

where $\psi(2^j \tau - k)$ is the wavelet basis function, $h_{s,2^j+k}^{DWT}$ and $f_{2^j+k}^{DWT}$ are the expansion coefficients of the impulse response function and external excitation respectively.

Substituting Eqs. (3.5) and (3.6) into the convolution integral in Eq. (3.4), and using the orthogonal conditions of the wavelet basis functions (Daubechies, 1992) as follows,

$$\int_0^{t_n} \psi(2^j \tau - k) d\tau = 0 \quad (3.7)$$

$$\int_0^{t_n} \psi(2^j \tau - k) \psi(2^r \tau - s) d\tau = \begin{cases} 1/2^j & \text{when } r = j \text{ and } s = k \\ 0 & \text{otherwise} \end{cases} \quad (3.8)$$

The following formula can then be derived as

$$\ddot{\mathbf{x}}_s(t_n) = \dot{\mathbf{h}}_s^{DWT}(t_n) \mathbf{f}^{DWT} \quad (3.9)$$

where $\dot{\mathbf{h}}_s^{DWT}(t_n)$ and \mathbf{f}^{DWT} are the discrete wavelet transforms of $\dot{\mathbf{h}}_s(t_n - \tau)$ and $\mathbf{f}(\tau)$, respectively, and are given as

$$\dot{\mathbf{h}}_s^{DWT}(t_n) = [\dot{\mathbf{h}}_{s,0}^{DWT}(t_n), \dot{\mathbf{h}}_{s,1}^{DWT}(t_n), \dots, \dot{\mathbf{h}}_{s,2^j+k}^{DWT}(t_n)]$$

$$\mathbf{f}^{DWT} = [\mathbf{f}_0^{DWT}, \mathbf{f}_1^{DWT}, \dots, \mathbf{f}_{2^j+k}^{DWT}]^T$$

3.2.3 Force identification in wavelet domain

For the entire set of time history data, for example, $\ddot{\mathbf{x}}_s = [\ddot{x}_s(t_1), \ddot{x}_s(t_2), \dots, \ddot{x}_s(t_n)]^T$ the system input-output relationship for the structure can be expressed as,

$$\ddot{\mathbf{x}}_{s(n \times 1)} = \dot{\mathbf{h}}_s^{DWT}{}_{(n \times rl)} \mathbf{f}^{DWT}{}_{(rl \times 1)} \quad (3.10)$$

and

$$\dot{\mathbf{h}}_s^{DWT} = [\dot{\mathbf{h}}_s^{DWT}(t_1), \dot{\mathbf{h}}_s^{DWT}(t_2), \dots, \dot{\mathbf{h}}_s^{DWT}(t_n)]^T$$

where n , r and l are the number of time steps of the response data, the number of input excitations and the number of wavelet coefficients in the discrete wavelet transform, respectively.

The force identification by using the impulse response function in the wavelet domain will be adopted in the following studies. The measured responses $\ddot{\mathbf{x}}_{mea}(t)$ can be represented in the wavelet domain from Eq. (3.10) as follows,

$$\ddot{\mathbf{x}}_{mea}(t)_{(mm \times 1)} = \ddot{\mathbf{h}}^{DWT}_{(mm \times rl)} \mathbf{f}^{DWT}_{(rl \times 1)} \quad (3.11)$$

where m is the number of sensors. When the number of measurements is at least equal or larger than the number of external excitation on the structure, the pseudo-inverse $(\ddot{\mathbf{h}}^{DWT})^+$ exists (Penrose, 1955). The discrete wavelet coefficient of the unknown force can be obtained from Eq. (3.11) as

$$\mathbf{f}^{DWT} = (\ddot{\mathbf{h}}^{DWT})^+ \ddot{\mathbf{x}}_{mea}(t) \quad (3.12)$$

The unknown external excitation can be obtained by substituting Eq. (3.12) into Eq. (3.6).

3.3 Damage Detection with Unknown Input Force

In practice, the input excitations such as wind, seismic and vehicle loadings are difficult to be measured. In the cases, output only method is more promising for structural damage detection. In this section, a output only decentralized damage detection method is proposed. The dynamic response sensitivities of a structure with respect to the structural parameters are derived first, and then sensitivity-based model updating

technique is reviewed. The proposed decentralized method utilizes the solution of the Newton-SOR method for structural damage detection. Parallel computing is also applied during the processing of damage detection in order to improve the computational performance.

3.3.1 Sensitivities of dynamic responses

Assuming that the structural local damages are in the form of a change of a structural stiffness parameter, the stiffness matrix of the damaged structure is expressed as

$$\mathbf{K}^d = \sum_{i=1}^{ne} (1 - \alpha_i) \mathbf{K}_i \quad (3.13)$$

where \mathbf{K}_i is the stiffness matrix of the i -th finite element in the intact state, and \mathbf{K}^d is the global stiffness matrix in the damaged state. In addition, α_i ($0 \leq \alpha_i \leq 1$) is defined as the damage index, which is a fraction of the intact stiffness of the i -th finite element of the structure, and ne is the total number of elements in the structure. Further, $\alpha_i = 1$ denotes that the i -th structural element completely loses its stiffness, whereas $\alpha_i = 0$ indicates that the structural element is intact.

The sensitivity method can be applied to identify local damages in the structure when external excitations are available. Performing differentiation to both sides of Eq. (3.1) with respect to the damage index, we have

$$\mathbf{M} \frac{\partial \ddot{\mathbf{x}}}{\partial \alpha_i} + \mathbf{C} \frac{\partial \dot{\mathbf{x}}}{\partial \alpha_i} + \mathbf{K} \frac{\partial \mathbf{x}}{\partial \alpha_i} = - \frac{\partial \mathbf{K}}{\partial \alpha_i} \mathbf{x} - a_2 \frac{\partial \mathbf{K}}{\partial \alpha_i} \dot{\mathbf{x}} \quad (3.14)$$

The responses of the structure have been calculated from Eq. (3.1). The response sensitivities $\partial\ddot{x}/\partial\alpha_i$, $\partial\dot{x}/\partial\alpha_i$, and $\partial x/\partial\alpha_i$ can therefore be solved from Eq. (3.14) using Newmark method (Lu and Law, 2007b).

3.3.2 Sensitivity-based model updating

The model updating based on acceleration response sensitivity can be expressed in the Taylor's expansion without the second and higher order terms as

$$\Delta\ddot{x} = \ddot{x}_{mea} - \ddot{x}_{cal} = S\Delta\theta + O(\Delta\theta^2) \quad (3.15)$$

$$S = \frac{\partial\ddot{x}_{cal}}{\partial\theta} = \left[\frac{\partial\ddot{x}_{cal}}{\partial\alpha_1}, \frac{\partial\ddot{x}_{cal}}{\partial\alpha_2}, \dots, \frac{\partial\ddot{x}_{cal}}{\partial\alpha_{ne}} \right]$$

where \ddot{x}_{mea} and \ddot{x}_{cal} are the measured and calculated acceleration responses, respectively; $\theta = [\alpha_1, \alpha_2, \dots, \alpha_{ne}]$ is the damage index vector, and S is the sensitivity matrix of acceleration obtained from Eq. (3.14). The high order terms $O(\Delta\theta^2)$ are small and can be ignored.

Eq. (3.15) can be solved by the simple least-squares method as follows:

$$\Delta\theta = (S^T S)^{-1} S^T \Delta\ddot{x} \quad (3.16)$$

However, the matrix S is generally ill-conditioned and the damped least-squares method is used instead with

$$\Delta\theta = (S^T S + \lambda)^{-1} S^T \Delta\ddot{x} \quad (3.17)$$

where λ is the non-negative optimal regularization parameter and can be obtained by the L-curve method (Tikhonov *et al.*, 1995).

3.3.3 Damage detection from several sets of responses

Sensitivity-based model updating is used in the following studies, considering with different sets of measurement responses. In a short-term field measurement, the sensors are not fixed locations but roved at different parts of the structure in sequence. Therefore, the number of sensors and the data acquisition units can be reduced significantly. The capital cost of the hardware can be reduced to a fraction of that in the SHM system. In practice, there are many measurement points for a large civil structure and the measurement duration is long. The sensitivity matrix \mathbf{S} has $n \times m$ rows and n columns, causing a very heavy computational load. To improve the computational efficiency, a decentralized approach is proposed in the subsequent section. Compared with the conventional global sensitivity based methods, the proposed decentralized approach only requires the diagonal block of the sensitivity matrix for finite element model updating. The computational workload and computer memory in each iteration are thus reduced.

A large structure is divided into several smaller groups in physical zones based on its finite element formulation. Consequently, the unknown damage index θ can be divided into several subsets $\theta = [\theta_1, \theta_2, \dots, \theta_r]$, where θ_i contains all the unknown damage

$$\mathbf{G}'(\boldsymbol{\theta}^n) = \begin{bmatrix} \frac{\partial \mathbf{g}_1}{\partial \theta_1} & \frac{\partial \mathbf{g}_1}{\partial \theta_2} & \dots & \frac{\partial \mathbf{g}_1}{\partial \theta_r} \\ \frac{\partial \mathbf{g}_2}{\partial \theta_1} & \frac{\partial \mathbf{g}_2}{\partial \theta_2} & \dots & \frac{\partial \mathbf{g}_2}{\partial \theta_r} \\ \vdots & \vdots & & \vdots \\ \frac{\partial \mathbf{g}_r}{\partial \theta_1} & \frac{\partial \mathbf{g}_r}{\partial \theta_2} & \dots & \frac{\partial \mathbf{g}_r}{\partial \theta_r} \end{bmatrix} \quad (3.23)$$

When an iterative successive-over-relaxation (SOR) method is used to solve Eq. (3.21) for each Newton iteration, the whole process is called Newton-SOR method (Ortega and Rheinboldt, 1970). If P iterations are used inside the SOR loop the method is called P -step Newton-SOR method. The comprehensive descriptions of the method can be found in Ortega and Rheinboldt (1970). The SOR solution is used to reconstruct the Jacobian for the next Newton step so that the SOR solution is not required to have a high precision (Carey and Krishnan, 1982). Therefore, we only consider *One-step* Newton-SOR method. Compared with global method (the classic sensitivity method), the proposed decentralized approach only requires that the diagonal block of the sensitivity matrix is calculated for the finite element model updating. Within each iteration, the computational workload and computer memory are thus reduced significantly. Other methods to reduce the computational resources, for example, the substructuring approach (Weng *et al.*, 2009; Weng *et al.*, 2013), are not studied and compared in this thesis.

Eq. (3.21) can be written as Eq. (3.24) with $\mathbf{G}'(\boldsymbol{\theta}^n)$ decomposed as Eq. (3.25)

$$(\mathbf{L} - \mathbf{U})\boldsymbol{\theta}^{n+1} = \mathbf{G}'(\boldsymbol{\theta}^n)\boldsymbol{\theta}^n - \mathbf{G}(\boldsymbol{\theta}^n) \quad (3.24)$$

$$\mathbf{G}'(\boldsymbol{\theta}^n) = \mathbf{L} - \mathbf{U} \quad (3.25)$$

where \mathbf{L} and \mathbf{U} are a diagonal block matrix and a non-diagonal block matrix of $\mathbf{G}'(\boldsymbol{\theta}^n)$,

respectively. On the right-hand-side of Eq. (3.24), set $\mathbf{b} = \mathbf{G}'(\boldsymbol{\theta}^n)\boldsymbol{\theta}^n - \mathbf{G}(\boldsymbol{\theta}^n)$

$$\mathbf{L}\boldsymbol{\theta}^{n+1} = \mathbf{U}\boldsymbol{\theta}^{n+1} + \mathbf{b} \quad (3.26)$$

$$\mathbf{L}\boldsymbol{\theta}^{n+1,q} = \mathbf{U}\boldsymbol{\theta}^{n+1,q-1} + \mathbf{b}, \quad \boldsymbol{\theta}^{n+1,q} = \mathbf{L}^{-1}(\mathbf{U}\boldsymbol{\theta}^{n+1,q-1} + \mathbf{b}), \quad q=1, 2, 3, \dots \quad (3.27)$$

where the superscript q denotes the iteration number in the SOR iteration. Defining

matrix $\mathbf{V} = \mathbf{L}^{-1}\mathbf{U}$, we have

$$\mathbf{V} - \mathbf{I} = \mathbf{L}^{-1}\mathbf{U} - \mathbf{I} = \mathbf{L}^{-1}(\mathbf{U} - \mathbf{L}) \quad (3.28)$$

Then Eq. (3.27) can be rewritten as:

$$\boldsymbol{\theta}^{n+1,q} = \mathbf{V}\boldsymbol{\theta}^{n+1,q-1} + \mathbf{L}^{-1}\mathbf{b} \quad (3.29)$$

Expanding the term $\mathbf{V}\boldsymbol{\theta}^{n+1,q-1}$ in full, we have

$$\begin{aligned} \boldsymbol{\theta}^{n+1,q} &= \mathbf{V}^q \boldsymbol{\theta}^{n+1,0} + (\mathbf{I} + \mathbf{V} + \mathbf{V}^2 \dots \mathbf{V}^{q-1}) \mathbf{L}^{-1}\mathbf{b} \\ &= \boldsymbol{\theta}^{n+1,0} + (\mathbf{V}^q - \mathbf{I})\boldsymbol{\theta}^{n+1,0} + (\mathbf{I} + \mathbf{V} + \mathbf{V}^2 \dots \mathbf{V}^{q-1}) \mathbf{L}^{-1}\mathbf{b} \\ &= \boldsymbol{\theta}^{n+1,0} + (\mathbf{I} + \mathbf{V} + \mathbf{V}^2 \dots \mathbf{V}^{q-1})((\mathbf{V} - \mathbf{I})\boldsymbol{\theta}^{n+1,0} + \mathbf{L}^{-1}\mathbf{b}) \end{aligned} \quad (3.30)$$

Substituting \mathbf{b} and $\mathbf{V} = \mathbf{L}^{-1}\mathbf{U}$ into the last bracket on the right-hand-side of Eq. (3.30), we obtain

$$\begin{aligned} &(\mathbf{V} - \mathbf{I})\boldsymbol{\theta}^{n+1,0} + \mathbf{L}^{-1}\mathbf{b} \\ &= \mathbf{L}^{-1}(\mathbf{U} - \mathbf{L})\boldsymbol{\theta}^{n+1,0} + \mathbf{L}^{-1}((\mathbf{L} - \mathbf{U})\boldsymbol{\theta}^n - \mathbf{G}(\boldsymbol{\theta}^n)) \end{aligned} \quad (3.31)$$

The initial and ending values of the SOR iteration are the initial and ending values of the Newton iteration and they are: $\boldsymbol{\theta}^{n+1,0} \equiv \boldsymbol{\theta}^n$ and $\boldsymbol{\theta}^{n+1,q} \equiv \boldsymbol{\theta}^{n+1}$, respectively.

Substituting Eq. (3.31) into Eq. (3.30), we have

$$\boldsymbol{\theta}^{n+1} = \boldsymbol{\theta}^n - (\mathbf{I} + \mathbf{V} + \mathbf{V}^2 \dots \mathbf{V}^{q-1}) \mathbf{L}^{-1}\mathbf{G}(\boldsymbol{\theta}^n) \quad (3.32)$$

When $q \rightarrow \infty$, Eq. (3.32) is equivalent to the Newton method in Eq. (3.22). When $q=1$, we have the *One-step* Newton-SOR iteration as

$$\boldsymbol{\theta}^{n+1} = \boldsymbol{\theta}^n - \mathbf{L}^{-1} \mathbf{G}(\boldsymbol{\theta}^n) \quad (3.33)$$

Rewriting $\boldsymbol{\theta}^{n+1}$ into a vector of subsets $[\boldsymbol{\theta}_1^{n+1}, \boldsymbol{\theta}_2^{n+1}, \dots, \boldsymbol{\theta}_r^{n+1}]$, we have

$$\begin{bmatrix} \boldsymbol{\theta}_1^{n+1} \\ \boldsymbol{\theta}_2^{n+1} \\ \vdots \\ \boldsymbol{\theta}_r^{n+1} \end{bmatrix} = \begin{bmatrix} \boldsymbol{\theta}_1^n \\ \boldsymbol{\theta}_2^n \\ \vdots \\ \boldsymbol{\theta}_r^n \end{bmatrix} - \begin{bmatrix} \frac{\partial \mathbf{g}_1}{\partial \boldsymbol{\theta}_1^n} & 0 & 0 & 0 \\ 0 & \frac{\partial \mathbf{g}_2}{\partial \boldsymbol{\theta}_2^n} & 0 & 0 \\ 0 & 0 & \ddots & 0 \\ 0 & 0 & 0 & \frac{\partial \mathbf{g}_r}{\partial \boldsymbol{\theta}_r^n} \end{bmatrix}^{-1} \begin{bmatrix} \mathbf{g}_1(\boldsymbol{\theta}^n, \mathbf{f}_1) - \ddot{\mathbf{x}}_{mea,1} \\ \mathbf{g}_2(\boldsymbol{\theta}^n, \mathbf{f}_2) - \ddot{\mathbf{x}}_{mea,2} \\ \vdots \\ \mathbf{g}_r(\boldsymbol{\theta}^n, \mathbf{f}_r) - \ddot{\mathbf{x}}_{mea,r} \end{bmatrix} \quad (3.34)$$

or

$$\boldsymbol{\theta}_i^{n+1} = \boldsymbol{\theta}_i^n - \left[\frac{\partial \mathbf{g}_i}{\partial \boldsymbol{\theta}_i^n} \right]^{-1} \left[\mathbf{g}_i(\boldsymbol{\theta}^n, \mathbf{f}_i) - \ddot{\mathbf{x}}_{mea,i} \right], \quad (i=1, 2, \dots, r) \quad (3.35)$$

The damped least-squares method by Tikhonov *et al.* (1995) is applied to obtain the solution with bound for Eq. (3.35). Eq. (3.36) gives the regularization solution in the *One-step* Newton-SOR iteration as

$$\boldsymbol{\theta}_i^{n+1} = \boldsymbol{\theta}_i^n - \left[\left(\frac{\partial \mathbf{g}_i}{\partial \boldsymbol{\theta}_i^n} \right)^T \left(\frac{\partial \mathbf{g}_i}{\partial \boldsymbol{\theta}_i^n} \right) + \lambda_i \right]^{-1} \left(\frac{\partial \mathbf{g}_i}{\partial \boldsymbol{\theta}_i^n} \right)^T \left[\mathbf{g}_i(\boldsymbol{\theta}^n, \mathbf{f}_i) - \ddot{\mathbf{x}}_{mea,i} \right], (i=1, 2, \dots, r) \quad (3.36)$$

When a limited number of measurement points are available, and the number of unknown parameters is large, the solution may not be unique. The increasing of measurement points and optimizing the sensor placements may provide more structural information in the measurement sets and thus the non-uniqueness problem in the

identified results can be avoided. In the following examples, the non-uniqueness issue does not occur

3.3.4 Parallel computing

Traditionally, all unknown parameters of a structure are updated at the same time, and the operations are conducted in the serial computation manner on a single-core CPU. That is the computer instructions are executed one by one in sequence. Note that in the *One-Step* Newton-SOR method, the identified vector θ_i^{n+1} is a function of $[\theta_1^n, \theta_2^n, \dots, \theta_r^n]$ and the excitation force f_i . The unknown parameters θ_i^{n+1} and θ_j^{n+1} ($i \neq j$) can be computed at the same time by performing the instructions using multithreads with different core of the CPUs or multiple CPUs. Therefore in this paper, the Parallel Computing Toolbox in MATLAB is used to execute instructions to update θ_i^{n+1} ($i=1, 2, \dots, r$) in different cores (or threads) of the CPU. The parallel for-loops (parfor) are used to manage the computation and data between the MATLAB session and the computing resources. The framework of the parallel computation is shown in Figure 3.1. The process of updating of each subset of parameters is shown in Figure 3.2. The iteration continues until a prescribed convergence condition is satisfied, which is defined as

$$\frac{\|\theta^{n+1} - \theta^n\|}{\|\theta^{n+1}\|} \times 100\% \leq Tol \quad (3.37)$$

where Tol is the convergence criterion.

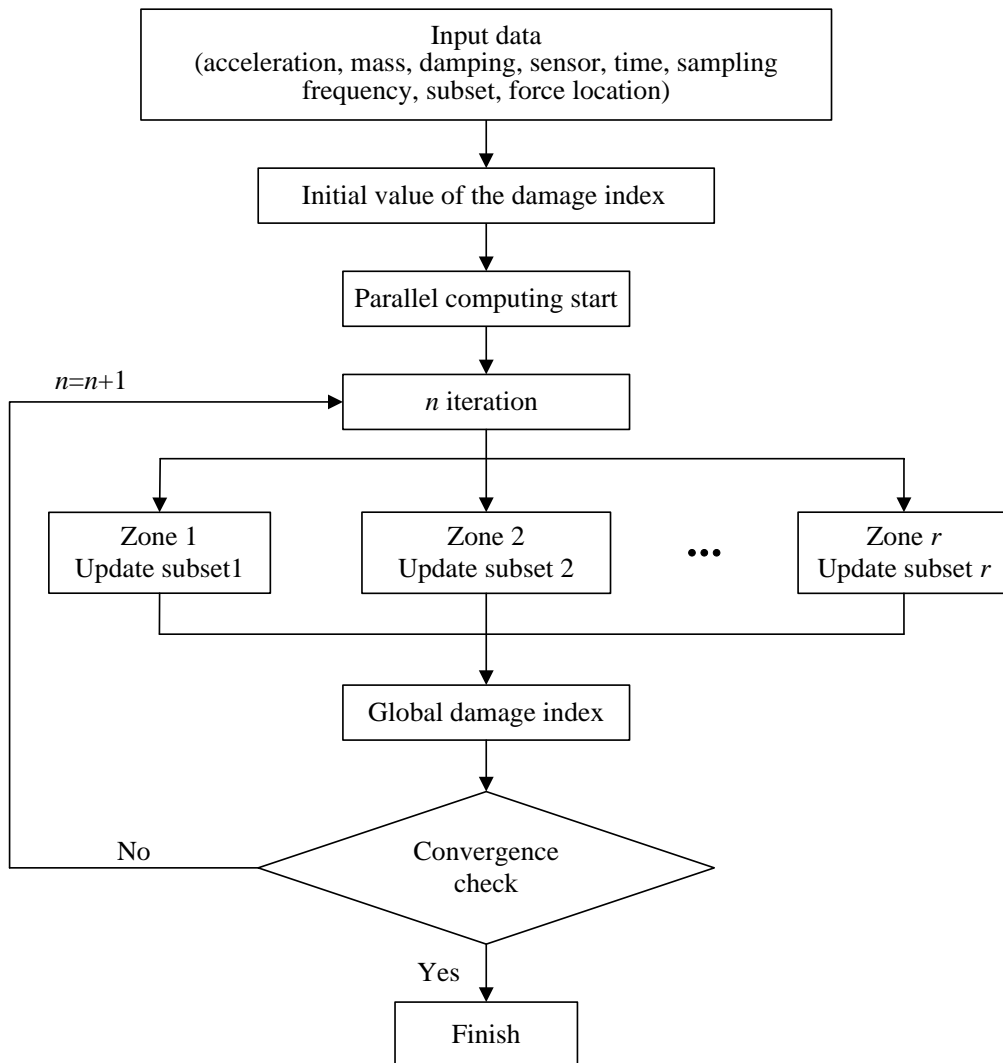


Figure 3.1 Framework of the parallel computation

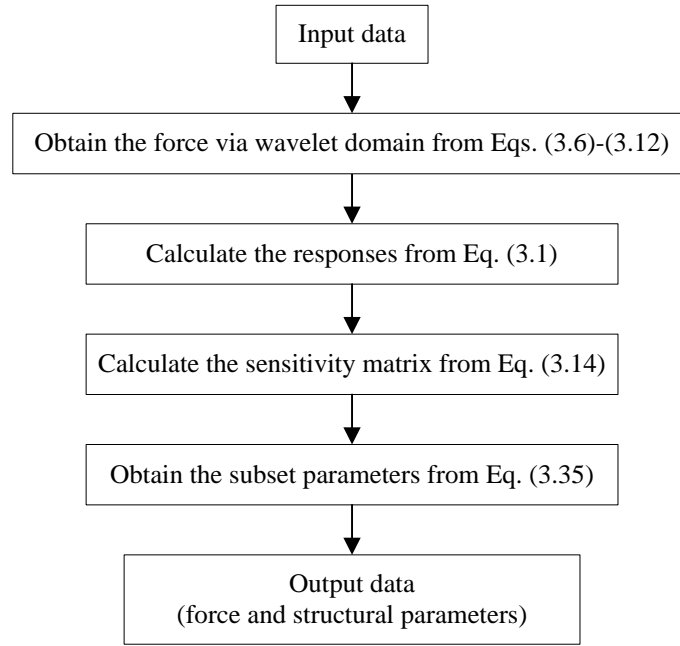


Figure 3.2 Computation for each zone

3.4 Numerical Study

A simply-supported planer truss structure as shown in Figure 3.3 with forty-six members serves for the simulation study. The truss has a pin support at Node 1 and roller support at Node 19. The cross-sectional area of the bar is 0.0016 m^2 . Rayleigh damping is adopted for the system with $\zeta_1=0.01$ and $\zeta_2=0.01$ assumed for the first two modes. The mass density of the material is $7.8 \times 10^3 \text{ kg/m}^3$ and the elastic modulus of the material is 206 GPa.

The truss structure is divided into three zones arbitrarily. The first zone consists of members 1 to 15 with unknown parameters $\alpha_1 \sim \alpha_{15}$. The second zone consists of members 16 to 31 with unknown parameters $\alpha_{16} \sim \alpha_{31}$, and the third zone consists of

members 32 to 46 with unknown parameters $\alpha_{32} \sim \alpha_{46}$. Each zone has 4 accelerometers as shown in Figure 3.4, two measuring horizontal acceleration and two verticals. The initial value of the modulus of material of the whole structure are equal to the health status. The convergence criterion in Eq. (3.37) is set to 10^{-3} and 10^{-6} for the case with and without noise in the measured responses, respectively.

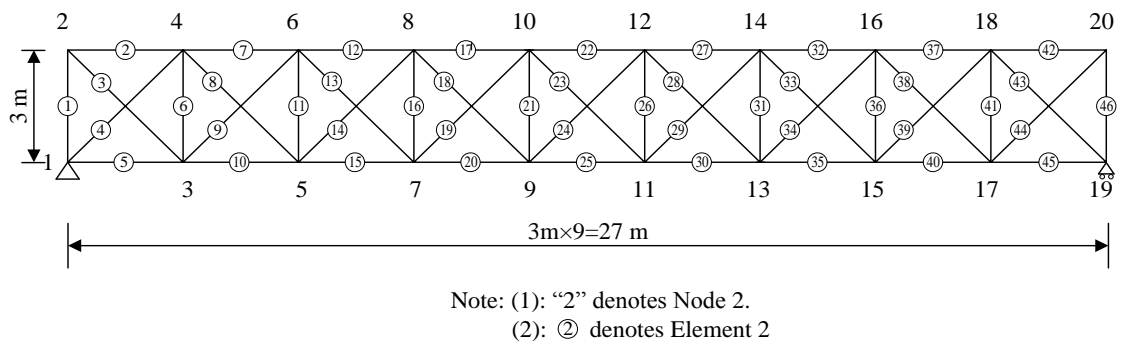
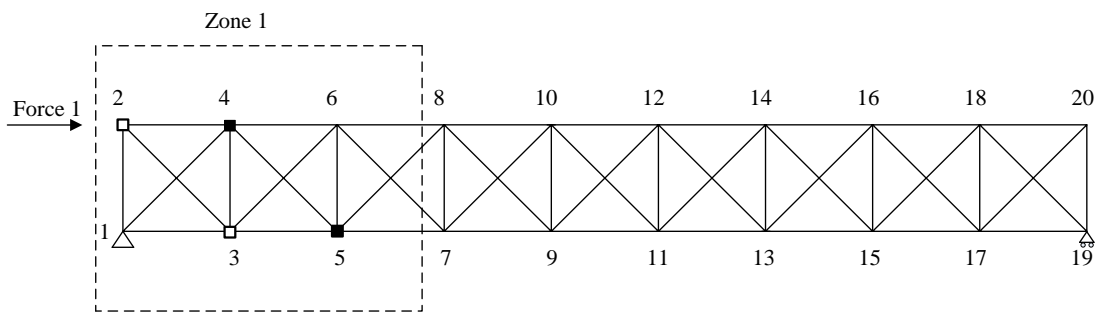
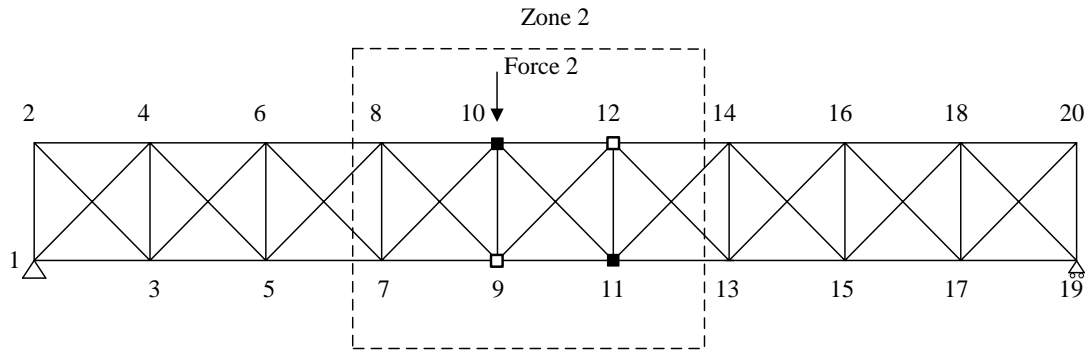


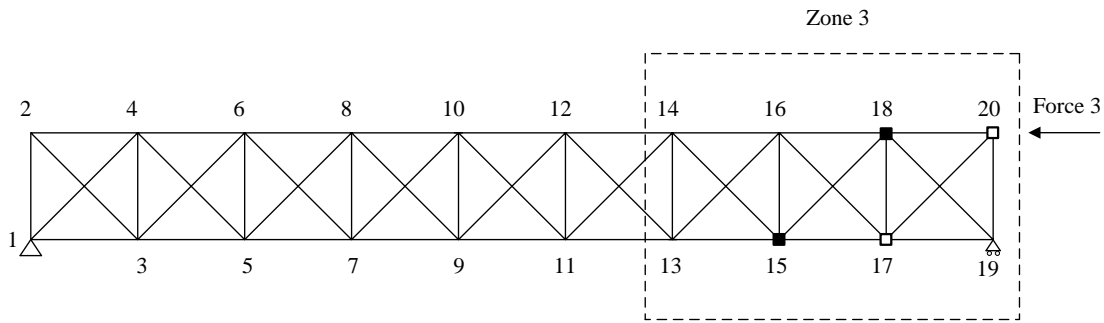
Figure 3.3 Truss structure



(a) Test 1



(b) Test 2



(c) Test 3

Note: □ denotes horizontal measurement; ■ denotes vertical measurement

Figure 3.4 Location of sensors and excitation

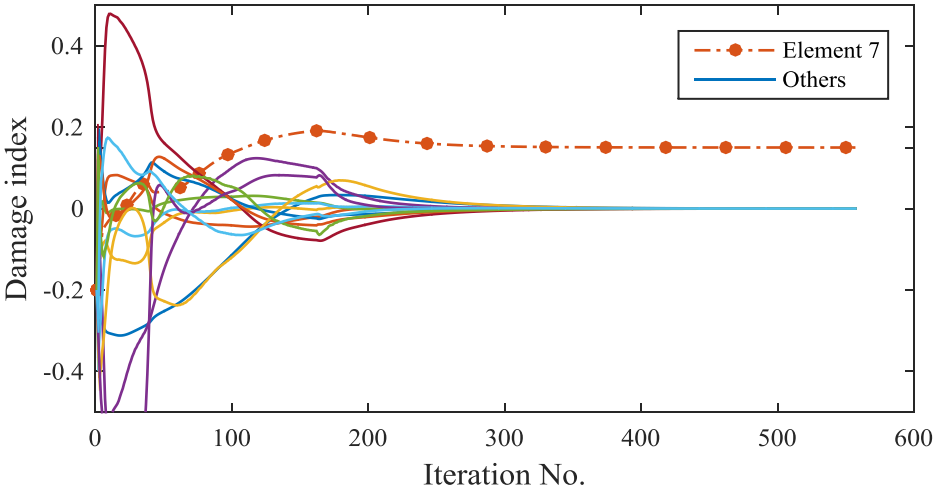
3.4.1 Damage detection without measurement noise

The structure is assumed to be at rest before applying white noise excitation at the selected node. Short-term field tests are carried out from zone 1 to zone 3 to obtain the vibration data as shown in Figure 3.4. The sampling rate is 200Hz. When there is no noise in the measurement responses, the response data of a duration of 2.5s is used for the studies.

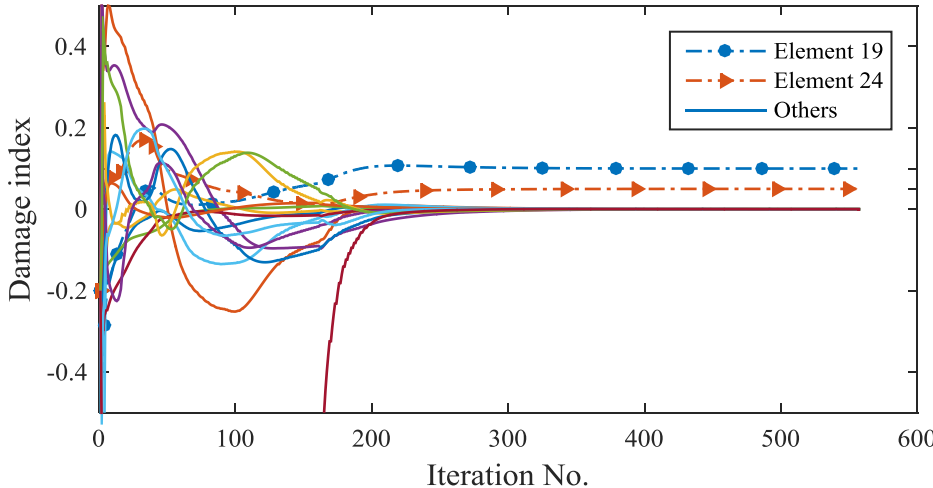
The modulus of elasticity of material is assumed to suffer a reduction of 15% in Elements 7 and 32, 10% in Element 19 and 5% in element 24 to simulate the damage in the structure. The 15% stiffness reduction of Element 7 is the structural damage in zone 1, while the stiffness reduction of Elements 19 and 24 are the damage in zone 2. Similarly, the Element 32 is in zone 3.

The dynamic responses of the structure are divided into three subsets. Each subset of vibration responses is obtained from the corresponding field test and they are used to identify the structural parameters in that zone. The solution from the *One-step* Newton-SOR method is used to identify the unknown structural parameters in each zone, because the structural damage is assumed to be more sensitive to the local responses but less sensitive to the responses that far away from the damage location. In each iteration, the subset unknown structural parameters are updated using the corresponding subset measurement responses in one CPU. After that, the global damage index is generated and sent to each CPU for performing the next iteration. The detailed procedures can be found in Figure 3.1 and 3.2. Figure 3.5 shows the evolution of damage indices of each subset with respect to iteration. All simulated damages are correctly identified after around 300 iterations. For the undamaged elements, the identified damage indices finally converged to zero and they are the same as the true values, which indicates that the proposed method can be used for structural damage detection accurately. Figure 3.6 shows the variation of the relative error with iterations. In this study, the convergence criterion is set at 10^{-6} , which may be too small. As the results convergence to true values after 300 iterations, the accuracy improvement in the further iterations is limited. The final identified unknown excitation force in zone 1 is shown in Figure 3.7, which

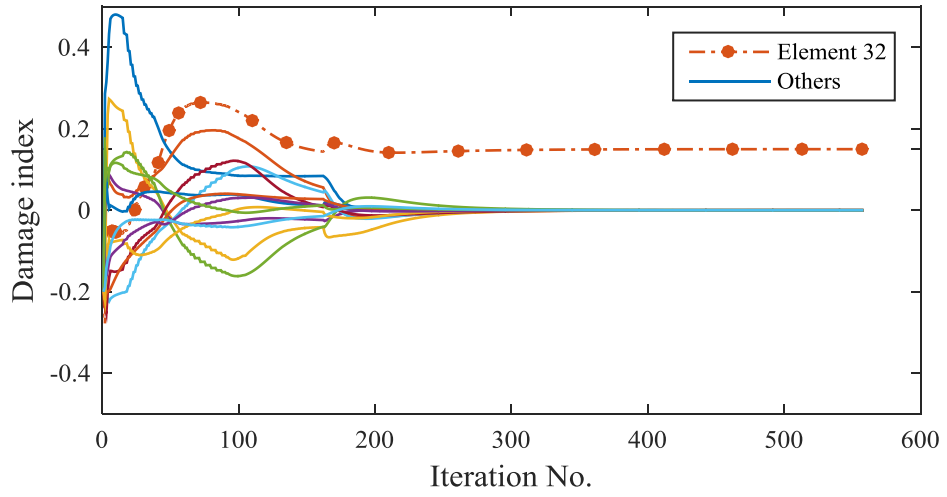
agrees with the true input force well with small error. The difference increases along with the time step, which may be caused by accumulation of numerical discrete error. However, the difference between the identified force and true input force is less than 0.1%. The results indicate that the proposed method is accurate, and it can be used for damage detection with unknown excitations.



(a) Subset 1



(b) Subset 2



(c) Subset 3

Figure 3.5 Evolution of the identified results without measurement noise

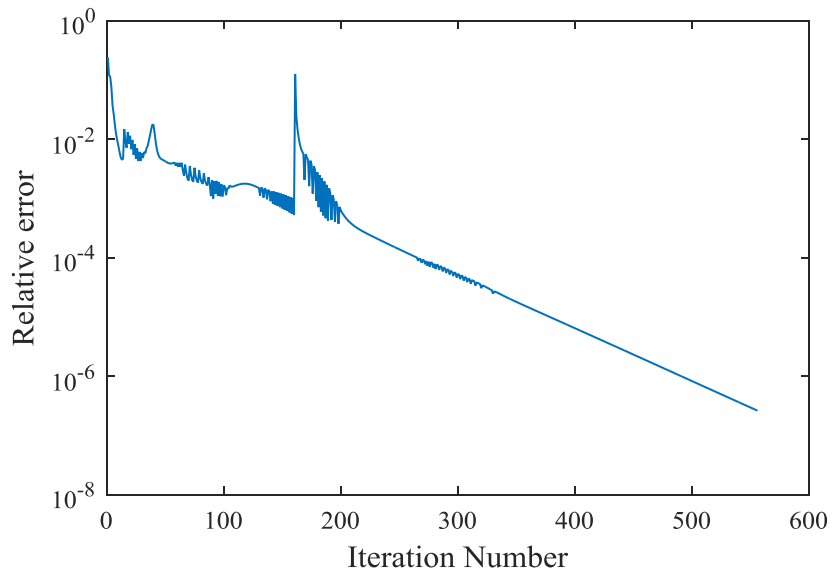
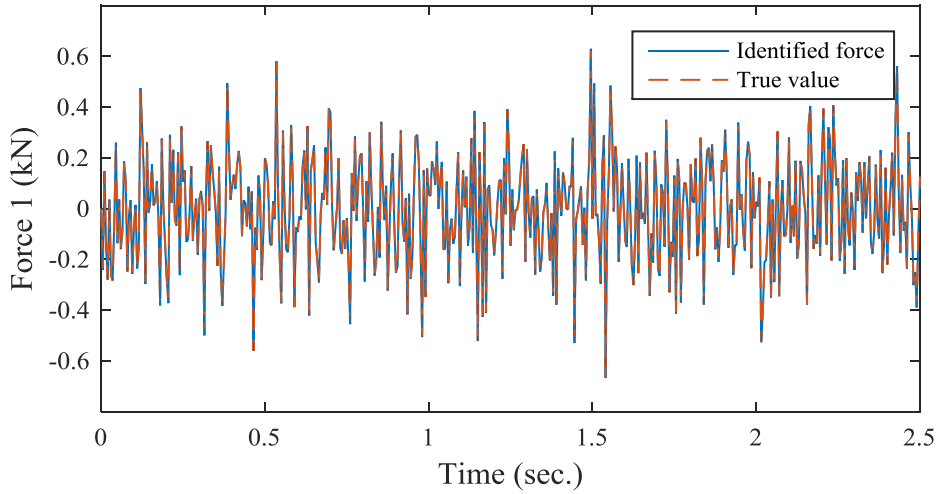
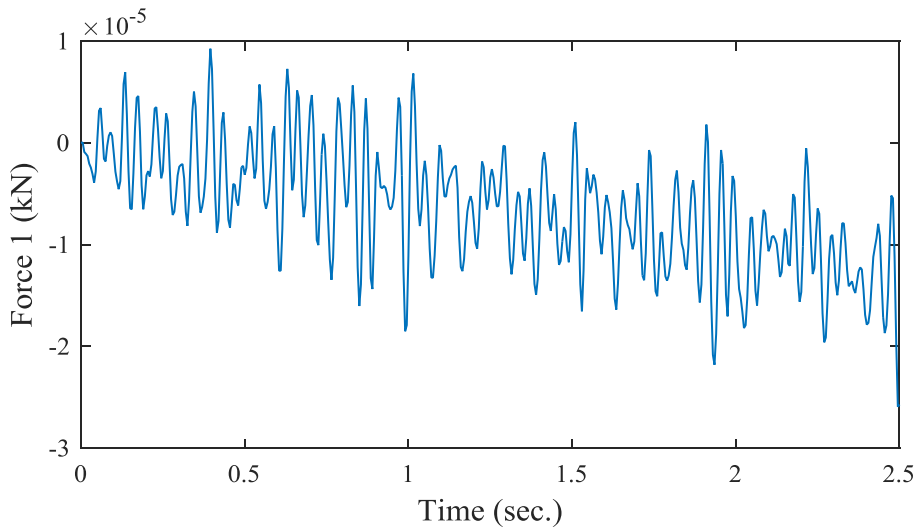


Figure 3.6 Relative error with iteration.



(a) Comparison of the identified input force with the true excitation force.



(b) Error of the identified input force.

Figure 3.7 Comparison of the identified input force without noise

3.4.2 Damage scenario with measurement noise

In practice, noise exists inevitably. The measurement noise effect on the identified resulted is studied. The measured response is simulated by adding a random component to the actual responses as

$$\ddot{\mathbf{x}}_{mea} = \ddot{\mathbf{x}} + E_p N_{noise} \sigma(\ddot{\mathbf{x}}) \quad (3.38)$$

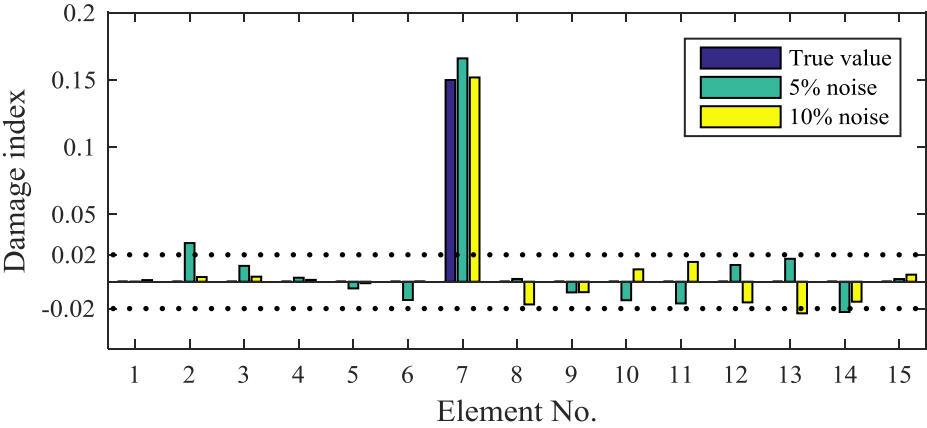
where E_p is the percentage noise level, N_{noise} is a standard normal distribution vector with zero mean and unit standard deviation, and $\sigma(\ddot{\mathbf{x}})$ is the standard deviation of the actual acceleration response. The 5 s response data are used in the damage identification. The error of the identified stiffness parameter is calculated from

$$\text{error} = \frac{\|\boldsymbol{\theta}_{identify} - \boldsymbol{\theta}_{true}\|}{\|\boldsymbol{\theta}_{true}\|} \times 100\% \quad (3.39)$$

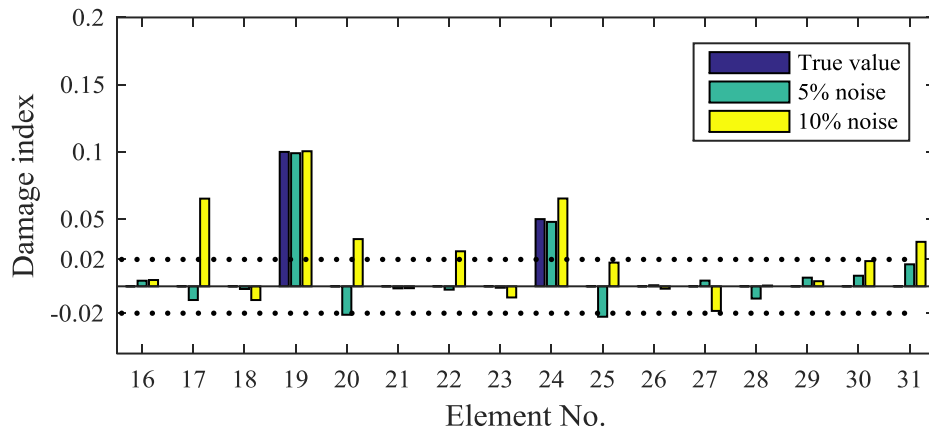
With the same procedures as described in the last section, the identified damage indices of each subset of parameters under different noise levels are shown in Figure 3.8. The damage location and severity are accurately identified. However, some undamaged elements are falsely identified. In the case of 5% noise, most of the errors are less than 2% and the maximum identification error is 3.72% at Element 34. In the case of 10% noise, several elements have relatively large errors. For example, 9.93% at Element 33, 6.52% at Element 17, and 5.56% at Element 36. The other identified errors are less than 5%. In the high noise environment, the proposed method may fail to detect some damaged elements. The errors of identification results at two noise levels are shown in Table 3.1. The error in the 1st zone with 5% noise in the responses is larger than that with 10% noise. The reason is unknown, probably due to the large randomness in the artificially generated noise in the responses.

The identified input force of zone 1 is shown in Figure 3.9, as compare with the true value. The accuracy of the identified force decreases with increasing noise level in the response as shown in Figures 3.9 (a) and (b). In each iteration, the unknown input

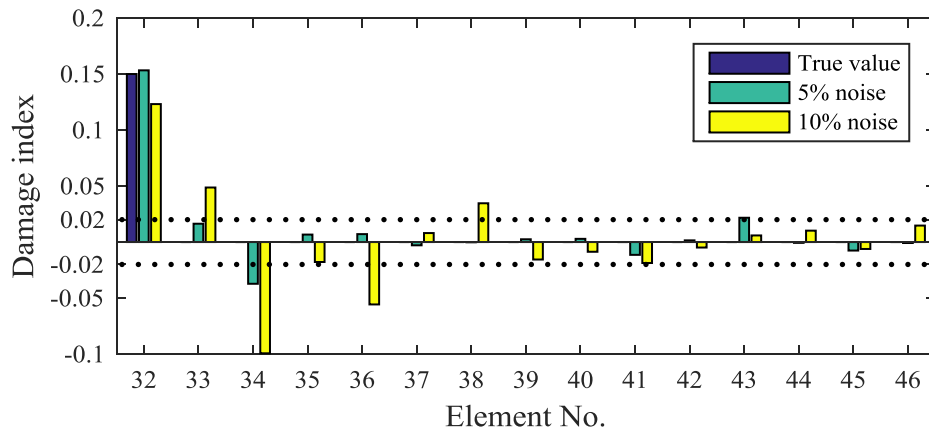
excitations are identified in the first stage and the subset unknown structural parameters are updated in the second stage. The errors of the force identification may affect the results of the unknown structural parameters. As shown in Figure 3.9, the identification force can be separated into a dynamic part and static part (linear trend). In the second stage of damage detection, the structure is subjected to the white noise as well as the identified low-frequency excitation. The static loading part changes very slowly and does not affect the dynamic acceleration responses. Therefore, the predicted responses match well with the measured dynamic responses. The other probable reason is that there are $4 \times 1000 \times 3$ data (four sensors for measurement and 5s of response data is used for the identification in each zone) used for the identification of the 46 unknown parameters and only 4×1000 data used for the identification of 5×200 unknown force values for one excitation in each subset study.



(a) Subset 1



(b) Subset 2

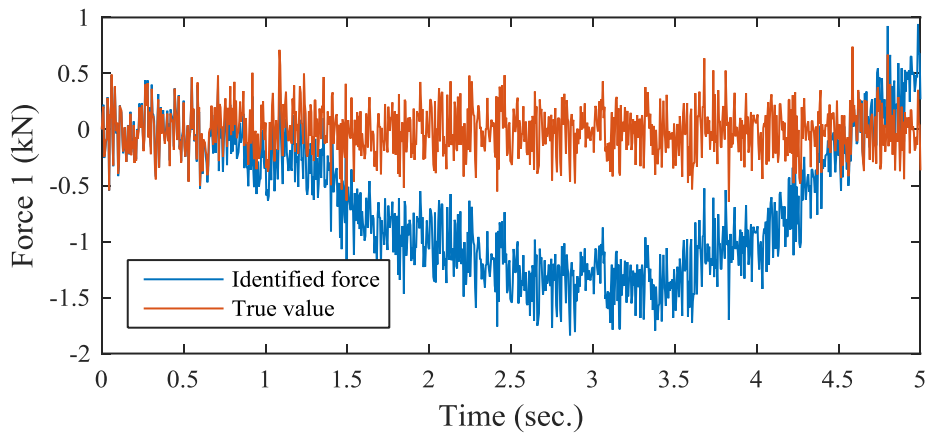


(c) Subset 3

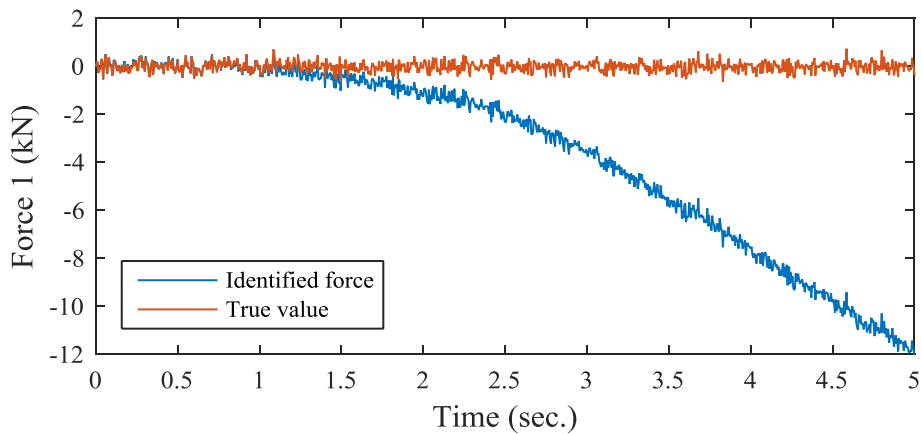
Figure 3.8 Identified stiffness reduction factor

Table 3.1 The identification error (%)

Noise level	The 1 th subset	The 2 nd subset	The 3 rd subset
5%	1.41	1.00	1.29
10%	1.08	2.35	3.57



(a) Comparison of the identified input force with 5% measurement noise



(b) Comparison of the identified input force with 10% measurement noise

Figure 3.9 Comparison of the identified input force with measurement noise

3.4.3 Damage detection with unknown damping ratios

The accuracy of the proposed method has been proved in Sections 3.4.1 and 3.4.2. However, the damping coefficients have been assumed to be known. In this section, the damping ratios are assumed to be unknown and the 5% of measurement noise is

considered. Prior to damage detection, experimental modal testing is performed to obtain the modal properties of the structure. An impulse excitation with an amplitude of 300N and duration of 0.1s is applied at Node 10 of the above structure in the vertical direction. The first 60s responses at Node 11 in the vertical direction are collected. The Fourier transform of the responses is shown in Figure 3.10. The first three modes fall in the respective frequency ranges of 0.5 ~ 1 Hz, 2.2~2.6 Hz, and 3.2 ~3.7 Hz. The band-pass filters are then applied sequentially to the measured response to obtain three separate time histories each with one dominating frequency. The Logarithmic decrement method (Inman, 2008) is adopted to identify the damping ratios. The Logarithmic decrement δ is obtained from the natural logarithm of the ratio of the amplitudes of any two successive peaks.

$$\delta_i = \frac{1}{n} \ln \frac{\ddot{y}_i^*(t)}{\ddot{y}_i^*(t+\Delta T)} \quad (3.40)$$

where $\ddot{y}_i^*(t)$ is the amplitude at time t and $\ddot{y}_i^*(t+\Delta T)$ is the amplitude of the peak Δ periods away, and Δ is an integer number of successive, positive peaks.

The damping ratio is then calculated from the logarithmic decrement as:

$$\xi_i = \frac{1}{\sqrt{1 + \left(\frac{2\pi}{\delta_i}\right)^2}} \approx \frac{\delta_i}{2\pi} \quad (3.41)$$

The damping coefficients can be determined from the following:

$$a_1 = \frac{2\omega_i\omega_j}{\omega_j^2 - \omega_i^2} (\omega_j\xi_i - \omega_i\xi_j) \quad (3.42)$$

$$a_2 = \frac{2}{\omega_j^2 - \omega_i^2} (\omega_j\xi_j - \omega_i\xi_i) \quad (3.43)$$

where ζ_i and ζ_j correspond to two circular frequencies ω_i and ω_j , respectively. Usually, the damping coefficients can be obtained by using the first two damping ratios. The final identified damping ratios and damping coefficients of the structure are listed in Table 3.2. It should be noted that the first two damping ratios are the same as the true values. Damage detection is then subsequently performed, and the final identified damage indices are shown in Figure 3.11. The identified values are almost matching with the true ones but with a maximum error of 6% at Element 29. These results show that the proposed method can identify the structural damage when the damping ratio is unknown.

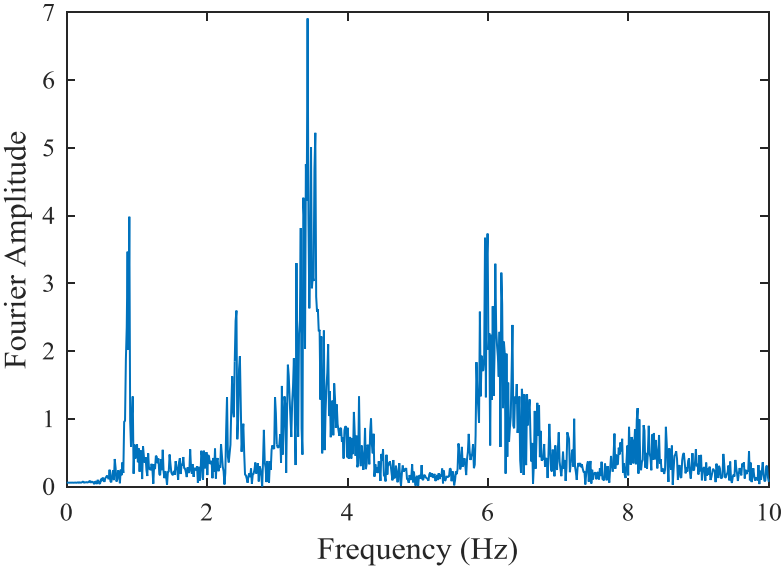


Figure 3.10 Fourier transform of the vertical acceleration of Node 10

Table 3.2 The identified modal frequencies and damping ratios

Frequency (Hz)	1 st	2 nd	3 rd
	0.87	2.45	3.44
Damping ratio	1 st	2 nd	3 rd
	1.00%	1.00%	1.22%
Damping coefficient	a_1	a_2	
True value	0.0807	9.5876×10^{-4}	
Identified value	0.0697	8.4899×10^{-4}	

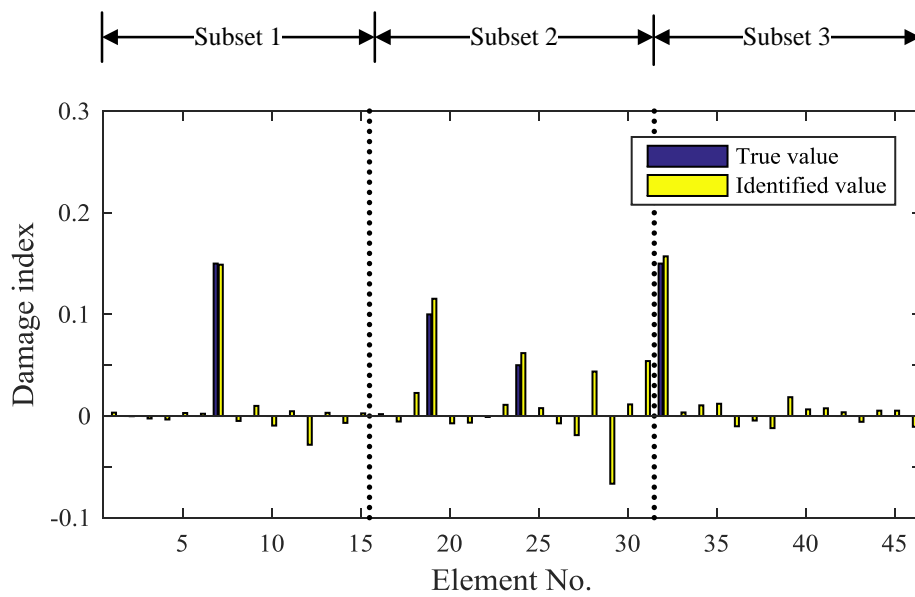


Figure 3.11 The identified results with unknown damping ratios

3.4.4 Modelling error effect and computation effort

Model errors due to the uncertainty of material parameters widely exist in civil structures. A numerical model can be built according to the geometric and material

information of the physic structure. However, due to the uncertainty of material parameters, the numerical model is not accurate for structural damage detection. A more accurate finite element model should be updated using the vibration responses in the undamaged stage. The finite element model updating with the proposed decentralized method is studied in this section. The effect of the random modelling error is investigated with a normal random distributed error with 5% coefficient of variation included in the initial value of the modulus of material of the structure. The coefficients of damping are known. They are identified using the logarithmic decrement method. Figures 3.12 and 3.13 present the identified results without measurement noise and with 10% measurement noise, respectively. The result obtained from the no measurement noise case has a good accuracy with the actual value, which can verify the accuracy of the proposed method again. The results of the case with 10% measurement noise is a little bit larger but satisfactory due to the combined effect of the modelling error and measurement noise. These results are similar to that in damage detection cases (Sections 3.4.1 and 3.4.2).

Table 3.3 compares the computational time required for model updating with and without using parallel computing. The table shows that using the parallel computing improves the computational efficiency. Nominally, the computational time in using the parallel computing should be 60% less than without using parallel computing. It is, however, only 56% less for the noise free case as shown in Table 3.3, and only 38% ~ 40% less for the noisy cases. When there is no noise in the measured response, only the 2.5 s responses are used for damage detection. In the noisy cases, the 5 s responses are used for model updating, which requires longer time for the housekeeping work of

reading and writing data. Therefore, the improvement in the efficiency of model updating with long duration of measurement data is less than that with short duration of measurement data.

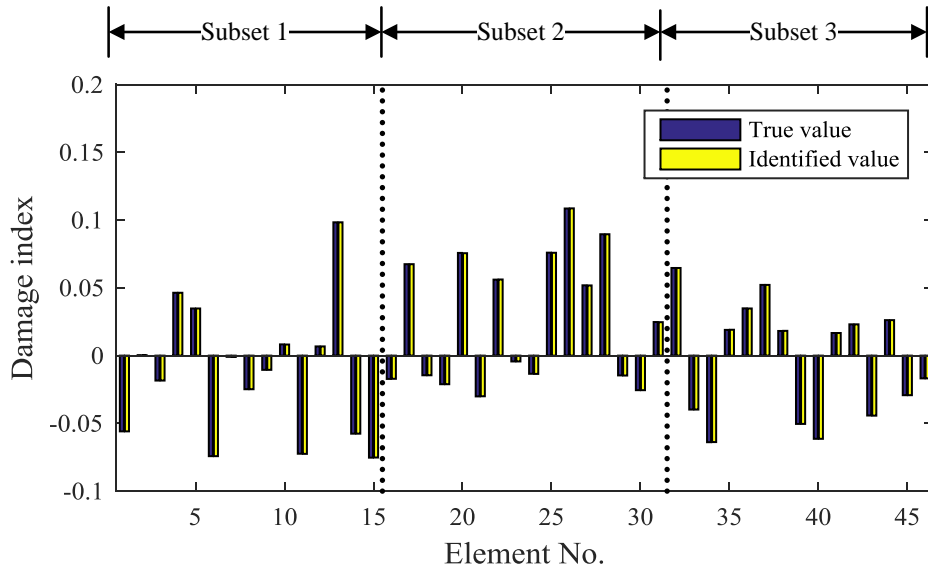


Figure 3.12 Identified result including model error and without measurement noise

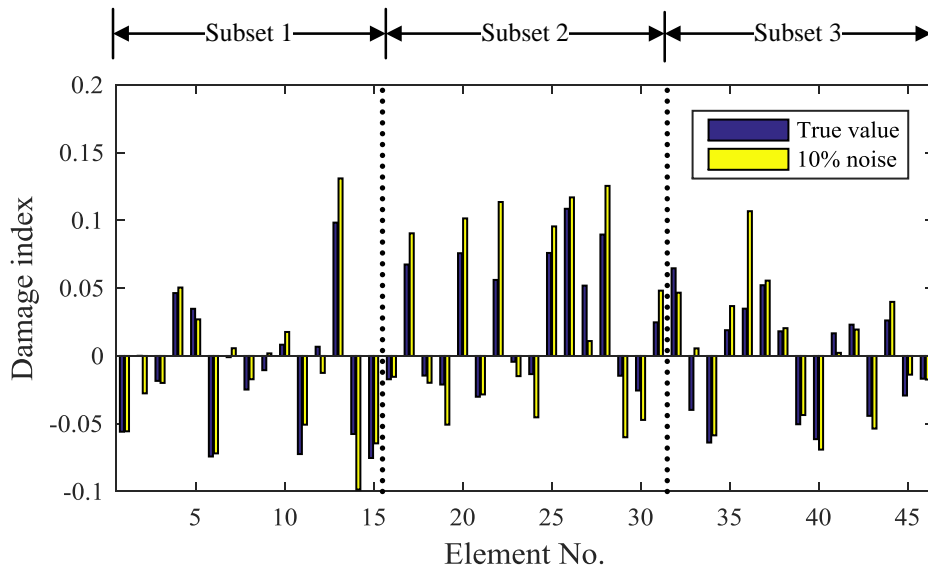


Figure 3.13 Identified result including model error and measurement noise

Table 3.3 Computational time in model updating

	CPU Time (hours)		
	Noise free	5% noise	10% noise
Number of iterations	483	350	247
Without using Parallel Computing Toolbox	0.81	2.1	1.5
With the use of Parallel Computing Toolbox	0.35	1.3	0.9
Percentage improvement	56.8%	38.1%	40.0%

3.5 Summary

A decentralized damage detection method for large-scale structures is proposed in this chapter. The structure is divided into several smaller zones and each zone is tested in sequence. The external excitations in each zone are identified in the wavelet domain, and the unknown structural parameters are updated by using the Newton-SOR method in the time domain. The external excitations and the structural parameters are updated iteratively with the parallel computing technology included in the model updating of the structure. Numerical studies on a planar frame structure indicate that the method is effective for damage detection with few sensors and even with 10% noise in the measurement data. An approximately 37% improvement is achieved in the required computational time when parallel computing is used.

CHAPTER 4

DECENTRALIZED DAMAGE DETECTION OF NONLINEAR STRUCTURES USING OUTPUT MEASUREMENT ONLY

4.1 Introduction

In Chapter 3, an output-only decentralized method was proposed for structural damage detection. The output responses are represented by convolution integral of impulse response function and input force in the wavelet domain. The unknown excitation force can then be identified based on the linear relationship of the input force and output responses. However, the proposed force identification method can only be used for the linear systems. In this chapter, structural damage detection under seismic loading is studied, in which the nonlinear behaviour of structure is represented by a mass-spring-damper models (shear-building model). The hysteretic behaviors due to stiffness

degradation are simulated with Duffing model (Worden and Hensman, 2012; Yang *et al.*, 2014).

Extended and unscented Kalman filter based methods are promising for nonlinear system identification and have been intensively studied (Yang *et al.*, 2006b; Wu and Smyth, 2007a; Lei *et al.*, 2012b; Xie and Feng, 2012). In the extended Kalman filter technique, both unknown structural parameters, velocity, and displacement are included in the extended state vector and a large number of unknowns may cause the state space equation unstable. Therefore, the method is usually applied to identification of small-scale structures with several unknown parameters. To improve the decentralized damage detection method for nonlinear structure, the Kalman filter technique is used to identify the unknown ground motion.

In this chapter, the Kalman filter technique is used for the state estimation only, and the unknown input forces are identified from the state vector with the optimization method. Since the unknown structural parameters are not included in the state vector, the dimension of the state vector is not large and the force identification can then be achieved even for large-scale structures. Structural parameters of the whole structure are divided into several subsets and then updated by using the Newton-SOR method, similarly to the approach in the last chapter. Both the external excitations and structural parameters are iteratively updated until a defined convergence criterion is satisfied.

4.2 Theoretical Development

4.2.1 Equation of motion

The equation of motion of a structure under the external excitation can be written as

$$\mathbf{M}\ddot{\mathbf{x}}(t) + \mathbf{F}_c(\dot{\mathbf{x}}(t)) + \mathbf{F}_s(\mathbf{x}(t), \boldsymbol{\theta}) = \mathbf{B}\mathbf{f}(t) \quad (4.1)$$

where \mathbf{M} is the $n \times n$ mass matrix; \mathbf{x} , $\dot{\mathbf{x}}$, and $\ddot{\mathbf{x}}$ are the displacement, velocity and acceleration vectors, respectively; $\mathbf{F}_c(\dot{\mathbf{x}}(t))$, $\mathbf{F}_s(\dot{\mathbf{x}}(t), \boldsymbol{\theta})$, and $\mathbf{f}(t)$ are the dissipating force vector, the stiffness force vector and the excitation force vector, respectively; \mathbf{B} is the mapping matrix relating with the location of the applied forces, and $\boldsymbol{\theta} = [\alpha_1, \alpha_2, \dots, \alpha_{ne}]$ is the unknown parameter vector of the structure with the number of elements as ne . It should be noted that the structural system could be linear or nonlinear, depending on the definition of the dissipating and stiffness force vectors.

The state vector is defined as

$$\mathbf{X}(t) = \begin{bmatrix} \mathbf{x}(t) \\ \dot{\mathbf{x}}(t) \end{bmatrix} \quad (4.2)$$

Transforming the equation of motion in Eq. (4.1) as a state equation, we have

$$\dot{\mathbf{X}}(t) = \mathbf{J}(\mathbf{X}(t), \boldsymbol{\theta}, \mathbf{f}(t)) = \begin{pmatrix} \dot{\mathbf{x}}(t) \\ \mathbf{M}^{-1}(\mathbf{B}\mathbf{f}(t) - \mathbf{F}_c(\dot{\mathbf{x}}(t)) - \mathbf{F}_s(\mathbf{x}(t), \boldsymbol{\theta})) \end{pmatrix} \quad (4.3)$$

Usually, only a limited number of accelerometers are deployed on structures to measure the vibrational acceleration responses. The measurement vector can be written as

$$\begin{aligned} \mathbf{Y}(t) &= \mathbf{d}\ddot{\mathbf{x}}(t) + \mathbf{v}(t) \\ &= \mathbf{D}\mathbf{f}(t) - \mathbf{d}\mathbf{M}^{-1}(\mathbf{F}_c(\dot{\mathbf{x}}(t)) + \mathbf{F}_s(\mathbf{x}(t), \boldsymbol{\theta})) + \mathbf{v}(t) \end{aligned} \quad (4.4)$$

where $\mathbf{D} = \mathbf{d}\mathbf{M}^{-1}\mathbf{B}$, \mathbf{d} is associated with the locations of accelerometers and $\mathbf{v}(t)$ is the measurement noise vector assumed to be a Gaussian white noise vector with zero mean and a covariance matrix $E(\mathbf{v}_i\mathbf{v}_j^T) = \mathbf{R}_{ij}\delta_{ij}$, in which δ_{ij} is the Kroneker delta and \mathbf{R}_{ij} is the variance matrix of the measurement noises.

Eq. (4.4) can be further expressed in the discrete form as (Yang *et al.*, 2006b; Yang *et al.*, 2007a)

$$\mathbf{Y}_k = \mathbf{h}(\mathbf{X}_k, \boldsymbol{\theta}) + \mathbf{D}\mathbf{f}_k + \mathbf{v}_k \quad (4.5)$$

where $\mathbf{h}(\mathbf{X}_k, \boldsymbol{\theta}) = -\mathbf{d}\mathbf{M}^{-1}(\mathbf{F}_c(\dot{\mathbf{x}}_k) + \mathbf{F}_s(\mathbf{x}_k, \boldsymbol{\theta}))$ with $\dot{\mathbf{x}}_k$ and \mathbf{x}_k representing the corresponding discrete values of $\dot{\mathbf{x}}(t)$ and $\mathbf{x}(t)$ at the time instant $t = k\Delta t$, \mathbf{Y}_k is the l -dimensional observation (measured) vector at $t = k\Delta t$ (Δt is the time step), and \mathbf{X}_k , \mathbf{f}_k , and \mathbf{v}_k are the corresponding discrete values at time instant $t = k\Delta t$.

4.2.2 Force identification based on Kalman filter technique

The state vector will be estimated first by using the classic Kalman estimator (Lei *et al.*, 2012b), and the unknown excitations are identified by the least squares estimation. Based on the classic Kalman estimator, the state vector at time $t = (k+1)\Delta t$ can be estimated as follows

$$\hat{\mathbf{X}}_{k+1} = \tilde{\mathbf{X}}_{k+1} + \mathbf{K}_k^e \left\{ \mathbf{Y}_k - \mathbf{h}(\hat{\mathbf{X}}_k, \boldsymbol{\theta}) - \mathbf{D}\hat{\mathbf{f}}_k \right\} \quad (4.6)$$

and

$$\tilde{\mathbf{X}}_{k+1} = \hat{\mathbf{X}}_k + \int_{k\Delta t}^{(k+1)\Delta t} \mathbf{J}(\hat{\mathbf{X}}_k, \boldsymbol{\theta}, \hat{\mathbf{f}}_k) dt \quad (4.7)$$

where $\hat{\mathbf{X}}_{k+1}$, $\tilde{\mathbf{X}}_{k+1}$, $\hat{\mathbf{f}}_k$ are the estimation of \mathbf{X}_{k+1} , the state prediction of \mathbf{X}_{k+1} and the estimation of \mathbf{f}_k , respectively. \mathbf{K}_k^e is the Kalman gain matrix at time instant $t = k\Delta t$, given by

$$\mathbf{K}_k^e = \boldsymbol{\Phi}_k \mathbf{P}_k \mathbf{H}_k^T (\mathbf{H}_k \mathbf{P}_k \mathbf{H}_k^T + \mathbf{R})^{-1} \quad (4.8)$$

where

$$\boldsymbol{\Phi}_k = \mathbf{I} + \mathbf{A}_k \Delta t \quad (4.9)$$

$$\mathbf{A}_k = \frac{\partial \mathbf{J}(\hat{\mathbf{X}}_k, \boldsymbol{\theta}, \hat{\mathbf{f}}_k)}{\partial \hat{\mathbf{X}}_k} \quad (4.10)$$

$$\mathbf{H}_k = \frac{\partial \mathbf{h}(\hat{\mathbf{X}}_k, \boldsymbol{\theta})}{\partial \hat{\mathbf{X}}_k} \quad (4.11)$$

and \mathbf{P}_k is the error covariance matrix of $\hat{\mathbf{X}}_k$, which can be obtained in a recursive formula as (Lei *et al.*, 2012b)

$$\mathbf{P}_k = \boldsymbol{\Phi}_{k-1} \mathbf{P}_{k-1} \boldsymbol{\Phi}_{k-1}^T - \mathbf{K}_k^e \mathbf{H}_k \mathbf{P}_{k-1} \boldsymbol{\Phi}_{k-1} \quad (4.12)$$

When the measurements are available at the DOFs where the external excitations are applied, \mathbf{D} in Eq. (4.4) is a non-zero matrix. The unknown external excitations $\hat{\mathbf{f}}_{k+1}$ can then be identified from Eq. (4.5) by using the least square method through the following equation

$$\hat{\mathbf{f}}_{k+1} = (\mathbf{D}^T \mathbf{D})^{-1} \mathbf{D}^T \{ \mathbf{Y}_{k+1} - \mathbf{h}(\hat{\mathbf{X}}_{k+1}, \boldsymbol{\theta}) \} \quad (4.13)$$

4.2.3 Damage detection from subset responses

A large number of unknowns in a large structure can be divided into several smaller zones based on its finite element mesh configuration. Accordingly, the unknown system parameter vector θ can be separated as several system parameter subsets $[\theta_1, \theta_2, \dots, \theta_r]$, where θ_i contains all the unknown damage indices of the i -th ($1 \leq i \leq r$) zone. In this chapter, the accelerometers are fixed in a structure, rather than roving different zones. When an earthquake event happens, the vibration data can be recorded. The measured acceleration response vector from the sensors in the i -th zone is defined as $\ddot{\mathbf{x}}_{mea,i}$. The responses measured at each zone can be written as a separate function of the structural parameters and excitations as

$$\begin{aligned}
 \mathbf{g}_1(\theta_1, \theta_2, \dots, \theta_r, \mathbf{f}) - \ddot{\mathbf{x}}_{mea,1} &= 0 \\
 \mathbf{g}_2(\theta_1, \theta_2, \dots, \theta_r, \mathbf{f}) - \ddot{\mathbf{x}}_{mea,2} &= 0 \\
 \vdots & \\
 \mathbf{g}_i(\theta_1, \theta_2, \dots, \theta_r, \mathbf{f}) - \ddot{\mathbf{x}}_{mea,i} &= 0 \\
 \vdots & \\
 \mathbf{g}_r(\theta_1, \theta_2, \dots, \theta_r, \mathbf{f}) - \ddot{\mathbf{x}}_{mea,r} &= 0
 \end{aligned} \tag{4.14}$$

It is noteworthy that all responses are under the same ground motion. After the unknown ground motion is identified in the first stage with Eqs. (4.6) ~ (4.13), the unknown structural parameters can be then updated. The structural parameter identification problem is to find out the solution from Eq.(4.14), which can be assembled as Eq. (4.15)

$$\mathbf{G}(\theta) = 0 \tag{4.15}$$

By using Newton method (Ortega and Rheinboldt, 1970), we have

$$\mathbf{G}(\boldsymbol{\theta}) = \mathbf{G}(\boldsymbol{\theta}^n) + \mathbf{G}'(\boldsymbol{\theta}^n)(\boldsymbol{\theta}^{n+1} - \boldsymbol{\theta}^n) = 0 \quad (4.16)$$

$$\mathbf{G}'(\boldsymbol{\theta}^n)\boldsymbol{\theta}^{n+1} = \mathbf{G}'(\boldsymbol{\theta}^n)\boldsymbol{\theta}^n - \mathbf{G}(\boldsymbol{\theta}^n) \quad (4.17)$$

$$\boldsymbol{\theta}^{n+1} = \boldsymbol{\theta}^n - [\mathbf{G}'(\boldsymbol{\theta}^n)]^{-1} \mathbf{G}(\boldsymbol{\theta}^n) \quad (4.18)$$

where $\mathbf{G}'(\boldsymbol{\theta}^n)$ is the Jacobin matrix of $\mathbf{G}(\boldsymbol{\theta}^n)$ and can be calculated from Eq. (4.19).

$$\mathbf{G}'(\boldsymbol{\theta}^n) = \begin{bmatrix} \frac{\partial \mathbf{g}_1}{\partial \theta_1} & \frac{\partial \mathbf{g}_1}{\partial \theta_2} & \dots & \frac{\partial \mathbf{g}_1}{\partial \theta_r} \\ \frac{\partial \mathbf{g}_2}{\partial \theta_1} & \frac{\partial \mathbf{g}_2}{\partial \theta_2} & \dots & \frac{\partial \mathbf{g}_2}{\partial \theta_r} \\ \vdots & \vdots & & \vdots \\ \frac{\partial \mathbf{g}_r}{\partial \theta_1} & \frac{\partial \mathbf{g}_r}{\partial \theta_2} & \dots & \frac{\partial \mathbf{g}_r}{\partial \theta_r} \end{bmatrix} \quad (4.19)$$

Following the derivation discussed in Section 3.3.3, the iterative SOR method is embedded in Eq. (7.25). Considering the solution from *One-step* Newton-SOR method, the unknown structural parameters can be updated with

$$\begin{bmatrix} \boldsymbol{\theta}_1^{n+1} \\ \boldsymbol{\theta}_2^{n+1} \\ \vdots \\ \boldsymbol{\theta}_r^{n+1} \end{bmatrix} = \begin{bmatrix} \boldsymbol{\theta}_1^n \\ \boldsymbol{\theta}_2^n \\ \vdots \\ \boldsymbol{\theta}_r^n \end{bmatrix} - \begin{bmatrix} \frac{\partial \mathbf{g}_1}{\partial \theta_1^n} & 0 & 0 & 0 \\ 0 & \frac{\partial \mathbf{g}_2}{\partial \theta_2^n} & 0 & 0 \\ 0 & 0 & \ddots & 0 \\ 0 & 0 & 0 & \frac{\partial \mathbf{g}_r}{\partial \theta_r^n} \end{bmatrix}^{-1} \begin{bmatrix} \mathbf{g}_1(\boldsymbol{\theta}^n, \mathbf{f}) - \ddot{\mathbf{x}}_{mea,1} \\ \mathbf{g}_2(\boldsymbol{\theta}^n, \mathbf{f}) - \ddot{\mathbf{x}}_{mea,2} \\ \vdots \\ \mathbf{g}_r(\boldsymbol{\theta}^n, \mathbf{f}) - \ddot{\mathbf{x}}_{mea,r} \end{bmatrix} \quad (4.20)$$

or

$$\boldsymbol{\theta}_i^{n+1} = \boldsymbol{\theta}_i^n - \left[\frac{\partial \mathbf{g}_i}{\partial \theta_i^n} \right]^{-1} \left[\mathbf{g}_i(\boldsymbol{\theta}^n, \mathbf{f}) - \ddot{\mathbf{x}}_{mea,i} \right], \quad (i = 1, 2, \dots, r) \quad (4.21)$$

Tikhonov regularization technique (Tikhonov *et al.*, 1995) is applied to solve Eq. (7.27) and the solution is obtained as

$$\boldsymbol{\theta}_i^{n+1} = \boldsymbol{\theta}_i^n - \left[\begin{pmatrix} \frac{\partial \mathbf{g}_i}{\partial \boldsymbol{\theta}_i^n} \end{pmatrix}^T \begin{pmatrix} \frac{\partial \mathbf{g}_i}{\partial \boldsymbol{\theta}_i^n} \end{pmatrix} + \lambda_i \right]^{-1} \begin{pmatrix} \frac{\partial \mathbf{g}_i}{\partial \boldsymbol{\theta}_i^n} \end{pmatrix}^T [\mathbf{g}_i(\boldsymbol{\theta}^n, \mathbf{f}) - \ddot{\mathbf{x}}_{mea,i}], \quad (i=1, 2, \dots, r) \quad (4.22)$$

After each subset parameters $\boldsymbol{\theta}_i^{n+1}$ is solved from Eq. (7.28), the global structural parameters are obtained and the sensitivity matrix $\mathbf{G}'(\boldsymbol{\theta}^{n+1})$ is re-calculated. The analytical responses and sensitivities in each iteration are obtained based on the global structure. Although the proposed approach is conducted by formulating the global optimization as a set of optimization problems for several smaller zones, the convergence can be achieved by using the iterative identification scheme (Ortega and Rheinboldt, 1970), as demonstrated in the examples described in Section 4.3.

4.2.4 Computational procedure of the proposed approach

The proposed approach can be applicable for both linear and nonlinear structural identification. The procedures are summarized as follows:

Step 1: Divide the structure into smaller zones according to its finite element mesh configuration. The measured vibration responses are also divided into several subsets according to sensor locations.

Step 2: Define the initial value of parameters as $\boldsymbol{\theta}^0 = [\boldsymbol{\theta}_1^0, \boldsymbol{\theta}_2^0, \dots, \boldsymbol{\theta}_r^0]$ based on the baseline model.

Step 3: Identify the unknown excitation force from Eqs. (4.6) ~ (4.13) with the measured vibration data of the whole structure.

Step 4: Calculate responses of the whole structure from Eq. (4.1) for each test in a specific zone. The sensitivity of responses with respect to the structural parameters of each zone $\partial \mathbf{g}_i / \partial \boldsymbol{\theta}_i^{n+1}$ are obtained by using forward difference method or Newmark- β method (Law *et al.*, 2014).

Step 5: The parameters of each zone $\boldsymbol{\theta}_i^{n+1}$ are updated by using Eq. (7.28). The finite element model of the global structure is then assembled as $\boldsymbol{\theta}^{n+1} = [\boldsymbol{\theta}_1^{n+1}, \boldsymbol{\theta}_2^{n+1}, \dots, \boldsymbol{\theta}_r^{n+1}]$.

Step 6: Repeat Steps 3–5 until the convergence criterion in Eq. (4.23) is satisfied.

$$\frac{\|\boldsymbol{\theta}^{n+1} - \boldsymbol{\theta}^n\|}{\|\boldsymbol{\theta}^{n+1}\|} \times 100\% \leq Tol \quad (4.23)$$

where Tol is the defined tolerance value, and will be given in the following numerical and experimental studies.

It should be noted that like many output only damage detection methods (Koh *et al.*, 2003; Yang and Huang, 2007; Lei *et al.*, 2012b; Lei *et al.*, 2013), the proposed approach requires that: a) the number of measured responses is larger than that of the unknown excitations; and b) the responses at the locations of the applied excitations shall be available. These two conditions can be satisfied for engineering applications, for example, when performing damage detection for the civil structure under earthquake loading, the locations of the unknown ground motions is usually known and the number of placed sensors shall be larger than the number of a few excitation forces.

4.3 Numerical Studies

To validate the effectiveness and accuracy of the proposed approach for system identification of linear and nonlinear structures, numerical studies on a nonlinear multi-story shear frame and a planar steel truss are conducted. Only measured responses are used for the identification of the ground motion and structural parameters.

4.3.1 Model updating of a 6-DOFs nonlinear structure

Considering a six-storey nonlinear elastic Duffing-type shear building subjected to a ground motion acceleration $\ddot{x}_g(t)$, the system equation of motion is given by (Yang *et al.*, 2006b; Yang *et al.*, 2007a)

$$m_i \left(\sum_{j=1}^i \ddot{x}_j(t) \right) + c_i \dot{x}_i(t) - c_{i+1} \dot{x}_{i+1}(t) + k_i x_i(t) - k_{i+1} x_{i+1}(t) + K_i x_i^3(t) - K_{i+1} x_{i+1}^3(t) = m_i \ddot{x}_g(t) \quad (i=1 \sim 5) \quad (4.24)$$

$$m_i \left(\sum_{j=1}^i \ddot{x}_j(t) \right) + c_i \dot{x}_i(t) + k_i x_i(t) + K_i x_i^3(t) = m_i \ddot{x}_g(t), \quad (i=6) \quad (4.25)$$

where x_i is the inter-storey drift displacement between the i -th and $(i+1)$ -th stories ($i=1 \sim 5$), $m_1 = m_2 = \dots = m_6 = 600\text{kg}$, $c_1 = c_2 = \dots = c_6 = 1\text{kNs/m}$, $k_1 = k_2 = \dots = k_5 = 1.2 \times 10^5\text{N/m}$, $k_6 = 0.6 \times 10^5\text{N/m}$, $K_1 = K_2 = \dots = K_5 = 2 \times 10^8\text{N/m}^3$, and $K_6 = 10^8\text{N/m}^3$. The ground motion is simulated based on a similar procedure in a previous study (Xu *et al.*, 2009) and generated as a white noise acceleration history, which is then scaled to a maximum peak ground acceleration (PGA) of 0.3g and is filtered with a cutting frequency 20Hz. For

the elastic structure with no nonlinear terms, that is $K_1 = K_2 = \dots = K_6 = 0$, and the first three natural frequencies are $\omega_1=0.538$ Hz, $\omega_2=1.473$ Hz and $\omega_3=2.251$ Hz.

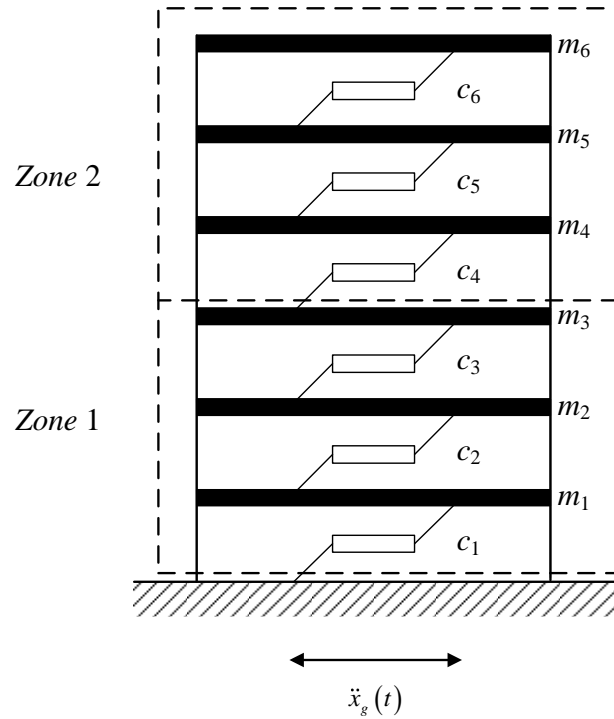


Figure 4.1 The nonlinear shear building model

Sensors are installed at each floor to measure the accelerations with a sampling frequency of 2000 Hz. In this example, the masses (m_1, m_2, \dots, m_6), damping (c_1, c_2, \dots, c_6) and stiffness (k_1, k_2, \dots, k_6) are assumed known. The parameters of the nonlinear Duffing model (K_1, K_2, \dots, K_6) and the input ground motion $\ddot{x}_g(t)$ are unknowns to be identified. Based on the proposed approach, the Kalman filter technique is used to identify the excitation force, and the system parameters are updated with the Newton-SOR method. The shear building structure is divided into two zones, namely, a lower level structure and an upper-level structure, as shown in Figure 4.1. The first zone

consists of three unknown parameters. i.e. $\theta_1=[K_1, K_2, K_3]$ and the second zone $\theta_2=[K_4, K_5, K_6]$. Each zone has three accelerometers to measure the vibration responses. The response data collected in the first one second are used for the identification. The convergence criterion in Eq. (4.23) is set to 10^{-6} for the case without noise and 10^{-3} for the case with noise. The initial value of unknown parameters are defined as $K_1=K_2=\dots=K_5=2.4 \times 10^8 \text{ N/m}^3$, and $K_6 = 1.2 \times 10^8 \text{ N/m}^3$. The purpose of this example is to verify accuracy of the proposed method for the identification of the unknown parameters in the nonlinear restoring force model. Therefore, the stiffness, mass and damping values are all given.

Firstly, the unpolluted acceleration responses are used to verify the accuracy of the proposed approach for the identification of nonlinear system parameters. Figure 4.2 shows the identified system parameters with iterations. The identified ground motion as shown in Figure 4.3 matches well with the true ground motion. The relative error of the ground motion identification is 0.115%. These results show that the proposed approach can identify the system parameters and unknown ground motion simultaneously with a very good accuracy.

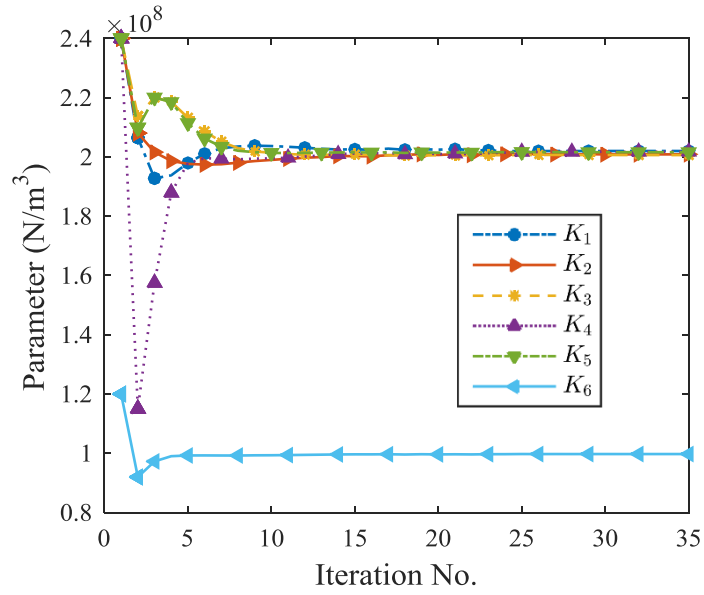


Figure 4.2 Identified system parameters with iterations

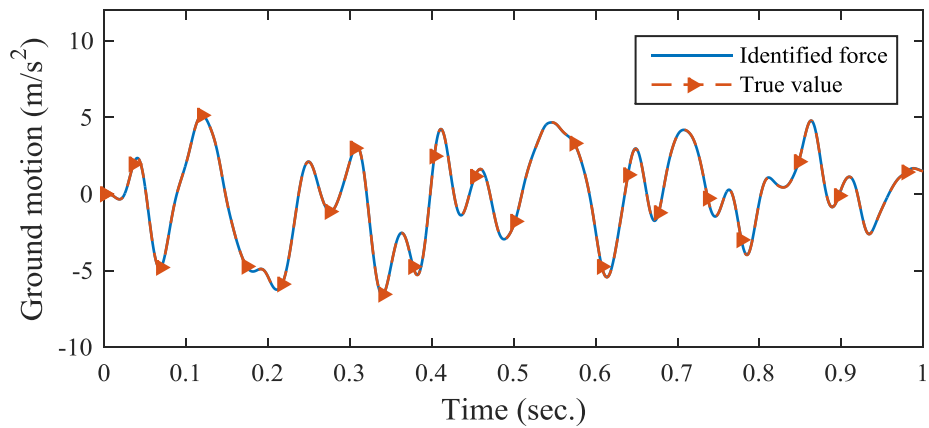


Figure 4.3 Identified ground motion using noise-free responses

To study the noise effect on the identification accuracy, the noisy response is simulated by adding a random white noise to the actual response as

$$\ddot{\mathbf{x}}_{mea} = \ddot{\mathbf{x}} + E_p N_{noise} \sigma(\ddot{\mathbf{x}}) \quad (4.26)$$

where E_p is percentage of the noise level, N_{noise} is a standard normal distribution vector with zero mean and unit standard deviation, and $\sigma(\ddot{x})$ is the standard deviation of the actual acceleration response. 5% and 10% noise levels are considered in this study. The 4th-order Butterworth band-pass filter of a frequency range 0.1~100 Hz is used to pre-process the signals and remove the high frequency noise.

The identified nonlinear system parameters using noisy measurement data are shown in Figure 4.4. The maximum identified error for 5% noise case is 4.25% at the floor 6, while the maximum identified error for 10% noise case is 5.63% at the floor 3. The other identification errors are small. The comparison between the identified and true ground motions is shown in Figure 4.5. The relative errors are 1.45% and 3.49% for the 5% and 10% noise cases, respectively. These results demonstrate that the proposed approach can well identify the nonlinear system parameters and the excitation force even under a significant measurement noise.

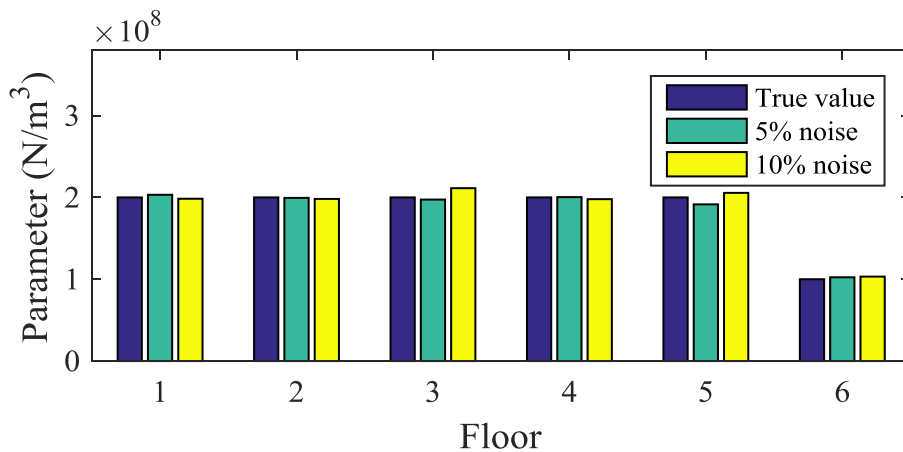


Figure 4.4 Identified system parameters with noise effect

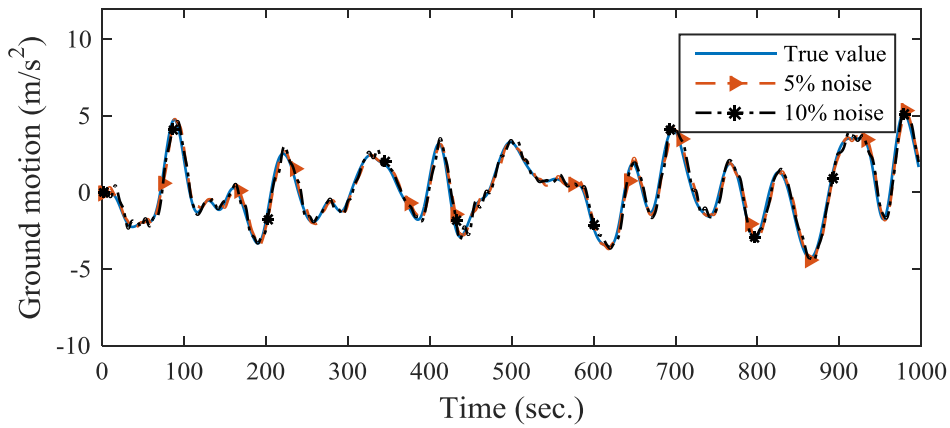
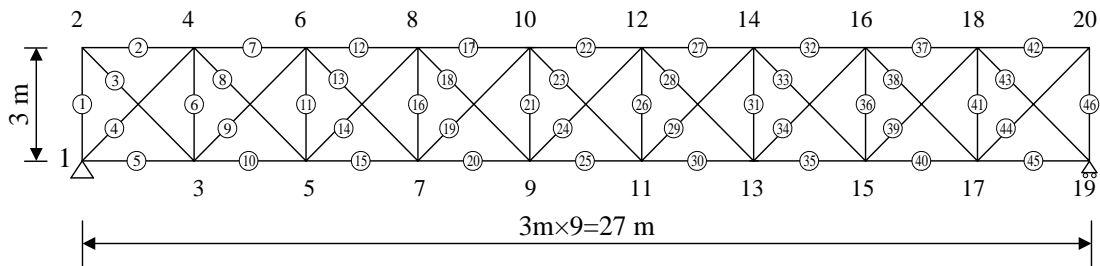


Figure 4.5 Identified ground motion with noise effect

4.3.2 Damage detection of a linear plane truss structure

A simply-supported plane truss structure used in Chapter 3 is selected for conducting a comparison study. The dimensions are shown in Figure 4.6. The structure is modeled with forty-six planar truss finite elements. The cross-sectional area of the bar is 0.0016 m^2 . Rayleigh damping with $\zeta_1=0.01$ and $\zeta_2=0.01$ is assumed as the damping ratios of the first two modes. The mass density is $7.8 \times 10^3 \text{ kg/m}^3$, and the elastic modulus is 206 GPa. The truss is pin-supported at Node 1 and roller-supported at Node 19.



Note: (1): “2” denotes Node 2.
 (2): ② denotes Element 2.

Figure 4.6 A linear planar truss structure model

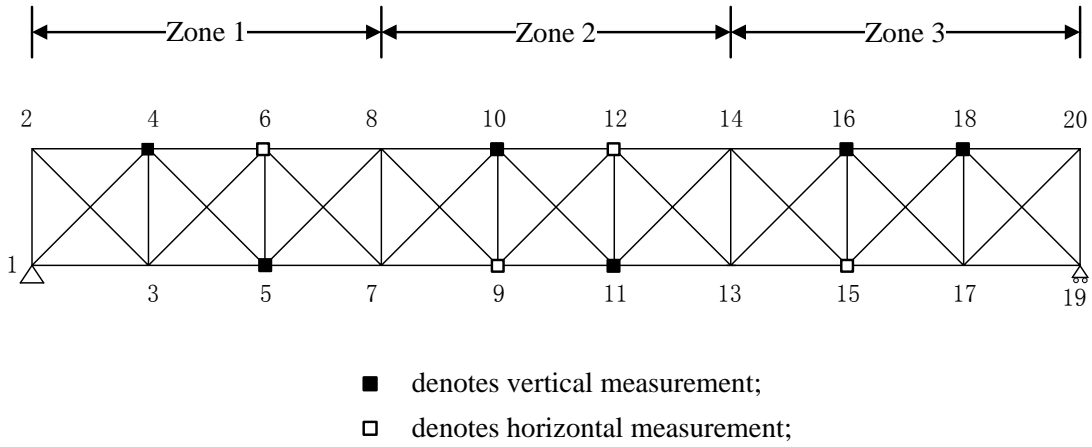


Figure 4.7 The sensor placement of the truss model

The truss structure is arbitrarily divided into three zones. The sensor layout is shown in Figure 4.7. In Zone 1, horizontal vibration (at Node 6) and vertical vibration (at Node 4, and 5) are measured. Zone 2 contains two accelerometers installed at Nodes 9 and 12 in the horizontal direction and two at Nodes 10 and 11 in the vertical direction. Zone 3 has two accelerometers at Nodes 16 and 18 in the vertical direction and one at Node 15 in the horizontal direction. The first zone, second zone and third zone consist of members 1 to 15 with unknown elemental stiffness parameters $\alpha_1 \sim \alpha_{15}$, members 16 to 31 with unknown elemental stiffness parameters $\alpha_{16} \sim \alpha_{31}$ and members 32 to 46 with unknown parameters $\alpha_{32} \sim \alpha_{46}$.

The proposed approach requires to identify the unknown input force and structural parameters at each iteration. Since the accuracy of the force identification results would affect the accuracy of damage identification, the accuracy of force identification with

different settings is studied in this section. To investigate the selection of different sampling rates and covariance matrices on the force identification accuracy, structural parameters are assumed as known. No ground motion is applied to the structure and only a vertical force on Node 10 is considered as unknown.

The effect of different sampling rates and covariance matrices on the force identification is studied. Table 4.1 shows the errors in the force identification results with four different sampling rates from 500Hz to 5000Hz and three covariance matrices in Kalman filter. Since the structure is at rest before the application of external force, the value of $\hat{\mathbf{X}}_0$ in Eq. (4.6) is selected as zero for all studies.

The identification results listed in Table 4.1 indicate that the sampling rate may significantly affect the accuracy of force identification, however, the definition of covariance matrix of measurement noise may not. The error in the identified force increases when the sampling rate decreases because the responses with a higher sampling rate consist of more information. Generally, the sampling frequency should be four or five times larger than the bandwidth of interested frequency. Based on this parametric study and considering the balance between the computational load and identification accuracy, the sampling rate and the covariance matrix are defined as 2000Hz and $0.01 \times \mathbf{I}$, respectively.

Table 4.1 Identification results with different sampling rates and covariance matrices

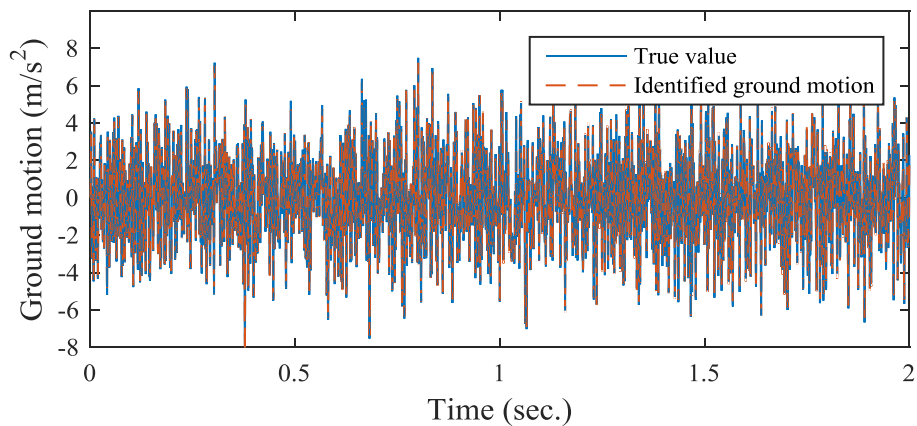
Sampling frequency (Hz)	Covariance matrix R		
	I	$0.01 \times I$	$0.001 \times I$
500	7.69%	7.21%	6.41%
1000	2.42%	2.18%	2.41%
2000	0.625%	0.64%	1.1%
5000	0.25%	0.22%	0.14%

Note: I is an identity matrix

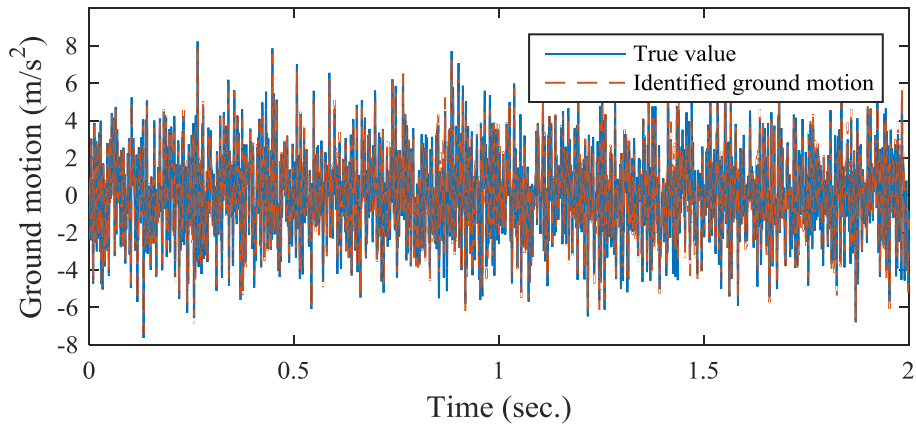
Structural damage detection with unknown ground motion is then studied. The structure is subjected to unknown ground motion in both directions. The applied ground motion is simulated based on a similar procedure in a previous study (Xu *et al.*, 2009) and generated as a white noise acceleration history, which is then scaled to have a maximum PGA of 0.6 g and low pass filtered with a frequency range from 0-400 Hz. The placed accelerometers for measuring the vibration responses in each zone are shown in Figure 4.7. Vibration measurements in a specific zone are only used for the identification of stiffness parameters associated with this zone. That is the measurements from Nodes 4 ~ 6 are used to update $\alpha_1 \sim \alpha_{15}$, the measurements from Nodes 9 ~ 12 are used to update $\alpha_{16} \sim \alpha_{31}$, and the measurements from Nodes 15, 16, 18 are used to update $\alpha_{32} \sim \alpha_{46}$. The unknown ground motions are identified with all of the responses. The sampling rate is 2000 Hz and 2 second vibration data are used for the identification. The health status of

the structure is known, and the structural damage is modelled by a reduction in the stiffness parameters. Three damages are considered in this study and one element is damaged in each zone. 10%, 20% and 15% stiffness reductions are assumed in elements 8, 24 and 38, respectively.

First, the acceleration responses without noise effect from the damaged structures are used. Figure 4.8 compares the true and identified excitation forces. The identified ground motion matches well with the true one. Figure 4.9 shows the identified damage indices of three subsets. The locations and severities of the three damaged elements in different zones are accurately identified. Small identification errors (less than 2%) are observed in the undamaged elements, which may be caused by the numerical errors in the proposed algorithm. These results demonstrate the accuracy of the proposed technique in the identification of structural damage and unknown ground motion.

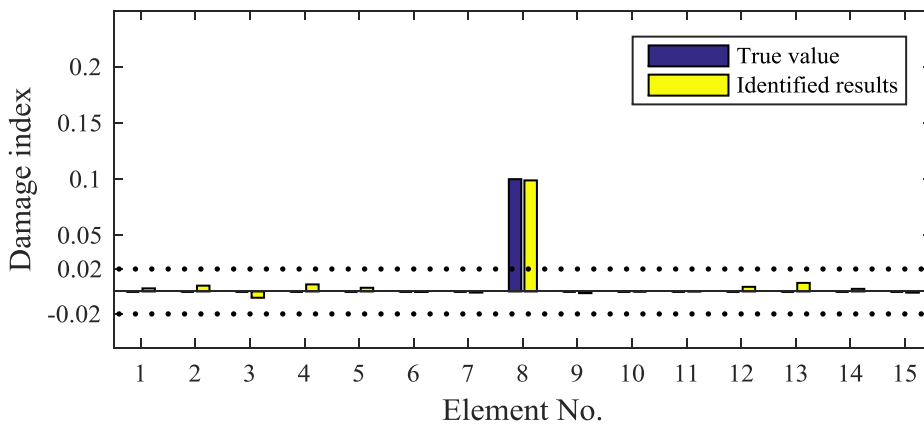


(a) Horizontal ground motion

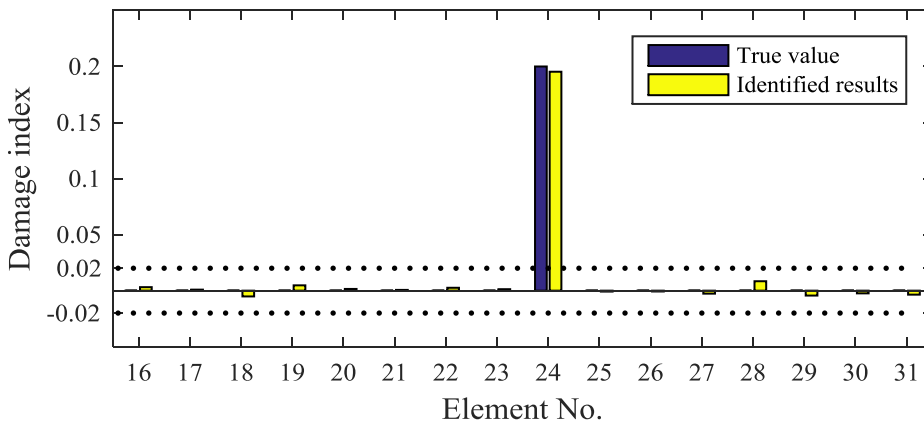


(b) Vertical ground motion

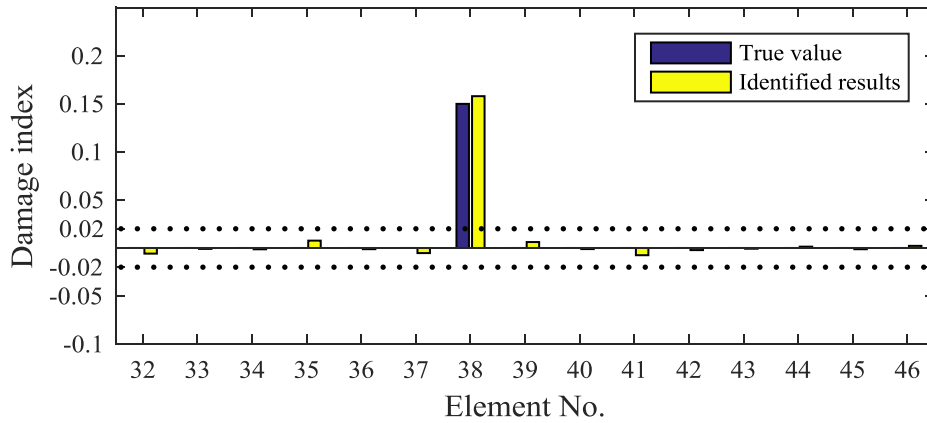
Figure 4.8 Identified and true ground motions without measurement noise



(a) Subset 1



(b) Subset 2

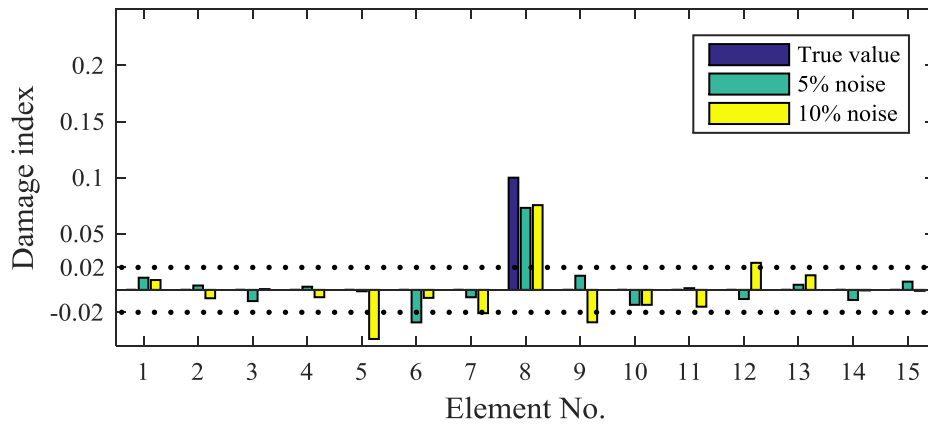


(c) Subset 3

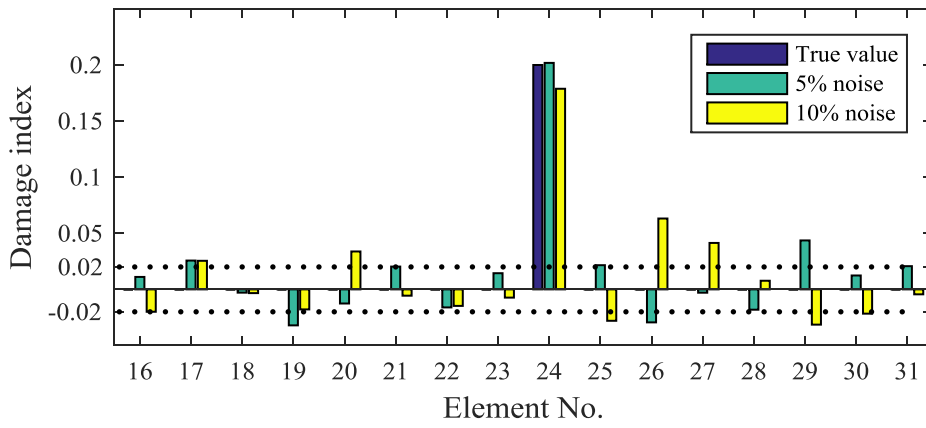
Figure 4.9 Damage identification results without noise effect

The robustness of the proposed method is then investigated. 5% and 10% noise are added in the measurement responses. The fourth-order Butterworth band-pass filter with a frequency range from 0.1 to 500 Hz is used to remove the high frequency noise. The final identified damage indices with different levels of measurement noise are shown in Figure 4.10. Both damage locations and severities in different zones are well identified. The maximum identified error for the 5% noise case is 4.36% at Element 29 and the other errors are less than 4%. There are two large identified errors, that is, 6.32% at Element 26 and 5.83% at Element 24, for 10% noise case. The identified unknown ground motions are compared with the true ones and shown in Figure 4.11. The identified ground motions generally show a good agreement with the true input ground motion, even the recorded data are polluted with noise. These results demonstrate that the proposed approach can accurately identify the structural damage and earthquake input when noise responses are used.

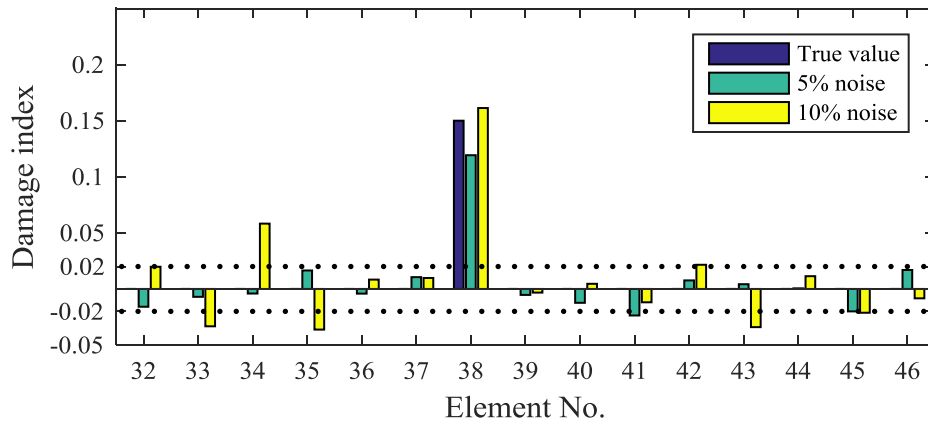
It should be noted that in the last chapter, it took about 3 hours for the model updating. However, the proposed approach in this chapter only takes less than 5 mins with the same simulation data since the input force is identified in a recursive procedure. The force identification in wavelet domain takes a long time, because of the large computational workload in the calculation of pseudo-inverse and wavelet transform (Li and Law, 2011; Li and Hao, 2014). The proposed method in Chapter 4 can be used to identify the unknown input force and parameters of linear and nonlinear structures. Compared with the example in Chapter 3, the advantages of the improved method, which can identify unknown structural parameters with less computation time, can be verified. Two advantages of the improved approach has been demonstrated through the numerical studies.



(a) Subset 1

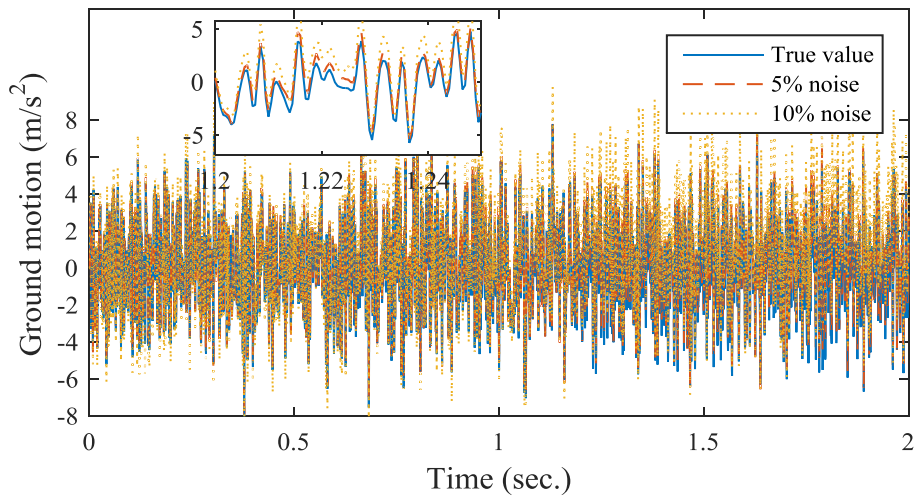


(b) Subset 2

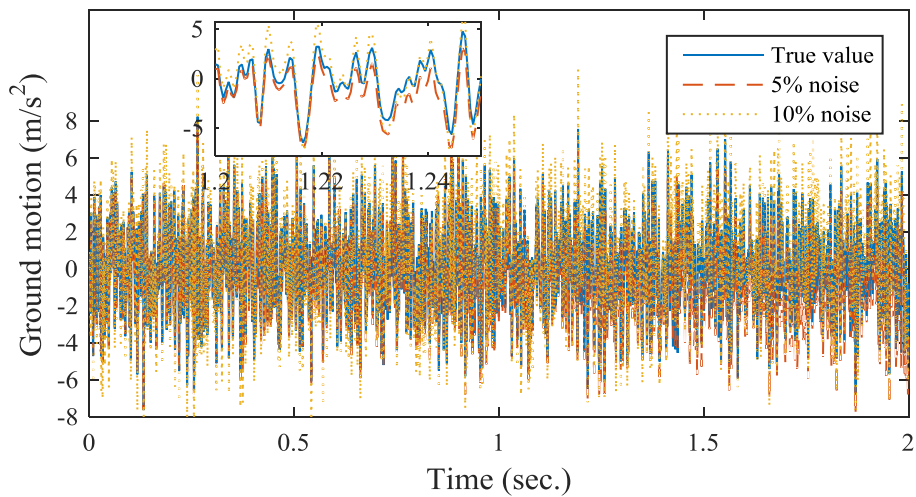


(c) Subset 3

Figure 4.10 Damage identification results with different noise levels



(a) Horizontal ground motion



(b) Vertical ground motion

Figure 4.11 Identified and true forces with different noise levels in the measurements

4.4 Experimental Verification

The experimental case study is used to verify the accuracy of the proposed method in Chapter 4. A laboratory-tested eight-story shear-type steel frame model, as shown in

Figure 4.12 is used. The height and width of steel structure are 2000 mm and 600 mm, respectively. The floor of each story was constructed by thick steel plates (100 mm×25mm), and the two columns of each story have the same cross section with a width of 50 mm and a thickness of 5 mm. The beams and columns were welded to form rigid joints. The bottom of two columns was welded onto a thick and solid steel plate, which is fixed to the strong floor. The dimensions of the frame model are shown in Figure 4.13. The initial elastic modulus of the steel is estimated as 200 GPa, and the mass density 7850 kg/m³.



Figure 4.12 Laboratory steel frame model

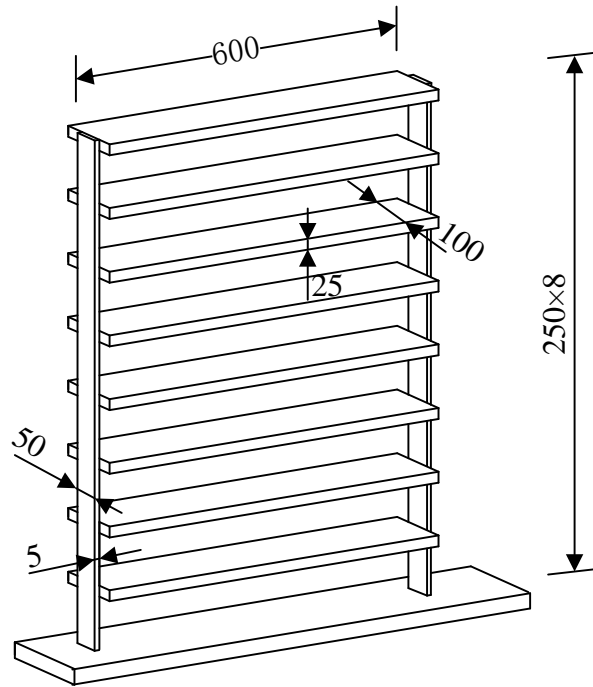


Figure 4.13 Dimensions of the steel frame model (unit: mm, not to scale)

4.4.1 Experimental setup and initial model updating

An SINOCERA LC-04A hammer with a rubber tip was used to apply the excitation on the model. KD1300 accelerometers were used to record the horizontal acceleration responses. A commercial data logging system INV306U and its associated signal analysis package DASP V10 were used for data acquisition. The initial shear-type building finite element model is built based on the dimensions and material properties of the frame. The discrepancy between the numerical finite element model and experimental model exist inevitably due to the modelling errors and uncertainties in the material properties and boundary conditions. Vibration testing data from the

experimental model under the healthy state are used to perform an initial model updating to minimize the difference between the experimental and analytical models.

Vibration test was performed by using the hammer to hit at the fourth floor of the frame model. Both applied force from the hammer and accelerations were recorded for 60s. Only the first 0.5 second data are selected for initial model updating. The sampling rate is set as 1024 Hz, and the cut-off frequency range for the band-pass filter is defined from 1 Hz to 100 Hz for all tests. In each floor, one accelerometer is installed to record the horizontal vibration response and totally, there are eight accelerometers installed in the frame structure. The finite element model of the shear frame is divided into two zones. The first zone consists of the 1st to 4th floors, and the second zone 5th to 8th floors. Accordingly, the measurement responses are divided into two subsets. Each subset of measurements was used to updating the corresponding structural stiffness parameters of the subset, while the unknown hammer force was identified from the measurements of both subsets. Both the structural stiffness parameters and excitation forces are updated iteratively with the proposed approach. Figure 4.14 shows the final identified structural stiffness parameters with their initial values. Slightly difference can be found due to the error between the numerical model and the experimental model. The identified input force matches well the recorded one, as shown in Figure 4.15.

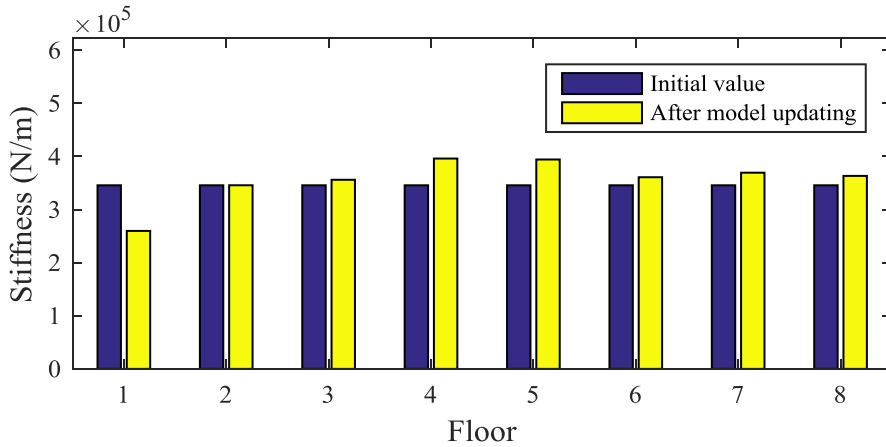


Figure 4.14 Initial model updating

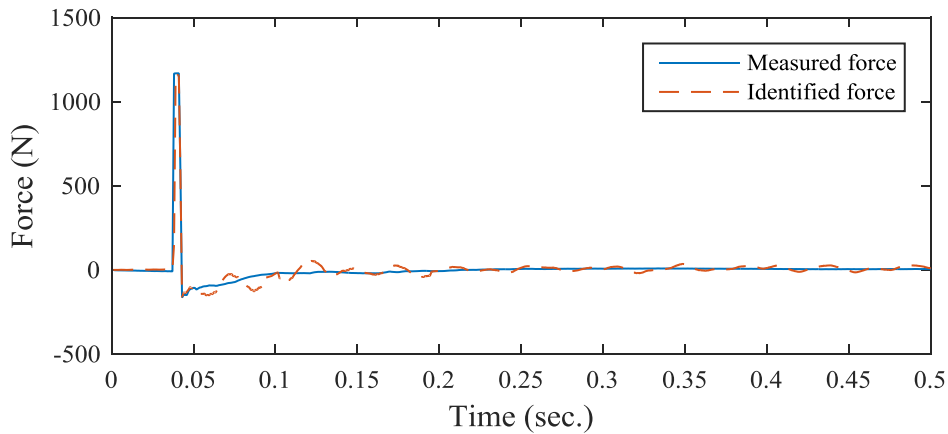


Figure 4.15 Identified force in the undamaged state

The measured and analytical natural frequencies of the frame in the undamaged state before and after model updating are listed in Table 4.2. The measured natural frequencies and model shapes are extracted by using the recorded input force and output responses with DIAMOND (Doebeling *et al.*, 1997). The maximum error in the frequencies after updating is only 0.26%. The measured and analytical mode shapes of the model are shown in Figure 4.16. The mode shapes after model updating match very

well with the measured mode shapes from the vibration tests. These indicate that the updated initial finite element model represents the undamaged frame accurately and serves as the baseline model in the subsequent damage detection.

Table 4.2 Measured and analytical natural frequencies of the frame
in the undamaged state

Mode	Tested	Before updating			After updating		
		Analytical (Hz)	Error (%)	MAC	Analytical (Hz)	Error (%)	MAC
1	4.645	4.810	-3.552	0.988	4.636	-0.1905	0.998
2	13.705	14.267	-4.101	0.975	13.714	0.0635	0.992
3	22.554	23.238	-3.033	0.978	22.558	0.0156	0.987
4	30.695	31.418	-2.355	0.981	30.776	0.2649	0.990
5	38.241	38.528	-0.7505	0.974	38.225	-0.0426	0.995
6	44.434	44.325	0.245	0.979	44.422	-0.0269	0.982
7	48.826	48.614	0.434	0.993	48.712	-0.2343	0.993
8	52.306	51.246	2.027	0.973	52.161	-0.2771	0.989

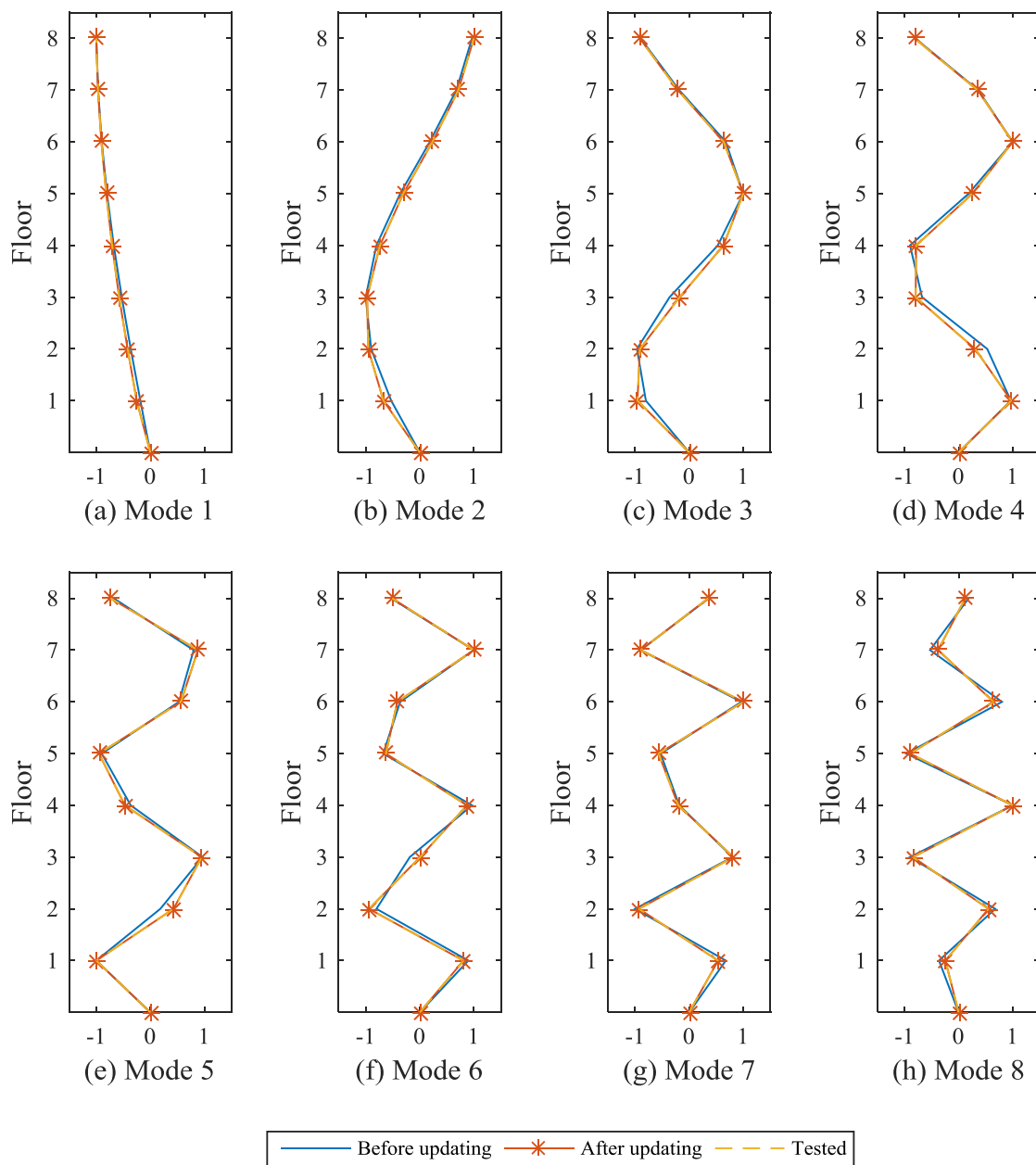
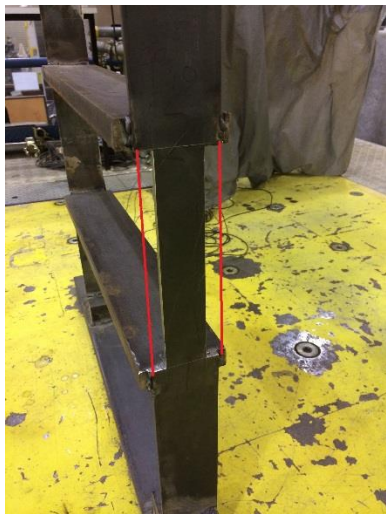


Figure 4.16 Mode shapes of the frame before and after updating

4.4.2 Decentralized damage detection

Structural damage was introduced by reducing the cross section of the column of the frame model. Two damage cases, i.e. Case 1 and 2, were introduced. Only a single damage was introduced in Case 1 with 40% cross section reduction in one column of the 2nd floor. This produced 20% reduction in the equivalent stiffness of the 2nd floor. Case 2 has multiple damages. Besides the damage in case 1, another damage was introduced with 20% cross section reduction in one column at the 7th floor of the frame model. This is equivalent to 10% stiffness reduction in the 7th floor. Those introduced damages in the second and seventh floors are shown in Figure 4.17.

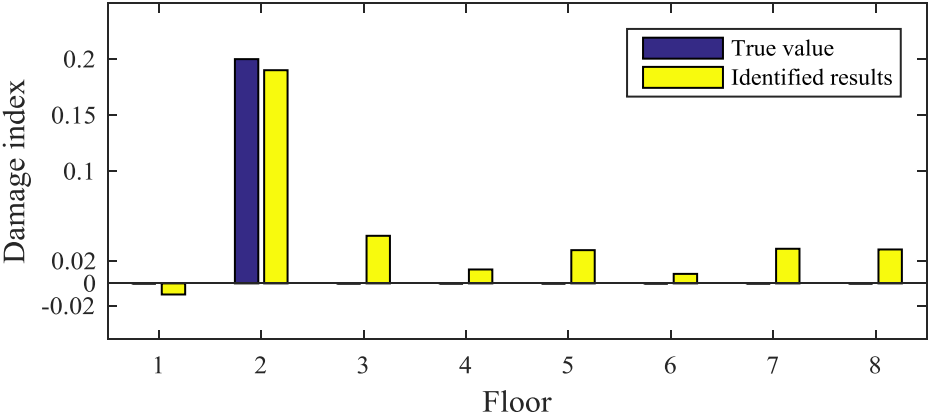


(a) Introduced damage at the 2nd floor

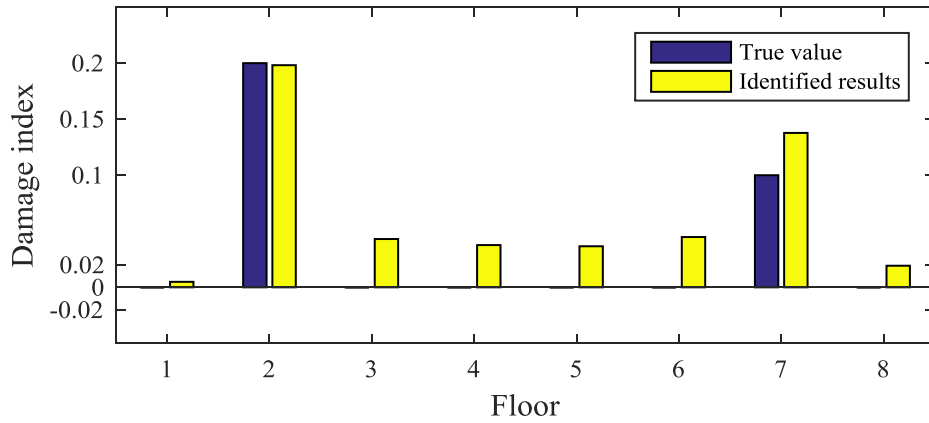
(b) Introduced damage at the 7th floor

Figure 4.17 Introduced damages of the frame model

The frame was tested similarly described in Section 4.4.1. The reduction of the mass caused by the damage is neglected. Measured responses are used to identify the structure damages and applied excitation force. The updated numerical model obtained in Section 4.4.1 is used as the baseline model. The identification results for the two cases are shown in Figure 4.18. In Case 1, the identified damage in the second floor is 19%, which is very close to the true value of 20%. For Case 2, the identified stiffness reductions are 19.8% at floor 2 and 10.4% at floor 7. It can be observed from the identification results of these two cases, that both damage locations and severities can be well identified with the proposed approach. Around 4% false identified stiffness reductions are observed in the 3rd floor to the 6th floor. The identified forces have a good agreement with the measured ones, as shown in Figure 4.19. These errors in the identified excitation force and stiffness parameters are due to the noises in the measurements and uncertainties in the finite element model.

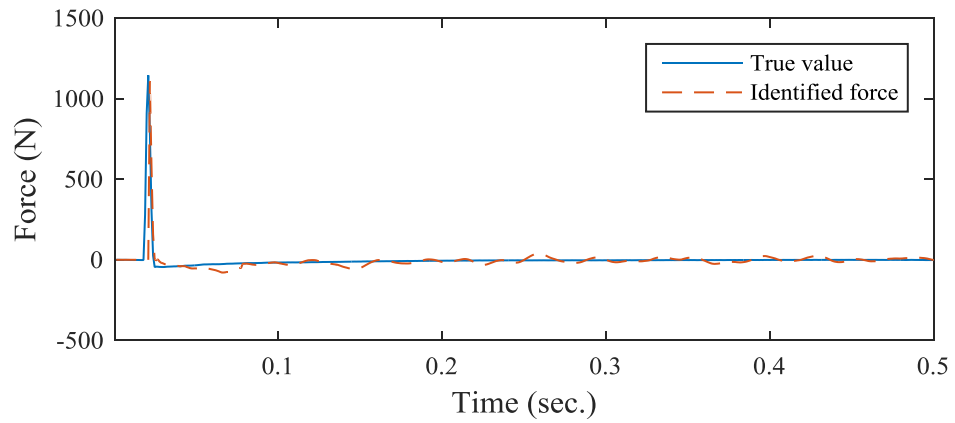


(a) Case 1

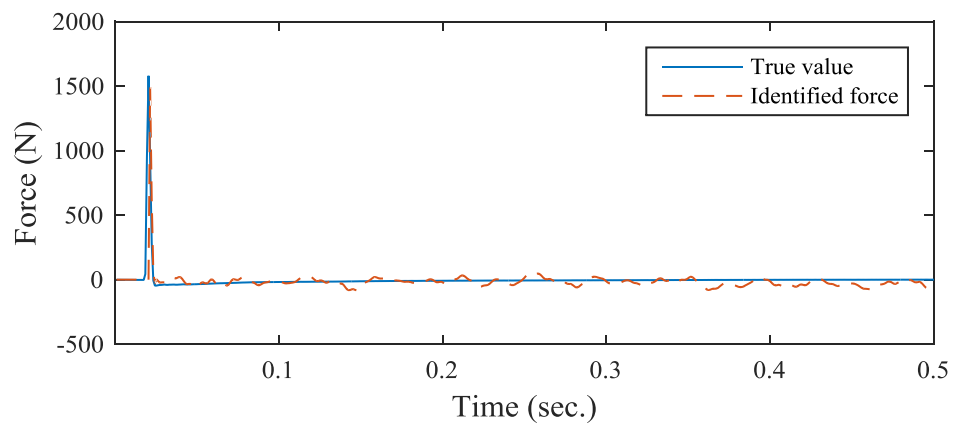


(b) Case 2

Figure 4.18 Damage identification results of the frame



(a) Case 1



(b) Case 2

Figure 4.19 Identified force of the frame in the damage cases

4.5 Summary

An improved decentralized damage detection identification approach is proposed for both linear and nonlinear structures with output only. The approach divides a large-scale structure into several zones. The Kalman filter technique is used to identify the unknown earthquake loading, and Newton-SOR method is adopted for identifying the unknown structural parameters of subsets using the vibration measurement of the subset only. The external excitations and structural parameters are updated iteratively. Numerical studies on a six-floor nonlinear system and a linear planar truss structure demonstrate that the proposed approach is effective for output-only structural identification with a few sensors, even at the presence of 10% noise included in the measured data. An experimental eight-story shear-type steel frame structure was also tested in the laboratory to validate the proposed approach. Two damage cases were introduced in the frame model. The applied excitation force and structure damage in both damage cases are well identified with the measured responses. It is demonstrated that the proposed approach can be used for both linear and nonlinear system identification by using only measured responses, and less computational time compared with the existing methods.

CHAPTER 5

NONLINEAR FINITE ELEMENT MODEL UPDATING WITH THE DECENTRALIZED APPROACH

5.1 Introduction

In Chapter 4, the nonlinear behaviour of a structure is modelled with a nonlinear mass–spring–dashpot model. For a complex civil structure, the dynamic responses predicted from such a model may be not accurate enough. Nonlinear finite element models can predict the dynamic responses of a large complex structure with more precision, which has been widely used in the structural analysis (De Borst *et al.*, 2012; Belytschko *et al.*, 2013). The nonlinear finite element model updating technique gains much attention in recent years. Several studies (Cooreman *et al.*, 2007; Rossi and Pierron, 2012; Astroza *et al.*, 2017; Ebrahimian *et al.*, 2017) have been proposed.

In this chapter, a nonlinear finite element model updating technique is proposed by using the decentralized approach. The dynamic responses of the structure are computed based on discrete finite element models and the nonlinear behaviour of the structure is simulated with distributed plastic model (Taucer *et al.*, 1991). Following the studies in Chapter 3 and 4, a large-scale structure is divided into some smaller zones according to its finite element configuration. The unknown structural material parameters of the whole structure are divided into several subsets according to their location. They are updated by using the vibration response at each zone with the Newton-SOR method. The proposed method is implemented in MATLAB and interfaced with OpenSees (McKenna, 2011) for calculation of dynamic response and response sensitivity. Numerical studies on a three-story two-bay reinforced concrete structure and a six-story one-bay steel building structure under ground motion input are employed to verify the accuracy of the proposed method. Different material parameters in the constitutive parameters (such as compressive strength f_c of concrete, yield stress f_y of reinforcement, etc) are treated as unknown variables to be updated. The results from the two structures show that the proposed method can update nonlinear material parameters accurately. The global model updating method is also studied to verify the efficiency and effectiveness of the proposed decentralized method. In this study, due to the long computational time for the nonlinear finite element analysis, the input earthquake is known.

5.2 Methodology

5.2.1 Nonlinear finite element analysis procedure

The equation of motion of an N -DOFs damped nonlinear system under ground motion excitation can be written as

$$\mathbf{M}\ddot{\mathbf{x}}(t) + \mathbf{C}\dot{\mathbf{x}}(t) + \mathbf{K}_r(\mathbf{x}(t), \boldsymbol{\theta}) = \mathbf{M}\mathbf{I}\ddot{x}_g(t) \quad (5.1)$$

where $\mathbf{x}(t)$, $\dot{\mathbf{x}}(t)$ and $\ddot{\mathbf{x}}(t)$ are vectors of displacements, velocity and acceleration responses of the structure, respectively; \mathbf{M} , and \mathbf{C} are the mass and damping matrices of the structure, $\boldsymbol{\theta}$ is the material parameter vector in the material constitutive model and $\mathbf{K}_r(\mathbf{x}(t), \boldsymbol{\theta})$ is the resisting force vector and depends on $\boldsymbol{\theta}$ and $\mathbf{x}(t)$; and $\ddot{x}_g(t)$ is the ground motion acceleration. The mass matrix of a structure can be estimated accurately from the geometry dimension and material density, and these are assumed invariant.

In this chapter, fiber beam-column elements are used for the nonlinear dynamic responses of frame structures under seismic input (Taucer *et al.*, 1991). The structural model is divided into several finite elements, and each section of element is further discretized into fibers. The computational framework of the nonlinear dynamic analysis is shown in Figure 5.1. The nonlinear analysis procedure contains state determination at element, section and fiber levels. The fiber strain can be computed from section/element deformation with the assumption that plane sections remain plane and normal to the reference longitudinal axis after deformation occurs. The stress and tangent module of each fiber can be computed from material constitutive models with fiber strain, and the section resisting forces can be calculated by summation of the axial force and biaxial bending moment contributions of all fibers. Finally, the element flexibility matrix can be formed by the integration of the section flexibility. This matrix can then be inverted

to obtain the element tangent stiffness matrix. This technique has been widely used in nonlinear analysis and design of frame-type structures. The details description of the technique can be found in (Taucer *et al.*, 1991).

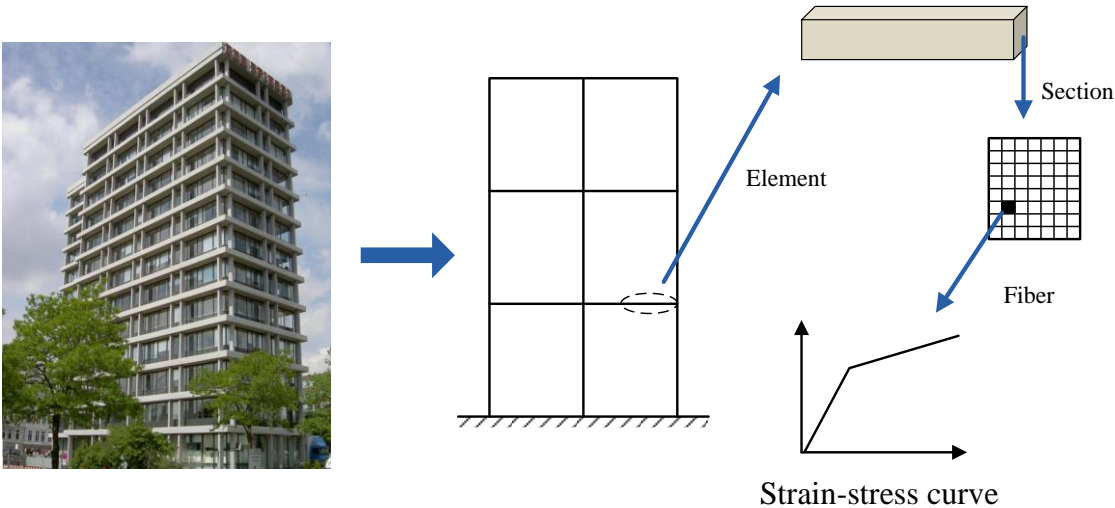


Figure 5.1 Computational framework of nonlinear dynamic analysis

5.2.2 Decentralized identification of nonlinear material parameters

Due to the distance for signal transmission and the ability for data processing, a SHM system contains central station and several sub-stations. The large structure is divided into several zones, and each sub-station is used for data acquisition in each zone. The proposed decentralized model updating method can be installed in each sub-station to update the structural parameters in each zone. The measurements in a large structure are divided into smaller groups in physical zones based on its finite element formulation.

The unknown damage index θ can be divided into r subsets $[\theta_1, \theta_2, \dots, \theta_r]$, where θ_i contains all the unknown material parameters of the i -th ($1 \leq i \leq r$) zone. Field measurement is conducted in different zones of the structure and the measured nonlinear dynamic responses from i -th zone $\ddot{\mathbf{x}}_{mea,i}$ can be written as a function as $\mathbf{g}_i(\theta_1, \theta_2, \dots, \theta_r, \ddot{\mathbf{x}}_g)$. When all of responses are collected, the measured responses from different zones can then be written as

$$\begin{aligned}
\mathbf{g}_1(\theta_1, \theta_2, \dots, \theta_r, \ddot{\mathbf{x}}_g) - \ddot{\mathbf{x}}_{mea,1} &= 0 \\
\mathbf{g}_2(\theta_1, \theta_2, \dots, \theta_r, \ddot{\mathbf{x}}_g) - \ddot{\mathbf{x}}_{mea,2} &= 0 \\
\vdots & \\
\mathbf{g}_i(\theta_1, \theta_2, \dots, \theta_r, \ddot{\mathbf{x}}_g) - \ddot{\mathbf{x}}_{mea,i} &= 0 \\
\vdots & \\
\mathbf{g}_r(\theta_1, \theta_2, \dots, \theta_r, \ddot{\mathbf{x}}_g) - \ddot{\mathbf{x}}_{mea,r} &= 0
\end{aligned} \tag{5.2}$$

The unknowns in this chapter are material parameters in the constitutive model, and the problem is to find the solution of Eq. (5.2). Eq. (5.2) can be written as Eq. (5.3) and solved using the Newton method (Ortega and Rheinboldt, 1970)

$$\mathbf{G}(\theta) = 0 \tag{5.3}$$

With

$$\mathbf{G}(\theta) = \mathbf{G}(\theta^n) + \mathbf{G}'(\theta^n)(\theta^{n+1} - \theta^n) = 0 \tag{5.4}$$

$$\mathbf{G}'(\theta^n)\theta^{n+1} = \mathbf{G}'(\theta^n)\theta^n - \mathbf{G}(\theta^n) \tag{5.5}$$

$$\theta^{n+1} = \theta^n - [\mathbf{G}'(\theta^n)]^{-1} \mathbf{G}(\theta^n) \tag{5.6}$$

where n denotes the number of iteration and $\mathbf{G}'(\theta^n)$ is the Jacobian matrix of $\mathbf{G}(\theta^n)$,

and

$$\mathbf{G}'(\boldsymbol{\theta}^n) = \begin{bmatrix} \frac{\partial \mathbf{g}_1}{\partial \theta_1} & \frac{\partial \mathbf{g}_1}{\partial \theta_2} & \dots & \frac{\partial \mathbf{g}_1}{\partial \theta_r} \\ \frac{\partial \mathbf{g}_2}{\partial \theta_1} & \frac{\partial \mathbf{g}_2}{\partial \theta_2} & \dots & \frac{\partial \mathbf{g}_2}{\partial \theta_r} \\ \vdots & \vdots & & \vdots \\ \frac{\partial \mathbf{g}_r}{\partial \theta_1} & \frac{\partial \mathbf{g}_r}{\partial \theta_2} & \dots & \frac{\partial \mathbf{g}_r}{\partial \theta_r} \end{bmatrix} \quad (5.7)$$

Following the derivation discussed in Section 3.3.3, the iterative SOR method is embedded in Eq. (5.6). Considering the solution from *One-step* Newton-SOR method, the unknown structural material parameters can be updated with

$$\begin{bmatrix} \boldsymbol{\theta}_1^{n+1} \\ \boldsymbol{\theta}_2^{n+1} \\ \vdots \\ \boldsymbol{\theta}_r^{n+1} \end{bmatrix} = \begin{bmatrix} \boldsymbol{\theta}_1^n \\ \boldsymbol{\theta}_2^n \\ \vdots \\ \boldsymbol{\theta}_r^n \end{bmatrix} - \begin{bmatrix} \frac{\partial \mathbf{g}_1}{\partial \theta_1^n} & 0 & 0 & 0 \\ 0 & \frac{\partial \mathbf{g}_2}{\partial \theta_2^n} & 0 & 0 \\ 0 & 0 & \ddots & 0 \\ 0 & 0 & 0 & \frac{\partial \mathbf{g}_r}{\partial \theta_r^n} \end{bmatrix}^{-1} \begin{bmatrix} \mathbf{g}_1(\boldsymbol{\theta}^n, \ddot{\mathbf{x}}_g) - \ddot{\mathbf{x}}_{mea,1} \\ \mathbf{g}_2(\boldsymbol{\theta}^n, \ddot{\mathbf{x}}_g) - \ddot{\mathbf{x}}_{mea,2} \\ \vdots \\ \mathbf{g}_r(\boldsymbol{\theta}^n, \ddot{\mathbf{x}}_g) - \ddot{\mathbf{x}}_{mea,r} \end{bmatrix} \quad (5.8)$$

or

$$\boldsymbol{\theta}_i^{n+1} = \boldsymbol{\theta}_i^n - \left[\frac{\partial \mathbf{g}_i}{\partial \theta_i^n} \right]^{-1} \left[\mathbf{g}_i(\boldsymbol{\theta}^n, \ddot{\mathbf{x}}_g) - \ddot{\mathbf{x}}_{mea,i} \right], \quad (i = 1, 2, \dots, r) \quad (5.9)$$

The least-squares method is applied to Eq. (5.9) and the resulting *One-step* Newton-SOR is obtained as

$$\boldsymbol{\theta}_i^{n+1} = \boldsymbol{\theta}_i^n - \left[\left(\frac{\partial \mathbf{g}_i}{\partial \theta_i^n} \right)^T \left(\frac{\partial \mathbf{g}_i}{\partial \theta_i^n} \right) \right]^{-1} \left(\frac{\partial \mathbf{g}_i}{\partial \theta_i^n} \right)^T \left[\mathbf{g}_i(\boldsymbol{\theta}^n, \ddot{\mathbf{x}}_g) - \ddot{\mathbf{x}}_{mea,i} \right], (i = 1, 2, \dots, r) \quad (5.10)$$

5.2.3 Dynamic response sensitivity considering material nonlinearity

Response sensitivity analysis has been studied for a long time and widely used for structural design optimization, probabilistic analysis and reliability analysis (Conte, 2001; Haukaas and Der Kiureghian, 2004). Many methods have been proposed, such as finite difference method, adjoint method, perturbation method, and direct differentiation method. The perturbation method is computationally efficient but not accurate. Forward finite difference method is the simplest method but time-consuming and easy to be negatively affected by the numerical error. The direct differentiation method is more accurate and computationally efficient than other methods (Shayanfar *et al.*, 2014; Ebrahimian *et al.*, 2015), and therefore, is employed in this section. The direct differentiation method in OpenSees is briefly introduced as follows (Ebrahimian *et al.*, 2015).

The acceleration and velocity at time step $(t+1)$ can be interpolated with implicit time integration scheme as

$$\ddot{\mathbf{x}}(t+1) = b_1 \mathbf{x}(t+1) + b_2 \mathbf{x}(t) + b_3 \dot{\mathbf{x}}(t) + b_4 \ddot{\mathbf{x}}(t) \quad (5.11)$$

$$\dot{\mathbf{x}}(t+1) = b_5 \mathbf{x}(t+1) + b_6 \mathbf{x}(t) + b_7 \dot{\mathbf{x}}(t) + b_8 \ddot{\mathbf{x}}(t) \quad (5.12)$$

where b_1 to b_8 are constant integration coefficients. Substitution of Eqs. (5.11) and (5.12) into Eq. (5.1), we have

$$b_1 \mathbf{M} \mathbf{x}(t+1) + b_5 \mathbf{C} \mathbf{x}(t+1) + \mathbf{K}_r(\mathbf{x}(t+1), \boldsymbol{\theta}) = \mathbf{P}(t+1) \quad (5.13)$$

where

$$\begin{aligned} \mathbf{P}(t+1) = & \mathbf{M}\mathbf{I}\ddot{\mathbf{x}}_g(t+1) - \mathbf{M} \left[b_2\mathbf{x}(t) + b_3\dot{\mathbf{x}}(t) + b_4\ddot{\mathbf{x}}(t) \right] \\ & - \mathbf{C} \left[b_6\mathbf{x}(t) + b_7\dot{\mathbf{x}}(t) + b_8\ddot{\mathbf{x}}(t) \right] \end{aligned} \quad (5.14)$$

Eq. (5.13) is differentiated with respect to each material parameter θ_i to obtain the response sensitivity, that is,

$$\begin{aligned} & \left[b_1\mathbf{M}\mathbf{x}(t+1) + b_5\mathbf{C}\mathbf{x}(t+1) + \frac{\partial \mathbf{K}_r(\mathbf{x}(t+1), \boldsymbol{\theta})}{\partial \mathbf{x}(t+1)} \right] \frac{\partial \mathbf{x}(t+1)}{\partial \theta_i} \\ & = -\frac{\partial \mathbf{K}(\mathbf{x}(t+1), \boldsymbol{\theta})}{\partial \theta_i} + \frac{\partial \mathbf{P}(t+1)}{\partial \theta_i} - \left(b_1 \frac{\partial \mathbf{M}}{\partial \theta_i} + b_5 \frac{\partial \mathbf{C}}{\partial \theta_i} \right) \mathbf{x}(t+1) \end{aligned} \quad (5.15)$$

In this chapter, only the material parameters in the material constitutive model are considered, therefore, $\partial \mathbf{M} / \partial \theta_i = 0$ and $\partial \mathbf{C} / \partial \theta_i = 0$. The last term on the right-hand side of Eq. (5.15) can be negligible. Similarly, taking derivative of Eq. (5.14) with respect to θ_i , we have

$$\begin{aligned} \frac{\partial \mathbf{P}(t+1)}{\partial \theta_i} = & \frac{\partial \mathbf{M}\mathbf{I}\ddot{\mathbf{x}}_g(t+1)}{\partial \theta_i} - \frac{\partial \mathbf{M}}{\partial \theta_i} \left[b_2\mathbf{x}(t) + b_3\dot{\mathbf{x}}(t) + b_4\ddot{\mathbf{x}}(t) \right] \\ & - \frac{\partial \mathbf{C}}{\partial \theta_i} \left[b_6\mathbf{x}(t) + b_7\dot{\mathbf{x}}(t) + b_8\ddot{\mathbf{x}}(t) \right] - \mathbf{M} \left[b_2 \frac{\partial \mathbf{x}}{\partial \theta_i}(t) + b_3 \frac{\partial \dot{\mathbf{x}}}{\partial \theta_i}(t) + b_4 \frac{\partial \ddot{\mathbf{x}}}{\partial \theta_i}(t) \right] \\ & - \mathbf{C} \left[b_6 \frac{\partial \mathbf{x}}{\partial \theta_i}(t) + b_7 \frac{\partial \dot{\mathbf{x}}}{\partial \theta_i}(t) + b_8 \frac{\partial \ddot{\mathbf{x}}}{\partial \theta_i}(t) \right] \\ = & -\mathbf{M} \left[b_2 \frac{\partial \mathbf{x}}{\partial \theta_i}(t) + b_3 \frac{\partial \dot{\mathbf{x}}}{\partial \theta_i}(t) + b_4 \frac{\partial \ddot{\mathbf{x}}}{\partial \theta_i}(t) \right] - \mathbf{C} \left[b_6 \frac{\partial \mathbf{x}}{\partial \theta_i}(t) + b_7 \frac{\partial \dot{\mathbf{x}}}{\partial \theta_i}(t) + b_8 \frac{\partial \ddot{\mathbf{x}}}{\partial \theta_i}(t) \right] \end{aligned} \quad (5.16)$$

The vectors $\partial \mathbf{x}(t) / \partial \theta_i$, $\partial \dot{\mathbf{x}}(t) / \partial \theta_i$ and $\partial \ddot{\mathbf{x}}(t) / \partial \theta_i$ are available from the last time step sensitivity computation. Therefore, $\partial \mathbf{P}(t+1) / \partial \theta_i$ can be obtained without difficulty.

The first term on the right-hand side of Eq. (5.15), $\partial \mathbf{K}_r(\mathbf{x}(t+1), \boldsymbol{\theta}) / \partial \theta_i$, represents the partial derivative of the internal resisting force vector with respect to the material parameter θ_i . The internal resisting force vector can be assembled from the element nodal resisting force vectors as

$$\mathbf{K}_r(\mathbf{x}(t+1), \boldsymbol{\theta}) = \sum_{i=1}^{ne} \left\{ K_{t+1}^{ele,i}(\mathbf{x}_i(t+1), \boldsymbol{\theta}) \right\} \quad (5.17)$$

where $K_{t+1}^{ele,i}$ denotes the i -th element nodal resisting force vector at time step $(t+1)$, and $\mathbf{x}_i(t+1)$ is the element nodal displacement vector in the element local coordinate system, and ne is the total number of the element. The element nodal resisting force vector is obtained from the integral of the section stress vector as

$$K_{t+1}^{ele,i} = \int \mathbf{B}^T \boldsymbol{\sigma}_{t+1}^{sec}(\boldsymbol{\varepsilon}_{t+1}^{sec}(\boldsymbol{\theta}), \boldsymbol{\theta}) dl \quad (5.18)$$

where \mathbf{B} is the strain-displacement transformation matrix, $\boldsymbol{\sigma}_{t+1}^{sec}$ is the section stress vector, and $\boldsymbol{\varepsilon}_{t+1}^{sec}$ is the section strain. Finally, the section stress vector is obtained by integrating the fiber stresses over the cross section as

$$\boldsymbol{\sigma}_{t+1}^{sec} = \int \mathbf{b} \sigma_{t+1}^{fib}(\boldsymbol{\varepsilon}_{t+1}^{fib}(\boldsymbol{\theta}), \boldsymbol{\theta}) dA \quad (5.19)$$

where \mathbf{b} is section kinematic vector, σ_{t+1}^{fib} is fiber stress, and $\boldsymbol{\varepsilon}_{t+1}^{fib}$ is fiber strain.

Substituting Eqs. (5.18) and (5.19) into Eq. (5.17), and the partial derivative computed as

$$\frac{\partial \mathbf{K}_r(\mathbf{x}(t+1), \boldsymbol{\theta})}{\partial \theta_i} = \sum_{i=1}^{ne} \left\{ \int \mathbf{B}^T \int \mathbf{b} \frac{\partial \sigma_{t+1}^{fib}(\boldsymbol{\varepsilon}_{t+1}^{fib}(\boldsymbol{\theta}), \boldsymbol{\theta})}{\partial \theta_i} dA dl \right\} \quad (5.20)$$

where $\frac{\partial \sigma_{t+1}^{fib}(\varepsilon_{t+1}^{fib}(\boldsymbol{\theta}), \boldsymbol{\theta})}{\partial \theta_i}$ is the derivative of the fiber stress with respect to the material parameter θ_i and can be computed by analytically differentiating the material constitutive law (Zhang and Der Kiureghian, 1993; Kleiber *et al.*, 1997; Conte *et al.*, 2003).

5.2.4 Implementation procedure of the model updating technique

The proposed method is implemented in Matlab and interfaced with OpenSees (McKenna, 2011) for structural response and response sensitivity computations. The implementation procedures of the proposed method are as follows.

Step 1: Divide the structure into smaller zones according to its finite element formulation and obtain the corresponding sets of responses from each zone.

Step 2: Setting the initial value of parameters as $\boldsymbol{\theta} = [\theta_1^0, \theta_2^0, \dots, \theta_r^0]$.

Step 3: Compute the sensitivity of responses with respect to the structural parameters of each zone with OpenSees.

Step 4: Update the parameters of each zone θ_i^{n+1} using Eq. (5.10).

Step 5: Repeat Steps 3 – 4 until the following convergence criterion in Eq. (5.22) is satisfied.

$$\frac{\|\boldsymbol{\theta}^{n+1} - \boldsymbol{\theta}^n\|}{\|\boldsymbol{\theta}^{n+1}\|} \times 100\% \leq Tol \quad (5.21)$$

Tol is tolerance of convergence criterion, which is 1.0×10^{-8} in for the case without noise and 1.0×10^{-5} for the case with noise.

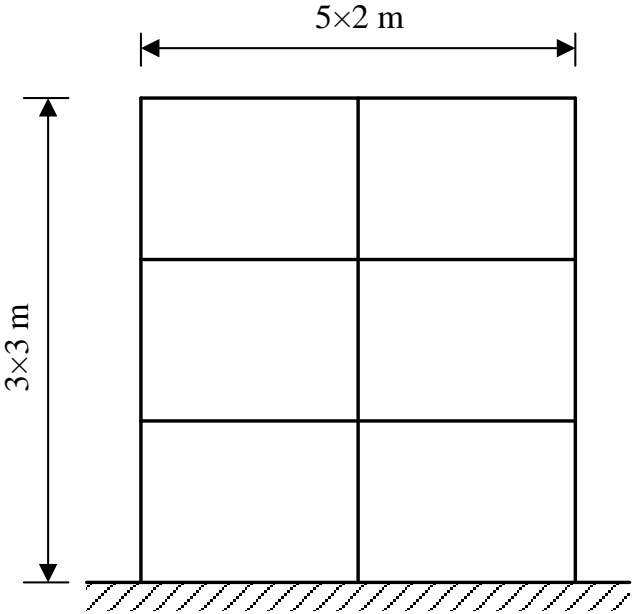
5.3 Numerical Examples

5.3.1 A reinforced concrete frame

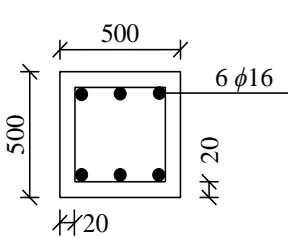
A 2D two-bay three-floor reinforced concrete structure is studied. The dimensions of the frame model are shown in Figure 5.2(a). Each bay of the structure has a width of 5 m and the height of each floor is 3 m. The cross sections of columns and beams are $0.5 \times 0.5 \text{ m}^2$ and $0.25 \times 0.4 \text{ m}^2$, respectively, as shown in Figures 5.2(b-c). This structure is modelled with displacement-based fiber-section beam-column elements using OpenSees. The column and beam at each floor are further divided into five elements and ten elements, respectively, along the longitudinal direction. Therefore, the finite element model of the structure consists of 102 nodes, 105 elements, and 306 DOFs. Different material parameters are selected to simulate the nonlinear behavior of the structure. The longitudinal reinforcement is modelled with uniaxial Menegotto-Pinto steel material (Barbato and Conte, 2006). The concrete is modelled with uniaxial smoothed Popovics-Saenz concrete material (Zona *et al.*, 2005). The stress-strain relations and the hysteresis curves of the steel and concrete are shown in Figures 5.3 (a-f). Section stress resultants are obtained by discretizing the frame sections into fibers, as shown in Figure 5.4. The material parameters of the longitudinal reinforcement, confined concrete, and unconfined concrete are shown in Table 5.1. These parameters are selected according to (Barbato *et al.*, 2013; Astroza *et al.*, 2014; Ebrahimian, 2015).

The nonlinear dynamic responses of the structure under seismic input are computed using Newmark method. The time history of the El-Centro earthquake (PGA=0.8g) is

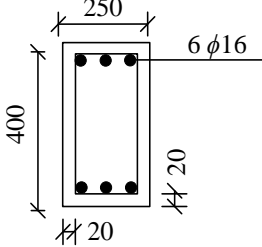
selected as the input for this study. Additional mass (4000 kg/m) is added to the beam element to simulate the weight of floors and other dead loads. The sampling frequency is 1000 Hz and the ground motion last for 20 seconds. Three accelerometers are installed in each zone to measure the horizontal responses, as illustrated in Figure 5.5. Based on the proposed method, the measurement responses in each zone are used to update the material parameters of the zone. For example, the dynamic responses from zone 2 are used to update the nine material parameters in the zone.



(a) The frame structure

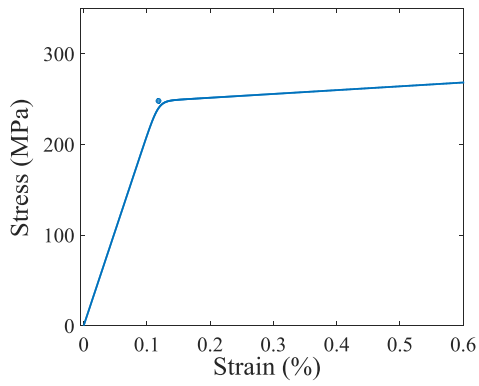


(b) Column (unit: mm)

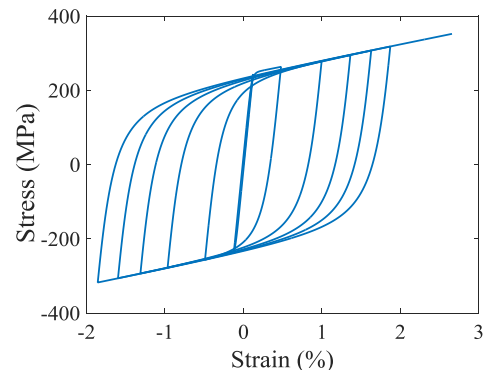


(c) Beam (unit: mm)

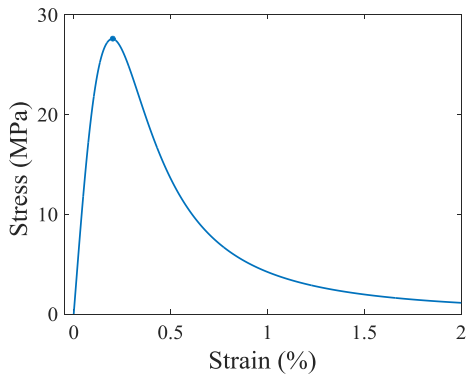
Figure 5.2 Dimensions of the reinforcement concrete structure



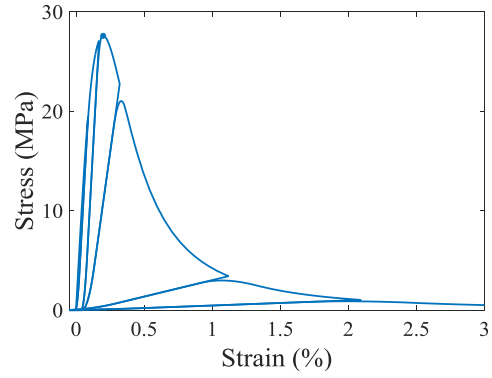
(a) Stain-stress curve of reinforcement



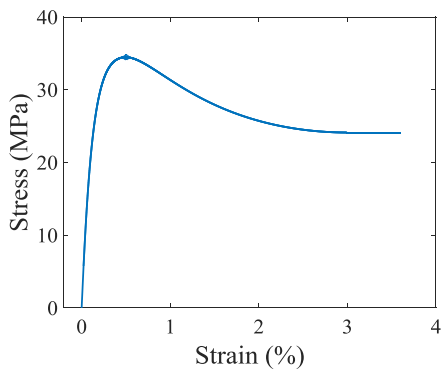
(d) Hysteresis loop of unconfined concrete



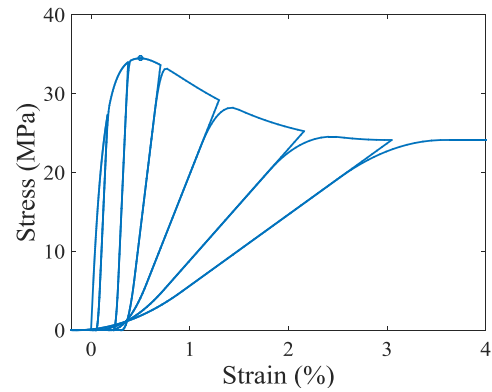
(b) Stain-stress curve of unconfined concrete



(e) Hysteresis loop of unconfined concrete

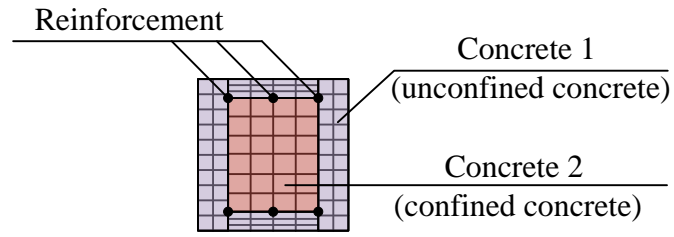


(c) Stain-stress curve of confined concrete

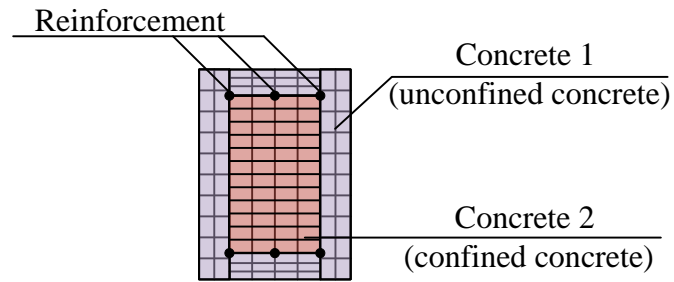


(f) Hysteresis loop of confined concrete

Figure 5.3 Material models



(a) Column



(b) Beam

Figure 5.4 Materials defined in the cross section

Table 5.1 Material parameters of the reinforcement concrete structure

Material	Unknown material parameters
Confined concrete	Compressive strength f_c 34.4738 MPa
	Concrete strain at maximum strength ε_c 0.005
	Initial tangent stiffness E_c 27.851 GPa
Unconfined concrete	Compressive strength f_{uc} 27.57904 MPa
	Concrete strain at maximum strength ε_{uc} 0.002
	Initial tangent stiffness E_{uc} 24.91 GPa
Reinforcement	Initial yield stress f_y 248.200 MPa
	Young's modulus E_s 210GPa
	Strain-hardening ratio b 0.02

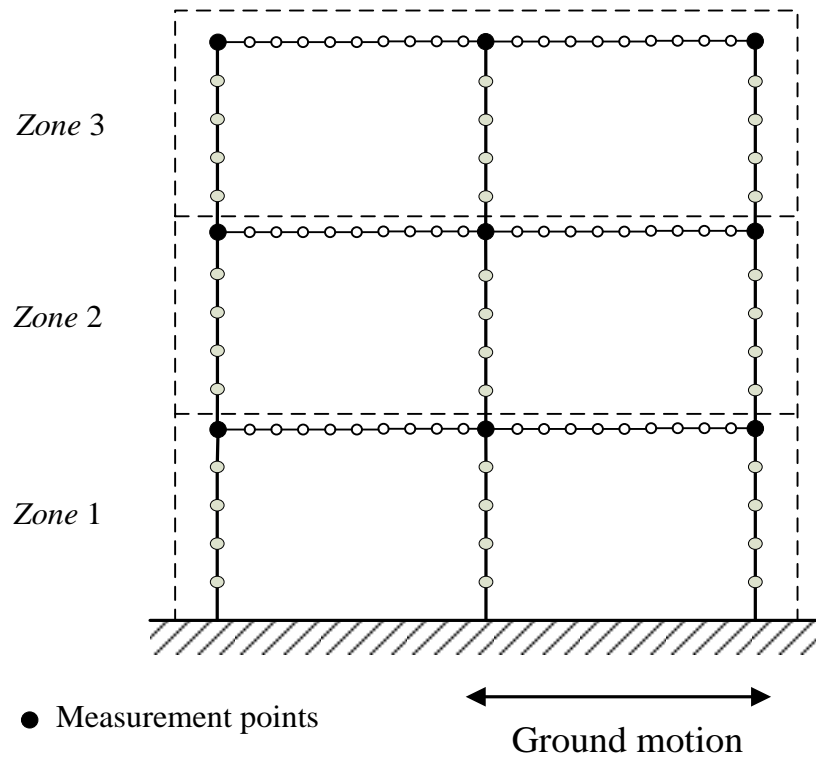


Figure 5.5 Finite element model of the frame structure

Modelling errors in reinforced concrete structures are usually significant (Barbato *et al.*, 2013). In this study, the model error is added to the material parameters of each floor. That means the material parameters in the constitutive model of each floor are the same. The material constitutive parameters such as compressive strength f_c , concrete strain at maximum strength ε_c , and initial tangent stiffness E_c of confined concrete; compressive strength f_{uc} , concrete strain at maximum strength ε_{uc} , and initial tangent stiffness E_{uc} of unconfined concrete; initial yield stress f_y , Young's modulus E_s , and strain-hardening ratio b of reinforcement are treated as unknown variables and the other empirical parameters controlling the curvature of the hysteretic loops are assumed as known constants. Therefore, there are 9 unknown material parameters in each zone, and

27 material parameters of the entire structure need to be identified. The initial value of material parameters used in this example are listed in Table 5.1. 10% random errors are added in the material parameters to simulate the uncertainty in the material parameters.

First, the acceleration responses under earthquake loading are used for this study. Figure 5.6 compares the computational time and relative errors from the proposed decentralized method and global model updating method. The global model updating method is based on classic Newton method or so-called sensitivity-based model updating method (Lu and Law, 2007a). In the decentralized method, the results converge to the true values after around 24 iterations (about 200 mins), while in the global method the results converge to its true values after around 15 iterations (500 mins). From these results, we can find that the Newton method converges fast and requires fewer iteration steps since this method has a second order convergence rate (Ortega and Rheinboldt, 1970). Both methods finally converge to the true values. However, the decentralized method requires less computation time. Figure 5.7 compares the identified results using the decentralized method with the true values. The identified results match the true values well, which could verify the accuracy of the proposed method for the identification of material parameters.

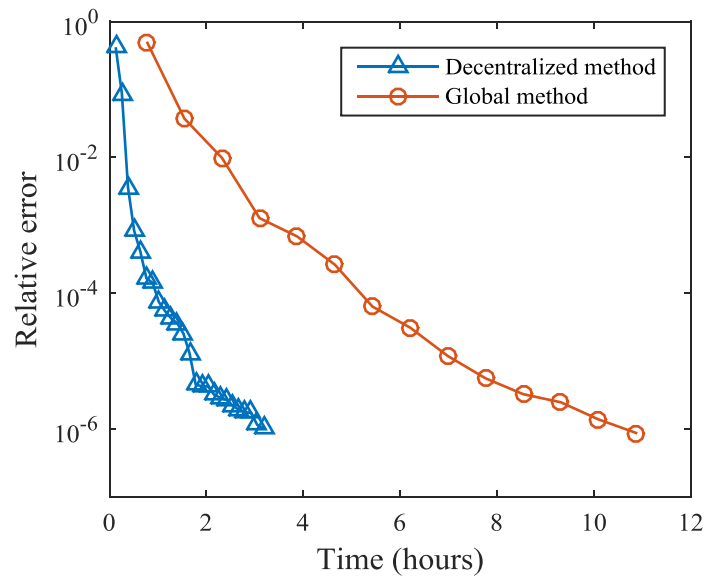
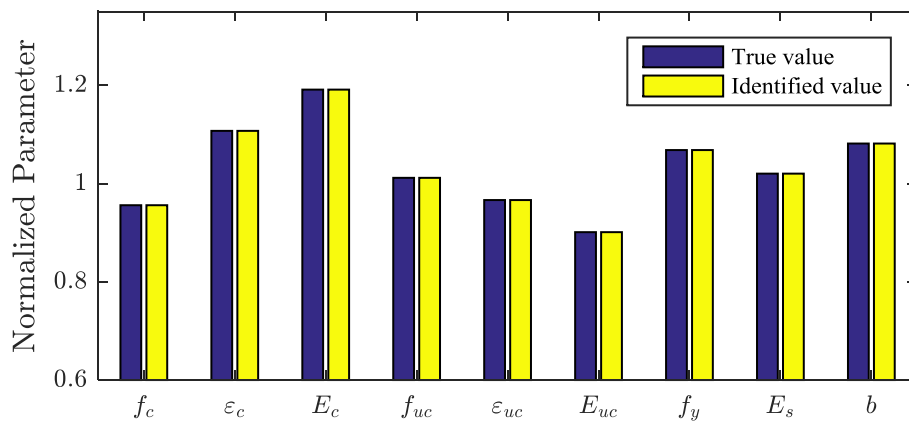
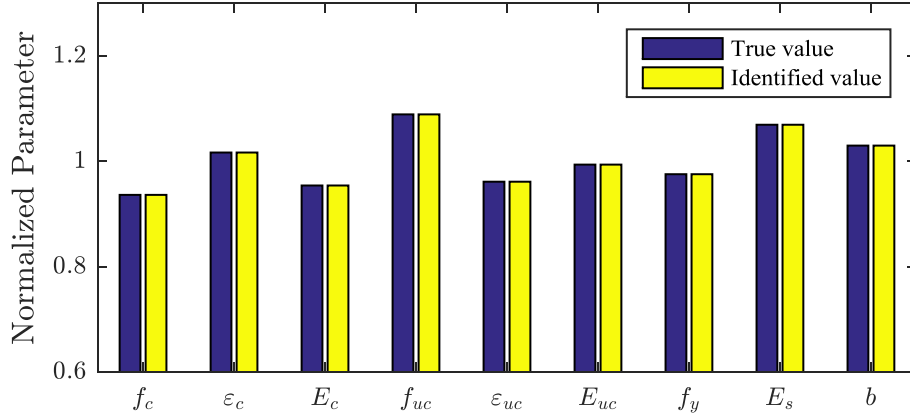


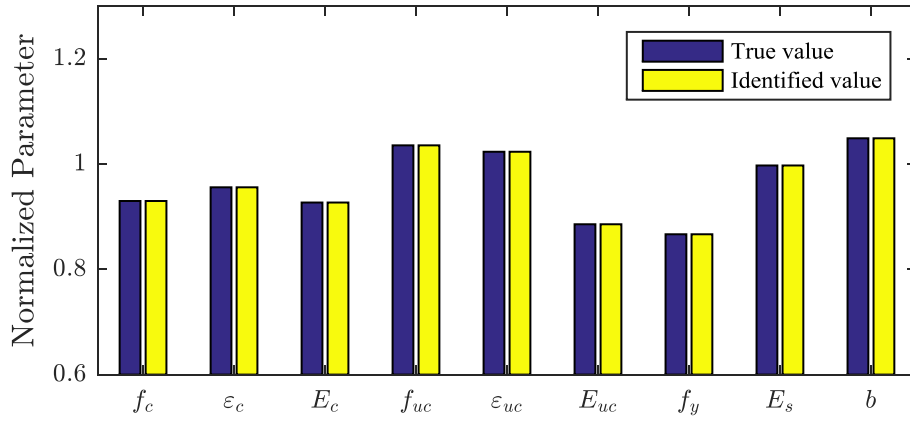
Figure 5.6 Comparison of the computation time of global method and decentralized method



(a) Subset 1



(b) Subset 2



(c) Subset 3

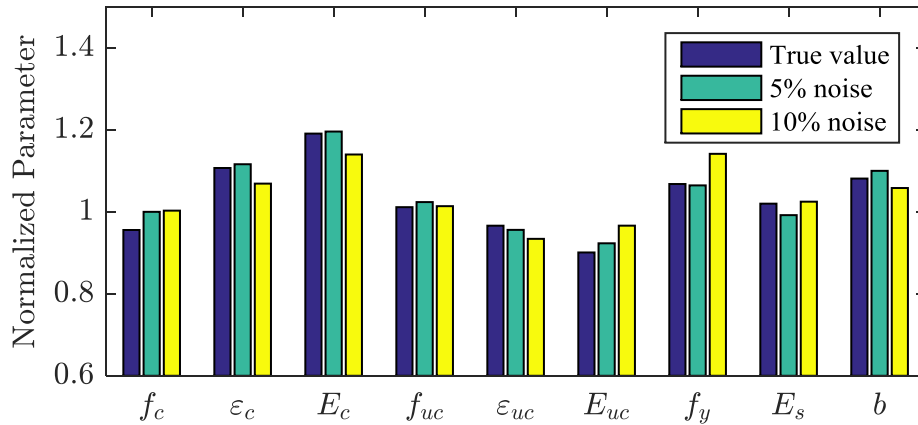
Figure 5.7 Identified results of reinforcement concrete structure

The effect of measurement noise on the identified results is considered. 5% and 10% measurement noise are studied. The polluted acceleration responses are simulated by adding a random component to the actual responses as

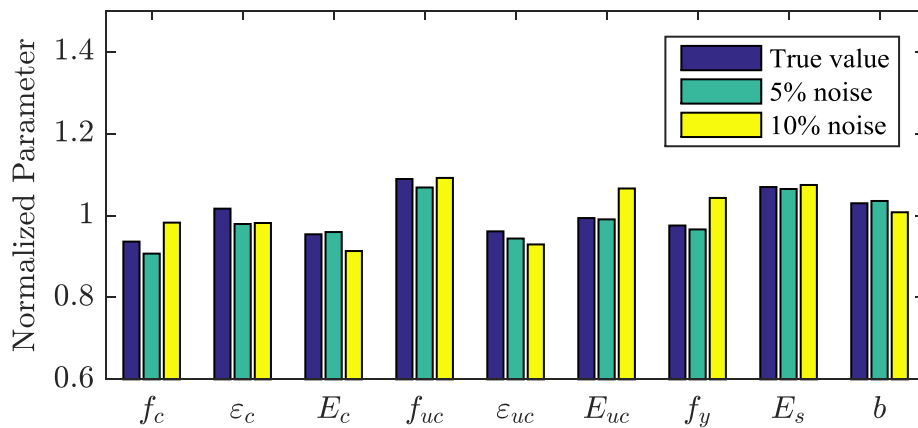
$$\ddot{\mathbf{x}}_{mea} = \ddot{\mathbf{x}} + E_p N_{noise} \sigma(\ddot{\mathbf{x}}) \quad (5.22)$$

where E_p is percentage of the noise level, N_{noise} is a standard normal distribution vector with zero mean and unit standard deviation, and $\sigma(\ddot{\mathbf{x}})$ is the standard deviation of the actual acceleration response.

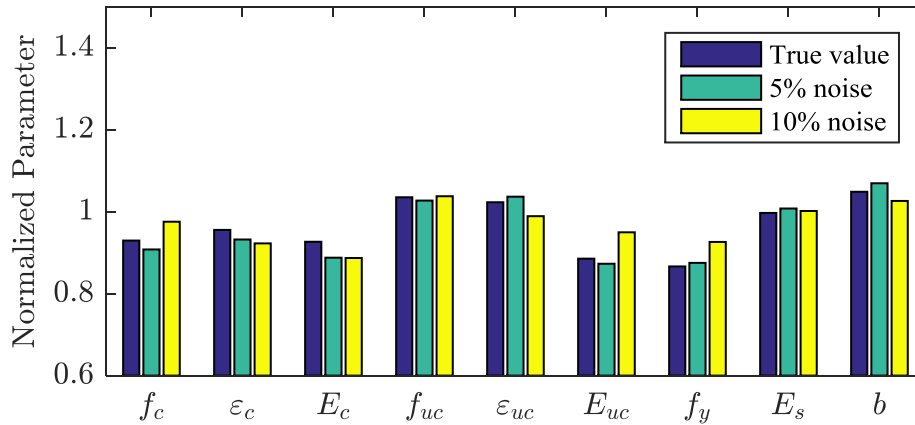
Figure 5.8 shows the identified normalized parameters of each subset with different noise levels. The error increases, in general, as the noise level increases. When 5% measurement noise is considered, some larger identification errors are 3.64% (f_c in subset 1), 4.45% (ε_c in subset 2), and 4.21% (E_c in subset 3). The other errors are very small. When 10% measurement noise is considered, the larger errors are 7.26% (E_{uc} in subset 1), 5.72% (b in subset 2), and 6.48% (ε_{uc} in subset 3). These identified results can verify the robustness of the proposed method.



(a) Subset 1



(b) Subset 2



(c) Subset 3

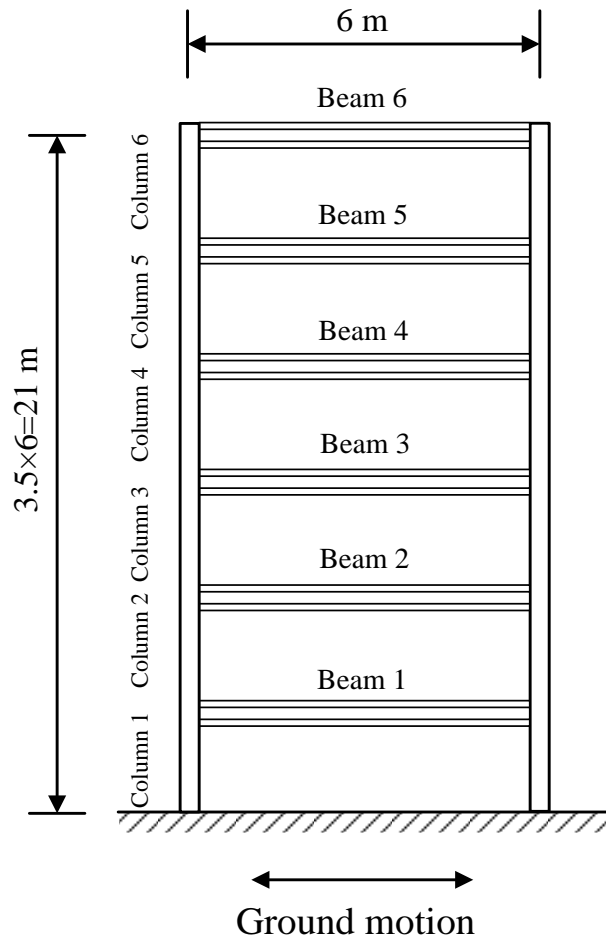
Figure 5.8 Identified material parameter of reinforcement concrete structure using noisy measurement data

5.3.2 A steel frame

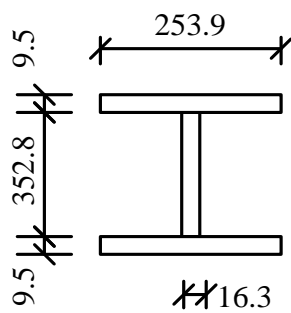
A 2D one-bay six-floor steel frame structure is employed in this section. The dimensions of the frame structure model are shown in Figure 5.9(a). The height of each floor is 3.5 m and the width of the building is 6 m. The beams of frame are made of W14×61 wide flange beam, while the columns of each floor have the same section with a width of 400 mm and a thickness of 8 mm. The cross sections of the column and beam are shown in Figures. 5.9 (b) and (c), respectively. The beams and columns are welded together to form rigid joints. The bottom of the frame is fixed on the strong floor. The column and beam at each floor are further divided into five elements. The structural elements are modelled with displacement-based fiber-section beam-column elements. Therefore, the finite element model of the structure consists of 86 nodes, 90 elements, and 258 DOFs, as shown in Figure 5.10. The constitutive behavior of steel

material is simulated with the uniaxial Menegotto-Pinto steel material (Barbato and Conte, 2006). The initial yield stress f_y , and Young's modulus E_s in the constitutive model of each column/beam are treated as unknown variables to be identified. Therefore, 4 unknown material parameters in each floor and totally 6×4 unknown material parameters will be identified. The initial material parameters used in this example are listed in Table 5.2. 10% model error is considered in the material parameters for this study.

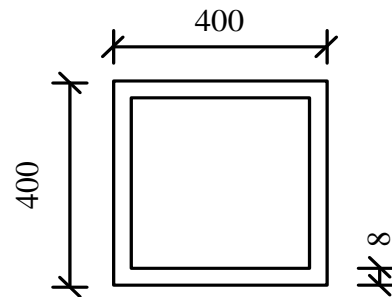
The dynamic responses of the building under earthquake loading are computed from the nonlinear finite element model. The time history of El-Centro earthquake (PGA=0.8g) is selected as the ground motion input. The sampling frequency is 1000 Hz. Totally, six accelerometers are installed in this structure to measure the responses of each floor. The sensors locations are selected at the beam and column joints as illustrated in Figure 5.10 and horizontal responses are recorded. The structure is divided into two zones. Based on the proposed method, the measurements are also divided into two subsets. The first subset of measurements contains the acceleration responses from 1st~3rd floor and the second subset of measurements contains the responses from 4st~6th floor. In the processing of model updating, each subset of response is used to update the corresponding material parameters in the same zone. The first 50 second vibration responses are used for model updating.



(a) dimension of reinforced concrete structure



(b) Cross section of beam (unit: mm)



(c) Cross section of column (unit: mm)

Figure 5.9 Dimension of the steel structure

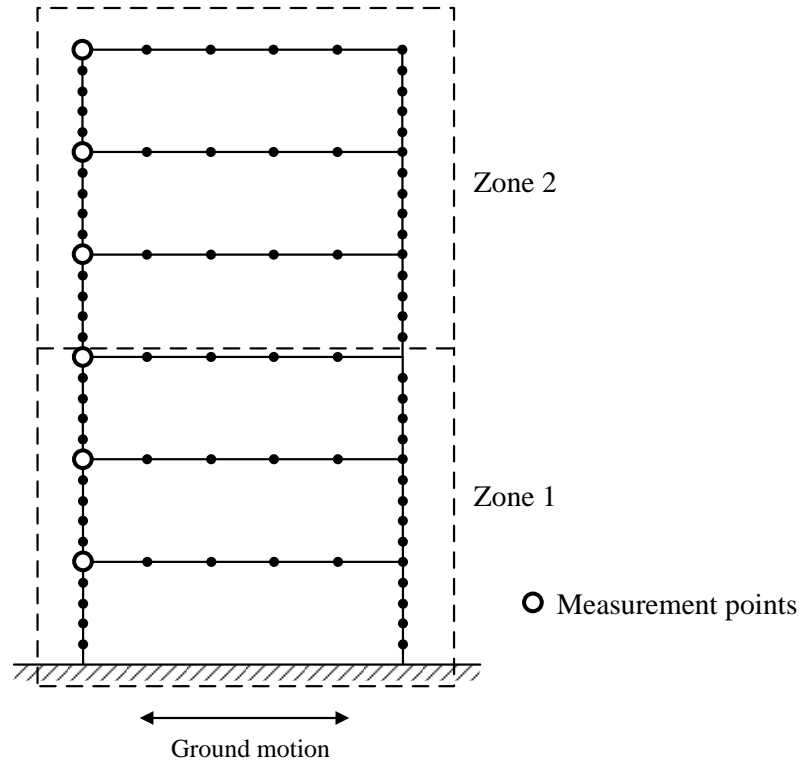


Figure 5.10 Finite element of the steel structure

Table 5.2 Material parameters of the steel structure

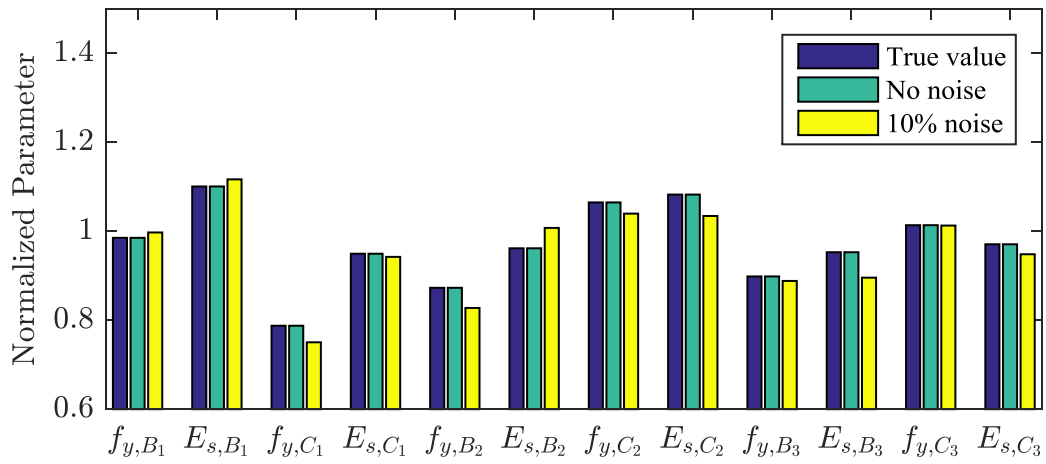
Member	Initial yield stress (f_y , MPa)	Young's modulus (E_s , GPa)	Strain-hardening ratio
Column 1~2	350	210	0.02
Beam 1~2			
Column 3~4	300	210	0.02
Beam 3~4			
Column 5~6	200	210	0.02
Beam 5~6			

The model updating results using the real measurement data are shown in Figure 5.11.

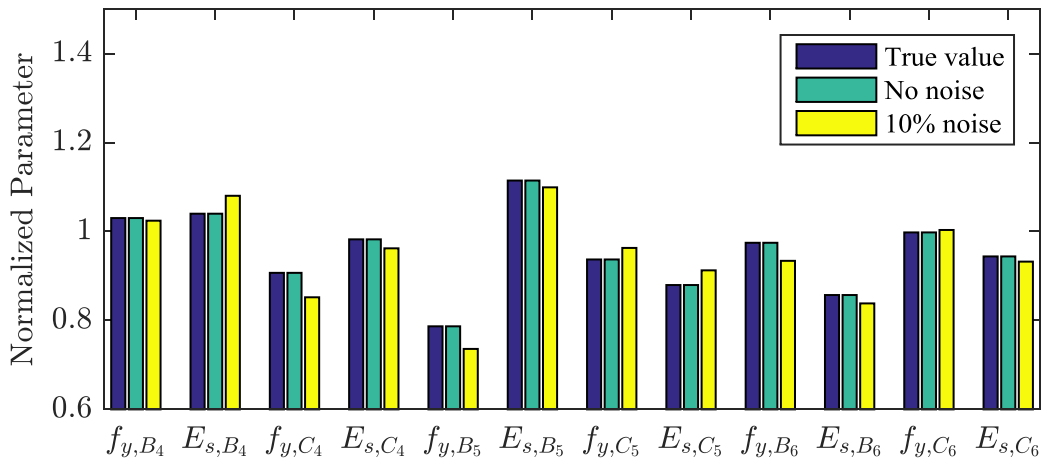
Again, the accuracy of the proposed decentralized model updating method is verified.

The identified normalized parameters without considering measurement noise match their true value well. When 10% noise is added in the actual responses, some identification errors occur. The largest identification error is 5.72% ($E_{s, B3}$) in Subset 1 and 5.49% ($f_{y, C4}$) in Subset 2. It should be noted that in this example, because the input ground motion is known, the identification error is smaller than that of output. Also, the number of iterations for model updating is small. Figure 5.12 shows the identify errors with computational time. It takes about 30 iterations for the decentralized method, while only 24 for the global model updating. The computational time for the decentralized method and global method is 6 hours and 12 hours, respectively. These results show the accuracy and robustness of the proposed method, again.

The proposed method can identify the material parameters with the nonlinear vibration responses. When the amplitude value of earthquake is low, most parts of the structure is still in the linear elastic stage. The dynamic response may insensitive to the material parameters. Figure 5.13 shows the results with different level of earthquake (PGA=0.6g, 0.8g, 1g). The results in the case of PGA=0.8g, and 1g match well with their true values. However, the results from a lower amplitude value of earthquake (PGA=0.6g) are different. The results of subset 1 from PGA=0.6g converge to their true vales, while the results of Subset 2 cannot converge to their true vales. The response sensitivity with respect to the yield stress $f_{y, B6}$ with different level of earthquake input are shown in Figure 5.14. The response sensitivity is too small when PGA= 0.6g, which may lead to the wrong identification results.



(a) Subset 1



(b) Subset 2

Figure 5.11 Normalized identified results of steel structure

(note: $f_{y, Bi}$ and $f_{y, Ci}$ mean the yield stress of the beam and column at i -th floor, respectively; $E_{s, Bi}$ and $E_{s, Ci}$ mean the Young's modulus of the beam and column at i -th floor, respectively)

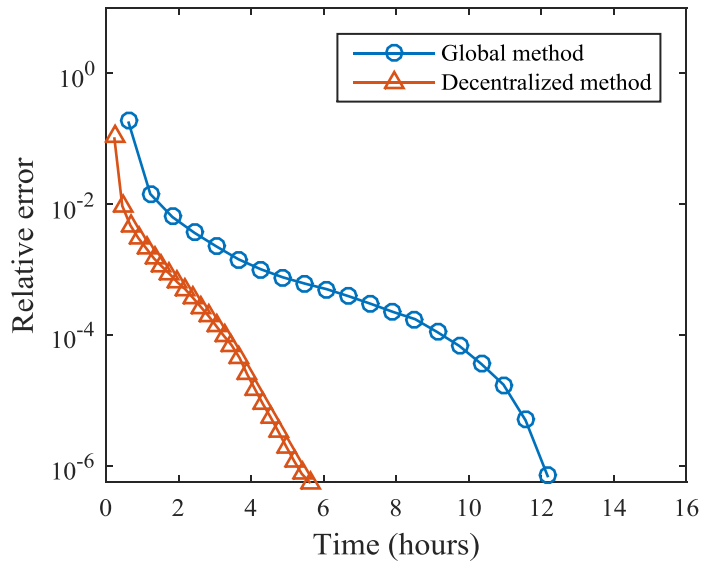
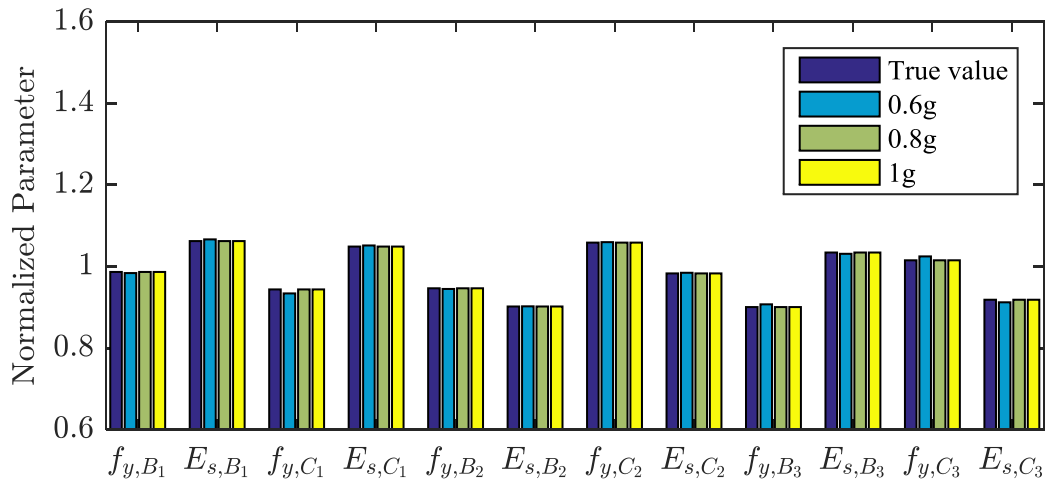
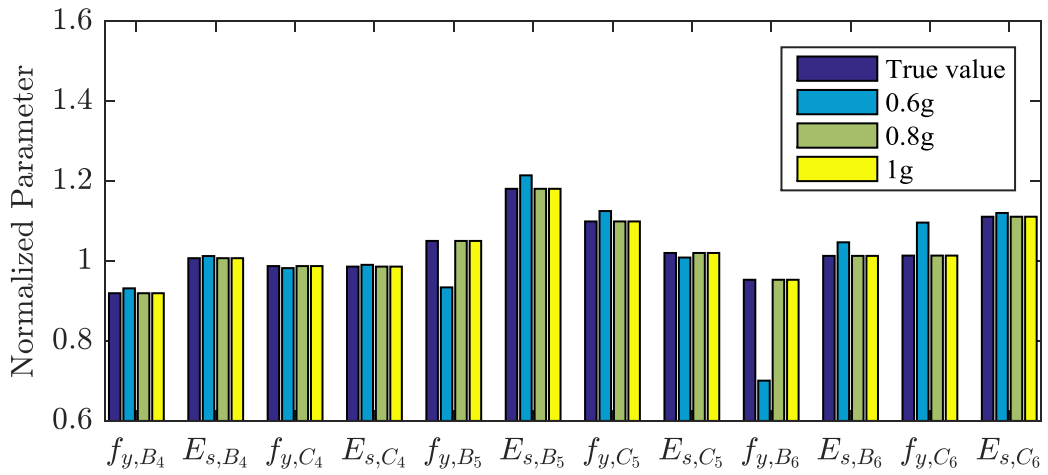


Figure 5.12 Comparison of computational time of steel structure with global method and decentralized method



(a) Subset 1



(b) Subset 2

Figure 5.13 Normalized identification results with different level of earthquake loading

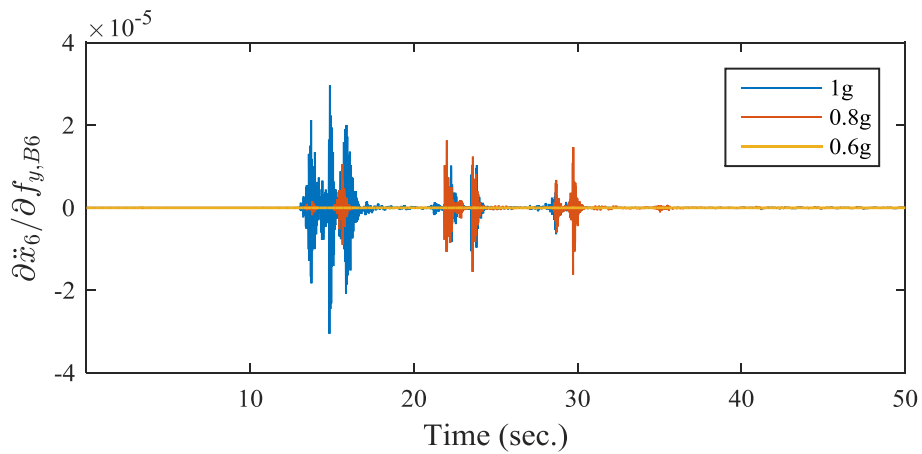


Figure 5.14 The sensitivity acceleration response at the top floor with respect to f_{y,B_6} at the top floor

5.4 Summary

In this chapter, a decentralized nonlinear model updating technique is proposed for civil infrastructure under earthquake loading. The nonlinear dynamic behavior of the structure is calculated based on a distributed plastic model. When the nonlinear dynamic responses are recorded, the material parameters in the constitutive model can be updated with the proposed method. The dynamic response sensitivity with respect to the material parameters is derived based on the direct difference method. Two numerical structures subjected to seismic input are used to verify the accuracy of the proposed method. One is a three-floor reinforcement concrete structure, and the other is a six-floor steel frame structure. Results show that the nonlinear parameters in the material constitutive model (such as, compressive strength f_c , concrete strain at maximum strength ε_c , initial tangent stiffness E_c , etc.) can be identified with high accuracy when 10% of the noise is considered. Comparison studies with the global model updating technique are also investigated. The results show that the proposed method can identify the unknown material parameters with less computational time than the global model updating method.

CHAPTER 6

CORRELATION FUNCTION BASED DAMAGE

DETECTION

6.1 Introduction

The following two chapters, we focus on developing time domain damage detection methods for civil structures under multiple unknown excitations. The time domain methods use the measured time history responses directly for structural damage detection. The error between the calculated dynamic responses (such as acceleration) and measured counterparts is minimized. Several methods, such as quadratic sum-squares error method (Yang *et al.*, 2009a), extended Kalman filter method (Yang *et al.*, 2006b; Lei *et al.*, 2012a), and least-squares method (Yang *et al.*, 2007b), etc. have been proposed for damage detection using acceleration responses. The output-only methods are more promising for damage detection under ambient excitations, because the ambient excitations (for example, wind loading) are usually difficult to measure. The wind loading of high-rise buildings and long span bridges are usually stationary and can

be approximated as ergodic and band-limited Gaussian noise processes (Shinozuka *et al.*, 1976; Quek *et al.*, 1999). However, the existing output-only methods require that the number of sensors should be larger than the total number of unknown excitations and the measurements (sensors) must be available at the DOFs where the external excitations act (Yang *et al.*, 2007a; Lei *et al.*, 2012a). These limitations are the necessary conditions for the existence of the analytical recursive solution (Lei *et al.*, 2012a), which discourages the use of most existing algorithms for a practical structure, and a new method for damage detection without these limitations should be developed.

Recently, the correlation-function based damage detection methods have been developed. Several studies have been explored (Yang *et al.*, 2007c; Yang *et al.*, 2009b; Li and Law, 2010; Wang *et al.*, 2010). In this chapter, a correlation function-based damage detection method is proposed for civil structures under multi-excitations without above mentioned limitations. The correlation function under multiple excitations is derived as two parts. One is associated with the UIR function that depends on structural parameters. The other is a constant part that depends on the energy of the excitation force. The structural parameters are then obtained through the model updating technique. Numerical and experimental studies are performed to demonstrate the effectiveness of the proposed method. Results show that the proposed method can identify the structural damage when the number of sensors is less than the total number of unknown excitations. Also, the responses at the force location are not necessary to be measured.

6.2 Correlation Function of Vibration Response

6.2.1 Correlation function of response under single white noise excitation

The equation of motion of a damped structural system is given as

$$\mathbf{M}\ddot{\mathbf{x}}(t) + \mathbf{C}\dot{\mathbf{x}}(t) + \mathbf{K}\mathbf{x}(t) = \mathbf{B}f(t) \quad (6.1)$$

where \mathbf{M} , \mathbf{C} , and \mathbf{K} are the $N \times N$ mass, damping, and stiffness matrices, respectively; $f(t)$ is the excitation force; and \mathbf{B} is the mapping vector with 1 at the excitation location and 0 at others. $\mathbf{x}(t)$, $\dot{\mathbf{x}}(t)$, and $\ddot{\mathbf{x}}(t)$ are the $N \times 1$ displacement, velocity, and acceleration vectors, respectively. Assume that the structure has zero initial conditions and excitation force $f(t)$ is a white noise process.

The acceleration response of the structure at i -th DOF can be expressed as

$$\ddot{x}_i(t) = \int_{-\infty}^{\infty} \ddot{h}_i(t-\tau) f(\tau) d\tau \quad (6.2)$$

where $\ddot{h}_i(t-\tau)$ is the UIR function at i when the structure is subjected to a unit impulse force.

Let $R_{ij}(\tau)$ denote the correlation function of the accelerations at the i -th and j -th DOFs of the system, which can be written as follows (Bendat and Piersol, 1980; Li and Law, 2008):

$$R_{ij}(\tau) = E \left[\int_{-\infty}^t \ddot{h}_i(t - \mu_1) f(\mu_1) d\mu_1 \int_{-\infty}^{t-\tau} \ddot{h}_j(t - \tau - \mu_2) f(\mu_2) d\mu_2 \right] \quad (6.3)$$

where μ_1 and μ_2 are the small time variations. With the assumption of white noise excitation, the above equation can be rewritten as

$$R_{ij}(\tau) = \int_{-\infty}^t \int_{-\infty}^{t-\tau} \ddot{h}_i(t - \mu_1) \ddot{h}_j(t - \tau - \mu_2) E[f(\mu_1) f(\mu_2)] d\mu_1 d\mu_2 \quad (6.4)$$

The auto-correlation function of $f(t)$ is

$$E[f(\mu_1) f(\mu_2)] = S \delta(\mu_1 - \mu_2) \quad (6.5)$$

where S is a constant defining the excitation energy, and δ is the Dirac delta function.

When $\mu_1 = \mu_2$, Eqs. (6.4) and (6.5) give (Li and Law, 2008)

$$R_{ij}(\tau) = S \int_0^{+\infty} \ddot{h}_i(t) \ddot{h}_j(t - \tau) dt \quad (6.6)$$

Define

$$H_{ij}(\boldsymbol{\theta}) = \int_0^{+\infty} \ddot{h}_i(t) \ddot{h}_j(t - \tau) dt \quad (6.7)$$

Eq. (6.7) is the function of structural physical parameters only. $\boldsymbol{\theta}$ is a vector consisting of the stiffness parameters of each element. Consequently, Eq. (6.6) can be written as

$$R_{ij}(\tau) = H_{ij}(\boldsymbol{\theta}) S \quad (6.8)$$

Eq. (6.8) indicates that the correlation function depends only on structural parameters $H_{ij}(\boldsymbol{\theta})$ and constant S .

6.2.2 Correlation function of response under unit impulse excitation

Instrumented hammers have likewise been widely used in laboratory experiments. The excitation force can be described as a large constant force lasting a very short time duration as

$$f(t) = \begin{cases} A\delta(t), & 0 \leq t \leq \varepsilon \\ 0, & \text{else} \end{cases} \quad (6.9)$$

where A is a constant, and ε is the impulse duration.

Substituting Eq. (6.9) into Eq. (6.2), the acceleration response of the structure can be expressed as

$$\ddot{x}_i(t) = A \int_0^{\infty} \ddot{h}_i(t-\tau) \delta(\tau) d\tau \quad (6.10)$$

According to the property of Dirac delta function,

$$\ddot{x}_i(t) = A\ddot{h}_i(t) \quad (6.11)$$

Therefore, the correlation function $R_{ij}(\tau)$ can be written as

$$\begin{aligned} R_{ij}(\tau) &= \int_0^{+\infty} \ddot{x}_i(t) \ddot{x}_j(t-\tau) dt \\ &= \int_0^{+\infty} A\ddot{h}_i(t) A\ddot{h}_j(t-\tau) dt \\ &= A^2 \int_0^{+\infty} \ddot{h}_i(t) \ddot{h}_j(t-\tau) dt \end{aligned} \quad (6.12)$$

The correlation functions under a impulse excitation and a white noise excitation have the similar form as shown in Eq. (6.6) and Eq. (6.12), respectively. The UIR function $\ddot{h}_i(t)$ in both cases can be obtained in Eq. (6.1), where $f(t)$ is a Dirac delta function. The function can be regarded as a free vibration state with some specific initial conditions. Assuming that the system is initially in static equilibrium, the UIR function can be calculated using the Newmark method (Li *et al.*, 2013):

$$\begin{cases} \mathbf{M}\ddot{\mathbf{h}}(t) + \mathbf{C}\dot{\mathbf{h}}(t) + \mathbf{K}\mathbf{h}(t) = \mathbf{0} \\ \mathbf{h}(0) = \mathbf{0}, \dot{\mathbf{h}}(0) = \mathbf{M}^{-1}\mathbf{B} \end{cases} \quad (6.13)$$

where $\mathbf{h}(t)$, $\dot{\mathbf{h}}(t)$ and $\ddot{\mathbf{h}}(t)$ are the unit impulse displacement, velocity and acceleration vectors, respectively.

6.2.3 Correlation function of response under multiple excitations

Previous studies usually considered single excitation only. However, practical structures are generally subjected to external forces applied at multiple points. Multiple white noise or impulse excitations are investigated in this section. The equation of motion of an N -DOF damped structural system under multiple excitations is given as

$$\mathbf{M}\ddot{\mathbf{x}}(t) + \mathbf{C}\dot{\mathbf{x}}(t) + \mathbf{K}\mathbf{x}(t) = \sum_{i=1}^{nf} \mathbf{B}_i f_i(t) \quad (6.14)$$

where $f_i(t)$ is the i -th excitation force, \mathbf{B}_i is the mapping vector corresponding to excitation $f_i(t)$, and nf is the number of excitations.

The responses under the multiple excitations can be written as the superposition of those under single excitation. That is,

$$\ddot{\mathbf{x}}_i(t) = \ddot{\mathbf{x}}_{i,1}(t) + \ddot{\mathbf{x}}_{i,2}(t) + \cdots + \ddot{\mathbf{x}}_{i,nf}(t) = \sum_{p=1}^{nf} \ddot{\mathbf{x}}_{i,p}(t) \quad (6.15)$$

where $\ddot{\mathbf{x}}_{i,p}(t)$ is the response at the i -th DOF under the p -th single excitation force.

Let $R_{\ddot{x}_i, \ddot{x}_j}(\tau)$ denote the cross-correlation function of the accelerations at the i -th and j -th DOFs of the system under the multiple excitations. It can be written as

$$R_{\ddot{x}_i, \ddot{x}_j}(\tau) = R_{(\ddot{x}_{i,1} + \ddot{x}_{i,2} + \dots + \ddot{x}_{i,nf})(\ddot{x}_{j,1} + \ddot{x}_{j,2} + \dots + \ddot{x}_{j,nf})}(\tau) = \sum_{p=1}^{nf} \sum_{q=1}^{nf} R_{\ddot{x}_{i,p}, \ddot{x}_{j,q}}(\tau) \quad (6.16)$$

and

$$R_{\ddot{x}_{i,p}, \ddot{x}_{j,q}}(\tau) = \int_{-\infty}^t \int_{-\infty}^{t-\tau} \ddot{h}_{i,p}(t-\mu_1) \ddot{h}_{j,q}(t-\tau-\mu_2) E[f_p(\mu_1) f_q(\mu_2)] d\mu_1 d\mu_2 \quad (6.17)$$

where $\ddot{h}_{i,p}$ is the UIR function at i -th DOF under excitation at location p .

The excitations are uncorrelated and, consequently, $E[f_p(\mu_1) f_q(\mu_2)] = 0$ ($p \neq q$). This leads to

$$R_{\ddot{x}_{i,p}, \ddot{x}_{j,q}}(\tau) = 0 \quad (p \neq q). \quad (6.18)$$

Therefore, Eq. (6.16) can be expressed as

$$R_{\ddot{x}_i, \ddot{x}_j}(\tau) = \sum_{p=1}^{nf} R_{\ddot{x}_{i,p}, \ddot{x}_{j,p}}(\tau) \quad (6.19)$$

As discussed in Section 6.1.1, the auto-correlation function of $f_p(t)$ is

$$E[f_p(\mu_1) f_p(\mu_2)] = S_p \delta(\mu_1 - \mu_2) \quad (6.20)$$

Then,

$$R_{\ddot{x}_{i,p}, \ddot{x}_{j,p}}(\tau) = S_p H_{ij,p} \quad (6.21)$$

and

$$H_{ij,p} = \int_0^{+\infty} \ddot{h}_{i,p}(t) \ddot{h}_{j,p}(t-\tau) dt \quad (6.22)$$

Define

$$\mathbf{H}_{ij}(\boldsymbol{\theta}) = [H_{ij,1}, H_{ij,2}, \dots, H_{ij,p}, \dots, H_{ij,nf}] \quad (6.23)$$

$$\mathbf{s} = [S_1, S_2, \dots, S_p, \dots, S_{nf}]^T \quad (6.24)$$

Eq. (6.19) can then be further simplified as

$$R_{\ddot{x}_i, \ddot{x}_j}(\tau) = \sum_{p=1}^{nf} S_p H_{ij,p} = \mathbf{H}_{ij}(\boldsymbol{\theta}) \mathbf{s} \quad (6.25)$$

The correlation functions between responses at different points can be expressed as

$$\mathbf{R}(\tau) = \mathbf{H}(\boldsymbol{\theta}) \mathbf{s} = \mathbf{R}(\boldsymbol{\theta}, \mathbf{s}) \quad (6.26)$$

In practice, the correlation function of accelerations can be obtained as a discrete inverse Fourier transform of the cross-spectral density function, while the latter is computed directly from the vibration data (Caicedo *et al.*, 2004).

6.3 Damage Detection Using Correlation Function

The above sections show that the correlation function of acceleration responses, regardless of whether under single or multiple excitations, can be written as the product of a constant and a function of structural parameters. A damage detection method based on the correlation function is proposed in this section.

Assuming that structural damage is in the form of a change in the structural stiffness, the stiffness matrix of the damaged structure can then be expressed as

$$\mathbf{K}^d = \sum_{i=1}^{ne} (1 - \alpha_i) \mathbf{K}_i \quad (6.27)$$

where K_i is the stiffness matrix of the i -th element in the intact state, α_i ($0 \leq \alpha_i \leq 1$) is defined as the stiffness fraction to the intact stiffness of the i -th element, and ne is the total number of elements in the structure. $\alpha_i = 1$ denotes that the element loses its stiffness completely, whereas $\alpha_i = 0$ indicates that the element is intact. The nonzero value of α_i denotes the damage at element i .

The problem of system identification with correlation function is to determine the system parameters $\boldsymbol{\theta} = [\alpha_1, \alpha_2, \dots, \alpha_{ne}]$ from the measured correlation function using the model updating technique. The objective function for model updating is defined as the difference between the measured and calculated correlation functions

$$J(\boldsymbol{\theta}) = \|\mathbf{R}_{mea}(\boldsymbol{\theta}) - \mathbf{R}_{cal}(\boldsymbol{\theta})\| \quad (6.28)$$

where \mathbf{R}_{mea} is the measured correlation functions and \mathbf{R}_{cal} is the corresponding correlation functions calculated from the finite element model.

A two-stage method is employed in model updating. In the first stage, constant coefficient part s can be estimated from Eq. (6.26) as

$$s = \mathbf{H}(\boldsymbol{\theta})^+ \mathbf{R}_{mea} \quad (6.29)$$

given the initial value of $\boldsymbol{\theta}$, where $\mathbf{H}(\boldsymbol{\theta})^+$ is the pseudo-inverse of $\mathbf{H}(\boldsymbol{\theta})$.

In the second stage, the correlation function can be expressed as a first-order Taylor expansion (Lu and Law, 2007b)

$$\Delta \mathbf{R} = \mathbf{R}_{mea} - \mathbf{R}_{cal} = \frac{\partial \mathbf{R}_{cal}}{\partial \boldsymbol{\theta}} \Delta \boldsymbol{\theta} + O(\Delta \boldsymbol{\theta}^2) \quad (6.30)$$

$$\frac{\partial \mathbf{R}_{cal}}{\partial \boldsymbol{\theta}} = \left[\frac{\partial \mathbf{R}_{cal}}{\partial \alpha_1}, \frac{\partial \mathbf{R}_{cal}}{\partial \alpha_2}, \dots, \frac{\partial \mathbf{R}_{cal}}{\partial \alpha_i}, \dots, \frac{\partial \mathbf{R}_{cal}}{\partial \alpha_{ne}} \right] \quad (6.31)$$

The high order terms $O(\Delta\boldsymbol{\theta}^2)$ are small and can be ignored. $\partial \mathbf{R}_{cal}/\partial \boldsymbol{\theta}$ is the sensitivity matrix of the correlation function with respect to the structural parameters, which can be obtained using the Newmark method (Li and Law, 2008) or the forward difference method (Morton and Mayers, 2005) as

$$\begin{aligned} \frac{\partial \mathbf{R}_{cal}}{\partial \alpha_i} &= \lim_{\varphi \rightarrow 0} \frac{\mathbf{R}_{cal}([\alpha_1, \alpha_2, \dots, \alpha_i + \varphi, \dots, \alpha_{ne}], s) - \mathbf{R}_{cal}([\alpha_1, \alpha_2, \dots, \alpha_i, \dots, \alpha_{ne}], s)}{\varphi} \\ &= \frac{\mathbf{R}_{cal}([\alpha_1, \alpha_2, \dots, \alpha_i + \varphi, \dots, \alpha_{ne}], s) - \mathbf{R}_{cal}([\alpha_1, \alpha_2, \dots, \alpha_i, \dots, \alpha_{ne}], s)}{\varphi} \end{aligned} \quad (6.32)$$

where φ is the difference step for the finite difference method.

Eq. (6.30) can be solved by the damped least-squares method as

$$\Delta \boldsymbol{\theta} = \left[\left(\frac{\partial \mathbf{R}_{cal}}{\partial \boldsymbol{\theta}} \right)^T \left(\frac{\partial \mathbf{R}_{cal}}{\partial \boldsymbol{\theta}} \right) + \lambda \right]^{-1} \left(\frac{\partial \mathbf{R}_{cal}}{\partial \boldsymbol{\theta}} \right)^T \Delta \mathbf{R} \quad (6.33)$$

where λ is the non-negative optimal regularization parameter determined by the L-curve method (Tikhonov *et al.*, 1995).

The above correlation function-based damage detection procedure can be summarized as follows:

Step 1: Measure the structural responses under ambient white noise excitations or impulse excitations, and calculate the correlation functions.

Step 2: Set the initial values of the structural parameters $\boldsymbol{\theta}^0 = [\alpha_1^0, \alpha_2^0, \dots, \alpha_{ne}^0]$.

Step 3: Calculate $\mathbf{H}(\boldsymbol{\theta})$ from Eq. (6.23) and estimate constant value s from Eq. (6.29).

Step 4: Calculate the correlation function from Eq. (6.26) and the sensitivity matrix from Eq. (6.32).

Step 5: Update the structural parameters from $\boldsymbol{\theta}^{n+1} = \boldsymbol{\theta}^n + \Delta\boldsymbol{\theta}$, where $\Delta\boldsymbol{\theta}$ is obtained from Eq. (6.33).

Step 6: Repeat steps 3 to 5 until the following convergence condition in Eq. (6.34) is satisfied, where the tolerance in this paper is set to 10^{-5} in this study

$$\frac{\|\boldsymbol{\theta}^{n+1} - \boldsymbol{\theta}^n\|}{\|\boldsymbol{\theta}^{n+1}\|} \times 100\% \leq Tol \quad (6.34)$$

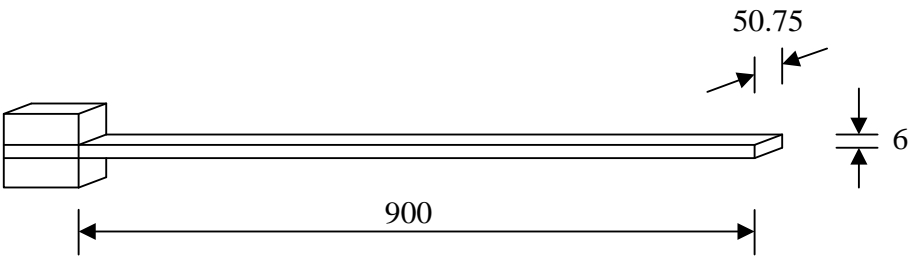
Step 7: For damage detection, the measurement responses before and after damage are both available. The stiffness parameters can be updated with these two sets of measurements. The structural damage then can be identified by comparing the changes in the element stiffness parameters.

6.4 Numerical Study

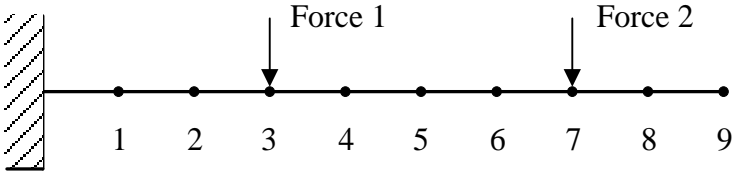
The steel cantilever beam (Hao and Xia, 2002) as shown in Figure 6.1 is used for the numerical study. The size of the cross-section is 50.75 mm×6.0 mm, and the mass density is 7.67×10^3 kg/m³. The structure is modeled with nine Euler–Bernoulli beam elements (i.e., $ne=9$). The initial Young's modulus in the intact state is 2.0×10^{11} N/m².

The structure is subjected to two white noise excitations as shown in Figure 6.1. One force is applied at Node 3 and the other at Node 7, both in the vertical direction. The force is assumed with a zero mean and unit standard deviation. The dynamic responses

computed from Eq. (6.1) are taken as the actual responses for the following studies. The sampling frequency was 1000 Hz and 1 hours force vibration responses are recorded. The auto/cross-correlation function is calculated from the measured responses, and the first 100 data of auto/cross-correlation function are selected for the numerical study.



(a) Configuration of the beam specimen (unit: mm)



(b) Finite element model of the cantilever beam

Figure 6.1 Cantilever beam

6.4.1 Structural stiffness identification

The real elastic modulus of the structural material is simulated by adding a random variation to the ideal ones (i.e., 2.0×10^{11} N/m²). The random variation has a normal distribution, with 10% standard deviation of its initial value. The cross-correlation function of accelerations at Nodes 4 and 6 ($R_{4,6}$) is used for system identification.

The real stiffness parameter of each element is identified using the proposed two-stage model updating technique. The initial value of the stiffness parameters for iteration are set the same at 2×10^{11} , as shown in Figure 6.2. The model updating results converge approximately after 10 iterations. The final identified stiffness parameters highly agree with the true values accurately without any false alarm, as shown in Figure 6.3. These results show the proposed output only method can identify the structural parameters. Moreover, the measurement at the force locations is not required.

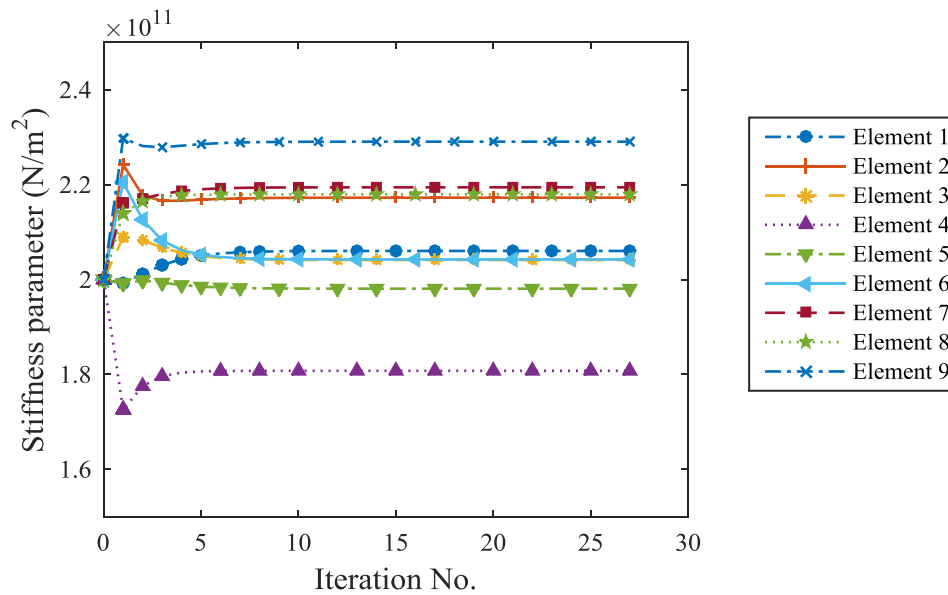


Figure 6.2 Evolution of identification results of the cantilever beam

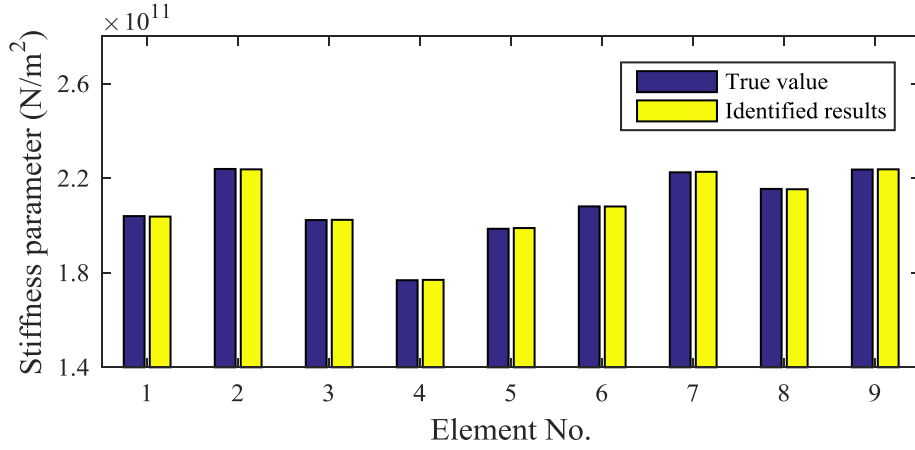


Figure 6.3 Model updating results without measurement noise

6.4.2 Effect of measurement noise

Random noise is added to the measured response to simulate the uncertainty of the measurements as

$$\ddot{\mathbf{x}}_{mea} = \ddot{\mathbf{x}} + E_p N_{noise} \sigma(\ddot{\mathbf{x}}) \quad (6.35)$$

where E_p is the percentage noise level, N_{noise} is the standard normal distribution vector with zero mean and unit standard deviation, and $\sigma(\ddot{\mathbf{x}})$ is the standard deviation of the actual acceleration response.

10% and 20% random noise are respectively added to the actual responses. Figure 6.4 shows the identified stiffness parameters under different noise levels. The maximum relative error was 1.1% at Element 2 for the case of 10% noise and 2.7% at Element 9 for the case of 20% noise. The results are satisfactory even when 20% noise is included.

These results show that the proposed method is insensitive to the measurement noise.

The effect of the measurement noise is analyzed as follows.

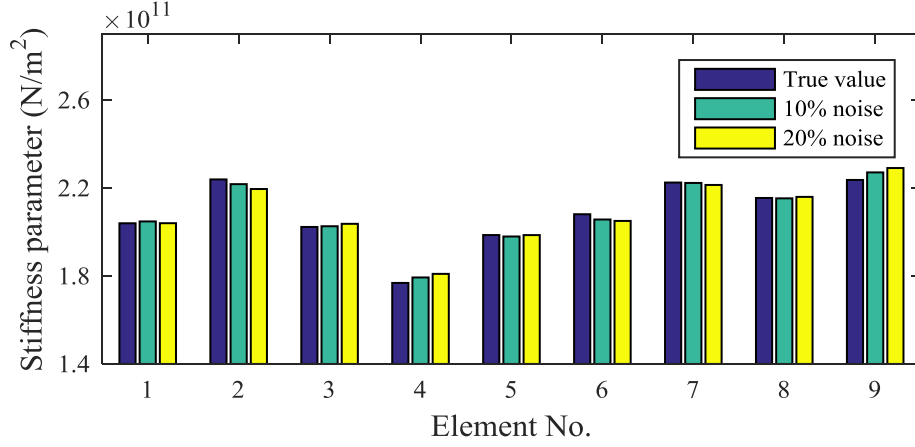


Figure 6.4 Model updating results with different noise levels

The correlation function of noised responses at i and j locations can be expressed as

$$\begin{aligned} \mathbf{R}_{\ddot{\mathbf{x}}_{mea,j}, \ddot{\mathbf{x}}_{mea,i}}(\tau) &= \mathbf{R}_{(\ddot{\mathbf{x}}_i + N_{noise,i}), (\ddot{\mathbf{x}}_j + N_{noise,j})}(\tau) \\ &= \mathbf{R}_{\ddot{\mathbf{x}}_i, \ddot{\mathbf{x}}_j}(\tau) + \mathbf{R}_{\ddot{\mathbf{x}}_i, N_{noise,j}}(\tau) + \mathbf{R}_{N_{noise,i}, \ddot{\mathbf{x}}_j}(\tau) + \mathbf{R}_{N_{noise,i}, N_{noise,j}}(\tau) \end{aligned} \quad (6.36)$$

For white noise, it has $\mathbf{R}_{\ddot{\mathbf{x}}_i, N_{noise,j}}(\tau) = 0$ and $\mathbf{R}_{N_{noise,i}, \ddot{\mathbf{x}}_j}(\tau) = 0$. Therefore, it has

$$\mathbf{R}_{\ddot{\mathbf{x}}_{mea,i}, \ddot{\mathbf{x}}_{mea,j}}(\tau) = \begin{cases} \mathbf{R}_{\ddot{\mathbf{x}}_i, \ddot{\mathbf{x}}_j}(\tau) & (i \neq j) \\ \mathbf{R}_{\ddot{\mathbf{x}}_i, \ddot{\mathbf{x}}_j}(\tau) + (E_p \sigma)^2 \delta(\tau) & (i = j) \end{cases} \quad (6.37)$$

In theory, the cross-correlation function is noise free, and the auto-correlation function contains noise only when $\tau=0$. Thus, the effect of measurement noise on the system identification results is very small as shown in Figure 6.5, where the cross-correlation function of $\mathbf{R}_{4,6}$ with 20% noise is almost the same as that without noise.

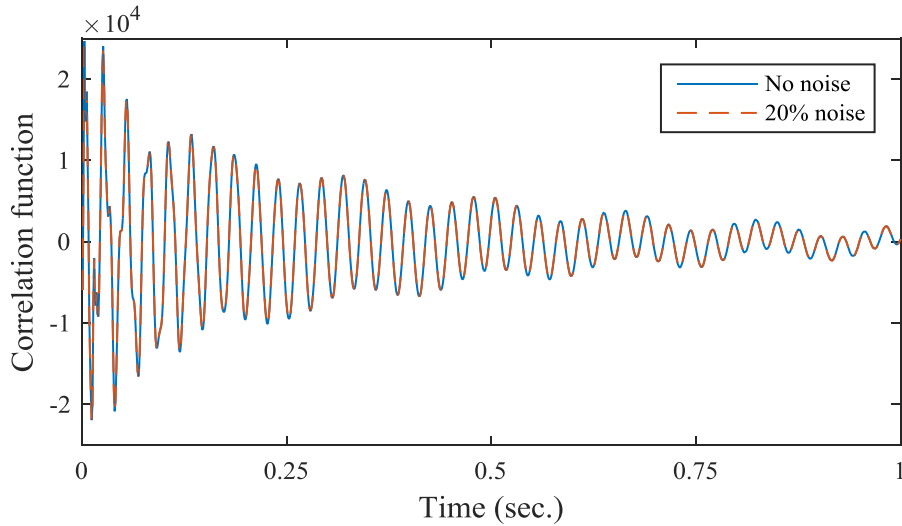


Figure 6.5 Comparison between the correlation functions $R_{4,6}$ with and without measurement noise

6.4.3 Effect of measurement point

The cross-correlation function of Nodes 4 and 6 are used in the above section. Responses from different measurement points may cause different identification results. In this section, the effect of measurement point will be studied. The excitation force and structural parameters used in Section 6.4.1 remain unchanged. The auto-correlation function of the vertical acceleration at one measurement point is employed for system identification each time. The identification errors with respect to different measurement point are shown in Figure 6.6. The identification errors for all cases are small and the maximum relative error is 2.3% at Element 6 when the auto-correlation function of the response at Node 8 is used. The effect of sensor location on the identification results is small and the proposed system identification technique is robust. These results

demonstrate that the proposed method is able to identify the structural damage when the number of sensors is less than the total number of unknown excitations.

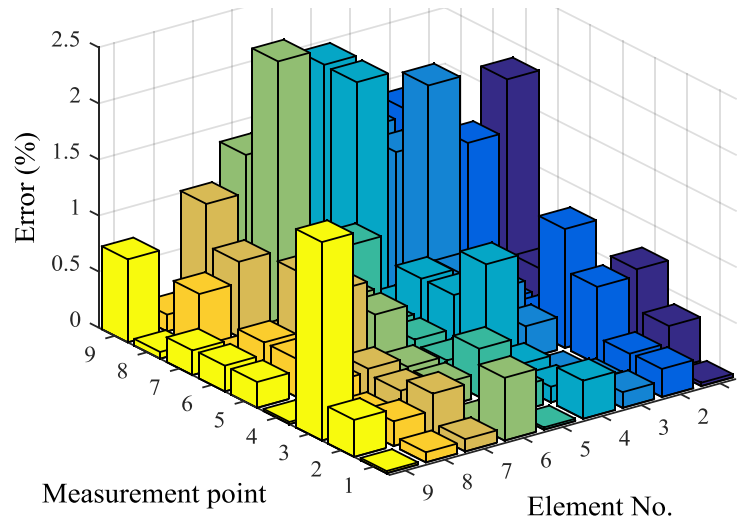


Figure 6.6 Identification error from different sensor locations

6.5 Experimental Study

A steel shear-type four-story building model was tested in the laboratory. The experiment is employed to verify the accuracy of the correlation-based damage detection method. The constructed building model is shown in Figure 6.7 and the dimensions are shown in Figure 6.8. The height of each floor is 300 mm, and the floor of each story is composed of 25 mm-thick steel plate. The two columns of each story have the same section shape with a width of 50 mm and a thickness of 5 mm. The beams and columns were welded together to form rigid joints. The bottom of the columns was welded onto a thick and solid steel plate, which was fixed to the strong floor. The elastic modulus of the steel is estimated to be 200 GPa, and the mass density is 7850 kg/m³.

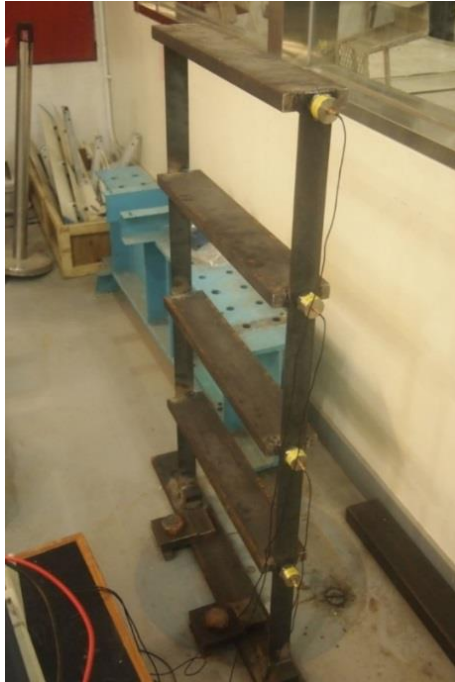


Figure 6.7 Laboratory tested steel frame model

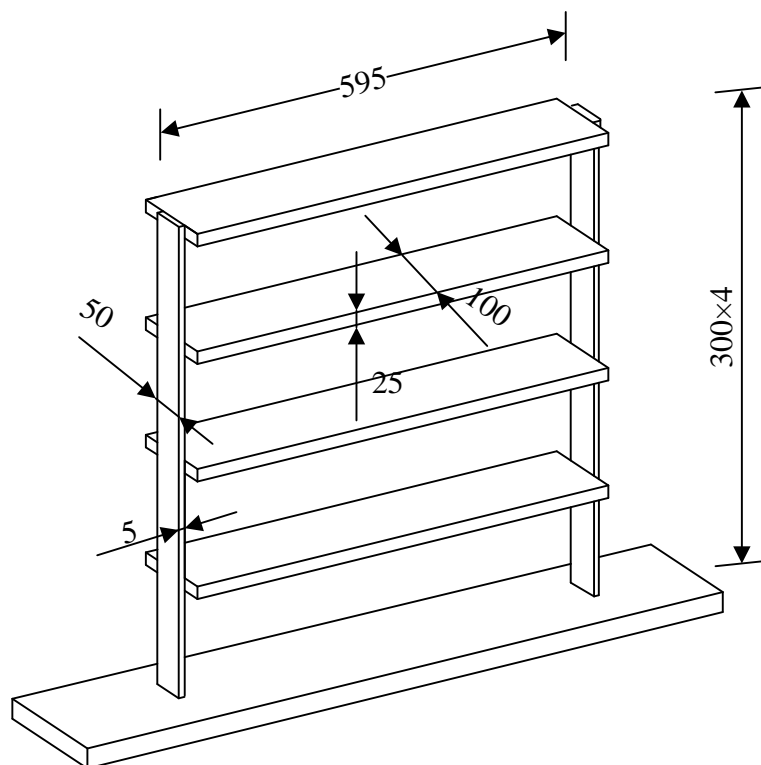


Figure 6.8 Dimensions of the frame (unit: mm)

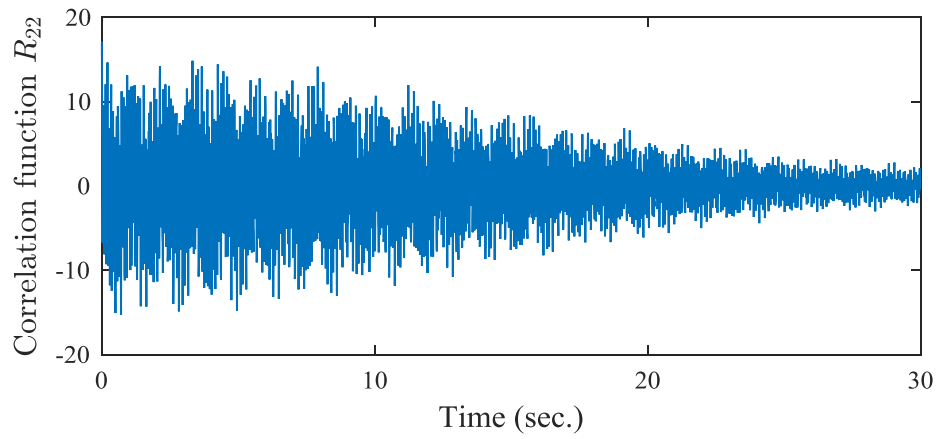
6.5.1 Experimental setup

A SINOCERA LC-04A hammer with a rubber tip was used to excite the frame. The horizontal acceleration responses at each floor were measured by using KD1300 accelerometers. A commercial data logging system INV306U and its associated signal analysis package DASP V10 were used for data acquisition. The sampling frequency was 1024 Hz, and the cut-off frequency range was preset at 1 Hz to 300 Hz for all test cases.

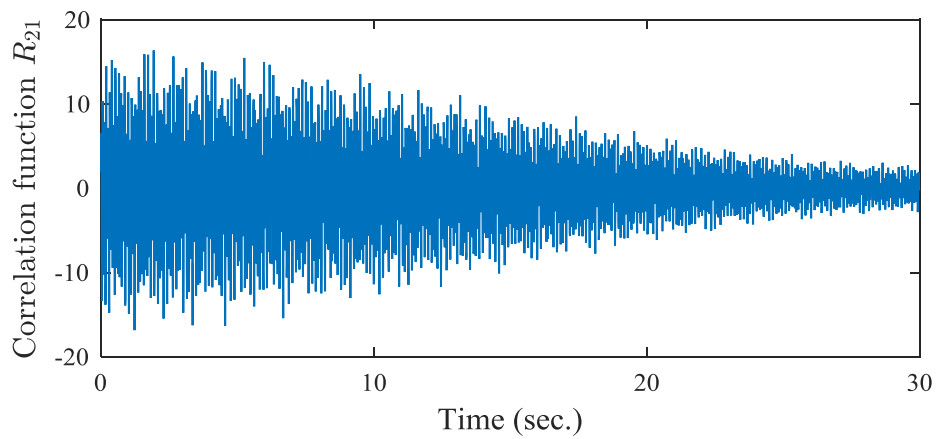
6.5.2 Modal testing and model updating in the undamaged state

The test was performed by using the hammer to hit the top floor of the frame. In each test, only output time history were recorded for 60 s. Typical curves of auto/cross-correlation functions ($R_{2,2}$ and $R_{2,1}$) are displayed in Figure 6.9. The first four natural frequencies of the undamaged structure were extracted from the measured input and output using modal analysis. The results are listed in Table 6.1 as compared with those calculated from the numerical model. In the numerical model, the stiffness of each floor is calculated from the physical configuration and material properties of the model, as listed in Table 6.2. The mass of columns, beams, and sensors are lumped at each floor. The calculated mass results are 13.1280, 13.0976, 13.0838, and 12.4948 kg for the first, second, third, and fourth floors, respectively. The analytical frequencies are very close to the measured counterparts. Thus, the model will be used for subsequent model

updating. The first four damping ratios were measured as $\zeta_1=0.74\%$, $\zeta_2=0.41\%$, $\zeta_3=0.34\%$, and $\zeta_4=0.27\%$.



(a) Auto-correlation function $R_{2,2}$



(b) Cross-correlation function $R_{2,1}$

Figure 6.9 Auto- and cross-correlation functions

Table 6.1 Frequencies of the structure in the undamaged state

Mode No.	Calculated (Hz)	Measured (Hz)	Relative difference (%)
1st	5.18	5.17	0.19
2nd	15.01	15.05	-0.27
3rd	23.19	23.52	-1.42
4th	28.60	29.20	-2.10

The correlation function between the measurement responses at the first to fourth floors and that at the second floor ($R_{2,1}$, $R_{2,2}$, $R_{2,3}$, and $R_{2,4}$) are used for the initial model updating in the undamaged state. The first 100 data of the correlation functions are employed for model updating. The updated stiffness parameters are listed in Table 6.2 (3rd column). They are very close to the initial ones.



Figure 6.10 Damage of the frame

Table 6.2 Identified flexural stiffness of columns in the undamaged and damage state

Story No.	Initial value (kN/m)	Before damage (kN/m)	After damage (kN/m)	Stiffness reduction (%)
1st	104.66	102.99	107.95	-4.8
2nd	122.21	124.75	73.14	41.4
3rd	122.21	130.16	133.18	-2.3
4th	122.21	117.30	116.83	0.4

6.5.3 Damage detection

Artificial damage was then introduced by reducing the width of two columns in the second floor from 50 mm to 30 mm, as shown in Figure 6.10, indicating 40% reduction in the stiffness of the columns. The frame was tested in a similar manner as in the undamaged state. The auto/cross-correlation functions ($R_{2,1}$, $R_{2,2}$, $R_{2,3}$, and $R_{2,4}$) are used to update the model in the damaged state. The initial model for damage detection is from the identification results in Section 6.5.2. The iteration process converges approximately after 10 runs, as shown in Figure 6.11. The updated stiffness parameters are shown in Table 6.2. The stiffness parameter of the second floor is reduced by 41.37% from 124.75 kN/m to 73.14 kN/m, which is the close to the actual value (40%). The parameters of the other columns remain almost unchanged, because there was not artificial damage happened. Therefore, both damage location and damage severity are correctly identified, and no false detection occurs.

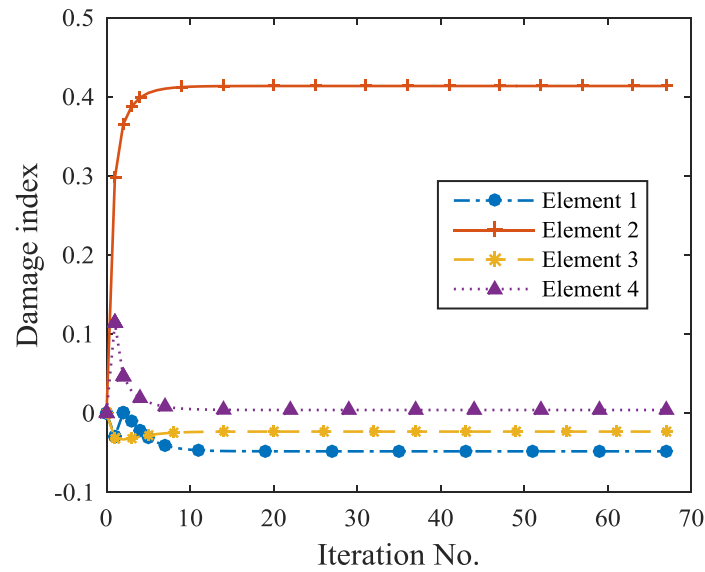


Figure 6.11 Iteration of damage identification results

6.6 Summary

Previous methods for damage detection under multiple unknown excitations are rare. In this chapter, a correlation function-based damage detection method is proposed when the structure is under multiple white noise or impulse excitations. The structural damage is detected by minimizing the error between the measured correlation functions and the calculated counterparts. The numerical study on a cantilever beam and experimental study on a steel frame model demonstrate the effectiveness and robustness of the proposed technique. Results show that the proposed method can identify the structural damage under multiple unknown excitations. The correlation function is insensitive to the measurement noise and the proposed method can detect the structural damage under the high noise condition. Moreover, the proposed method does not require the number of sensor larger than the number of excitations, as required in other methods.

CHAPTER 7

DECENTRALIZED DAMAGE DETECTION WITH AMBIENT LOADING VIA CORRELATION FUNCTION

7.1 Introduction

In Chapter 6, a correlation function-based damage detection method was presented for damage detection with multiple unknown input forces. The proposed method does not require that the number of sensor should be greater than the amount of unknown input force. However, the force location should be known in advance.

In this chapter, the proposed decentralized method is combined with correlation function based damage detection method. The new proposed method can identify the structural parameters with less computational time and without the limitations, in which the force location is unknown, and the number of sensor can be less than the number of unknown input forces. The excitation forces are assumed to be broadband white noise, and the ambient vibration responses are used for damage detection. On the basis of

NExT theory (James *et al.*, 1995; Caicedo *et al.*, 2004), the correlation functions of vibration responses can be treated as free vibration responses of the structure with non-zero initial conditions. The correlation function of the vibration signal can be represented in two parts. One part comprises the Markov parameters that depend on structural parameters, and the other part is a vector of the equivalent initial values. Structural damage is identified by minimizing the errors between the calculated and measured correlation functions. The decentralized technique proposed in previous chapters is used to determine the structural damage. Numerical and experimental studies are performed to demonstrate accuracy and effectiveness of the proposed method. Results show that the proposed technique can detect structural damage accurately and is insensitive to the measurement noise.

7.2 Representation of the Correlation Function of Vibration Response via NExT

7.2.1 Natural excitation technique (NExT)

The equation of motion of an n -DOF damped structural system under external excitation can be written as

$$M\ddot{\mathbf{x}}(t) + C\dot{\mathbf{x}}(t) + K\mathbf{x}(t) = \mathbf{B}f(t) \quad (7.1)$$

where $\mathbf{x}(t)$, $\dot{\mathbf{x}}(t)$ and $\ddot{\mathbf{x}}(t)$ are vectors of displacement, velocity and acceleration responses of the structure, respectively; M , C , and K , are the mass, damping, and

stiffness matrices of the structure, respectively, $\mathbf{f}(t)$ is the external excitation force vector, and \mathbf{B} is the mapping matrix relating the excitations to the DOFs of the structure. Rayleigh damping is assumed with the form $\mathbf{C} = a_1\mathbf{M} + a_2\mathbf{K}$, where a_1 and a_2 are damping coefficients determined from two modal damping ratios. Other damping models can also be used. The dynamic responses of the structure can be obtained from Eq. (7.1) by using the Newmark- β method.

The correlation function between two response vectors has been successfully used for modal parameter identification (James *et al.*, 1995). Caicedo *et al.* (2004) showed that the correlation function satisfies the homogeneous equation of motion provided that the excitation and responses are weakly stationary random processes.

Multiplying both sides of Eq. (7.1) by a reference response vector $\ddot{\mathbf{x}}_{ref}(t)$ and taking the expected value, one has

$$\mathbf{M}E[\ddot{\mathbf{x}}_{ref}(t)\ddot{\mathbf{x}}(t)] + \mathbf{C}E[\ddot{\mathbf{x}}_{ref}(t)\dot{\mathbf{x}}(t)] + \mathbf{K}E[\ddot{\mathbf{x}}_{ref}(t)\mathbf{x}(t)] = E[\ddot{\mathbf{x}}_{ref}(t)\mathbf{f}(t)] \quad (7.2)$$

where $E(\bullet)$ denotes the expectation value. Eq. (7.2) can be rewritten as

$$\mathbf{M}\mathbf{R}_{\ddot{\mathbf{x}}_{ref}\ddot{\mathbf{x}}}(\tau) + \mathbf{C}\mathbf{R}_{\ddot{\mathbf{x}}_{ref}\dot{\mathbf{x}}}(\tau) + \mathbf{K}\mathbf{R}_{\ddot{\mathbf{x}}_{ref}\mathbf{x}}(\tau) = \mathbf{R}_{\ddot{\mathbf{x}}_{ref}\mathbf{f}}(\tau) \quad (7.3)$$

where $\mathbf{R}_{\ddot{\mathbf{x}}_{ref}\ddot{\mathbf{x}}}(\tau)$ is the correlation function between $\ddot{\mathbf{x}}_{ref}$ and $\ddot{\mathbf{x}}$. $\mathbf{R}_{\ddot{\mathbf{x}}_{ref}\dot{\mathbf{x}}}(\tau)$, $\mathbf{R}_{\ddot{\mathbf{x}}_{ref}\mathbf{x}}(\tau)$ and $\mathbf{R}_{\ddot{\mathbf{x}}_{ref}\mathbf{f}}(\tau)$ are similarly defined.

The excitation and the system responses are uncorrelated because they are assumed weakly stationary random processes. This condition leads to the following equations (Bendat and Piersol, 2011):

$$\mathbf{R}_{\ddot{x}_{ref}f}(\tau) = 0, \mathbf{R}_{\ddot{x}_{ref}\dot{x}}(\tau) = \dot{\mathbf{R}}_{\ddot{x}_{ref}x}(\tau), \text{ and } \mathbf{R}_{\ddot{x}_{ref}\ddot{x}}(\tau) = \ddot{\mathbf{R}}_{\ddot{x}_{ref}x}(\tau) \quad (7.4)$$

Eq. (7.3) then becomes

$$\mathbf{M}\ddot{\mathbf{R}}_{\ddot{x}_{ref}x}(\tau) + \mathbf{C}\dot{\mathbf{R}}_{\ddot{x}_{ref}x}(\tau) + \mathbf{K}\mathbf{R}_{\ddot{x}_{ref}x}(\tau) = \mathbf{0} \quad (7.5)$$

Eq.(7.5) shows that the correlation function of responses can be treated as the free vibration response.

In practical applications, correlation function $R_{AB}(t)$ can be obtained as a discrete inverse Fourier transform of the cross-spectral density function (James *et al.*, 1995; Caicedo *et al.*, 2004) as

$$R_{AB}(t) = \frac{1}{N} \sum_{k=0}^{N-1} S_{AB}(k) \exp\left[j \frac{2\pi kt}{N}\right] \quad (7.6)$$

where $S_{AB}(k)$ is the discrete cross-spectral density function of the measured responses A and B , k is the discrete frequency index, and N is the total number of time steps.

7.2.2 Equivalent initial free vibration responses

Eq. (7.5) shows the system correlation function can be equivalent to the free vibration response of the same system as

$$\begin{cases} \mathbf{M}\ddot{\mathbf{z}}(t) + \mathbf{C}\dot{\mathbf{z}}(t) + \mathbf{K}\mathbf{z}(t) = \mathbf{0} \\ \ddot{\mathbf{z}}(t_0) = \ddot{\mathbf{z}}_0, \dot{\mathbf{z}}(t_0) = \dot{\mathbf{z}}_0, \mathbf{z}(t_0) = \mathbf{z}_0 \end{cases} \quad (7.7)$$

where $\mathbf{z}(t)$, $\dot{\mathbf{z}}(t)$, and $\ddot{\mathbf{z}}(t)$ are vectors of displacements, velocity, and acceleration responses, respectively, in the equivalent free vibration system; \mathbf{z}_0 , $\dot{\mathbf{z}}_0$, and $\ddot{\mathbf{z}}_0$ are the initial displacements, velocity, and acceleration, respectively.

Eq. (7.7) can be written in the form of state space as

$$\dot{\mathbf{Z}}(t) = \mathbf{A}_c \mathbf{Z}(t) \quad (7.8)$$

where

$$\mathbf{Z} = \begin{bmatrix} \mathbf{z}(t) \\ \dot{\mathbf{z}}(t) \end{bmatrix} \text{ and } \mathbf{A}_c = \begin{bmatrix} \mathbf{0} & \mathbf{I} \\ -\mathbf{M}^{-1}\mathbf{K} & -\mathbf{M}^{-1}\mathbf{C} \end{bmatrix}$$

Measurements are generally obtained at several sensor locations only. The observation equation is

$$\mathbf{y}(t) = \mathbf{C}_a \ddot{\mathbf{z}}(t) + \mathbf{C}_v \dot{\mathbf{z}}(t) + \mathbf{C}_d \mathbf{z}(t) \quad (7.9)$$

where $\mathbf{y}(t)$ is the vector of the output, \mathbf{C}_a , \mathbf{C}_v , and \mathbf{C}_d are the mapping matrices for the acceleration, velocity, and displacement output, respectively.

In many practical applications, only accelerations are measured. It then has

$$\mathbf{y}(t) = \mathbf{C}_a \ddot{\mathbf{z}}(t) = -\mathbf{C}_a \begin{bmatrix} \mathbf{M}^{-1}\mathbf{K} & \mathbf{M}^{-1}\mathbf{C} \end{bmatrix} \mathbf{Z}(t) = \mathbf{C}_o \mathbf{Z}(t) \quad (7.10)$$

$$\mathbf{C}_o = \begin{bmatrix} -\mathbf{C}_a \mathbf{M}^{-1}\mathbf{K} & -\mathbf{C}_a \mathbf{M}^{-1}\mathbf{C} \end{bmatrix} \quad (7.11)$$

Eqs. (7.10) and (7.8) constitute a deterministic state-space model and can be converted into the following discrete equations:

$$\mathbf{Z}_{i+1} = \mathbf{A}_d \mathbf{Z}_i \quad (7.12)$$

$$\mathbf{y}_i = \mathbf{C}_o \mathbf{Z}_i \quad (i=1, 2, 3, \dots, l) \quad (7.13)$$

where $\mathbf{Z}_i = \mathbf{Z}(i\Delta t)$ is the discrete state vector, $\mathbf{A}_d = \exp(\mathbf{A}_c \Delta t)$ is the discrete state matrix, and l is the total number of sampling points.

The output response \mathbf{y}_{i+1} can be solved from Eqs. (7.12) and (7.13) in terms of the previous input as

$$\mathbf{y}_{i+1} = \mathbf{C}_o \mathbf{Z}_{i+1} = \mathbf{C}_o \mathbf{A}_d \mathbf{Z}_i = \mathbf{C}_o \mathbf{A}_d^2 \mathbf{Z}_{i-1} \cdots = \mathbf{C}_o \mathbf{A}_d^{i+1} \mathbf{Z}_0 \quad (7.14)$$

Eq. (7.14) can then be rewritten as (Siringoringo and Fujino, 2006)

$$\begin{bmatrix} \mathbf{y}_1 \\ \mathbf{y}_2 \\ \vdots \\ \mathbf{y}_l \end{bmatrix} = \begin{bmatrix} \mathbf{C}_o \mathbf{A}_d \\ \mathbf{C}_o \mathbf{A}_d^2 \\ \vdots \\ \mathbf{C}_o \mathbf{A}_d^l \end{bmatrix} \mathbf{Z}_0 \quad (7.15)$$

or

$$\mathbf{Y} = \mathbf{H} \mathbf{Z}_0 \quad (7.16)$$

The constant matrices in \mathbf{H} are known as system Markov parameters (Siringoringo and Fujino, 2008), which are associated with the structural parameters.

From Eqs. (7.4), (7.5), (7.7), and (7.16), we find that the correlation function of the acceleration responses can be expressed as

$$\mathbf{R}_{\ddot{\mathbf{x}}_{ref} \ddot{\mathbf{x}}} = \ddot{\mathbf{R}}_{\ddot{\mathbf{x}}_{ref} \mathbf{x}} = \mathbf{H} \mathbf{Z}_0 \quad (7.17)$$

Eq. (7.17) shows that the correlation function can be written as two parts. One part is associated with the system Markov parameters and the other is the equivalent initial values of the dynamic system.

If the structural parameters are known, then the equivalent initial velocity and displacement can be obtained from

$$\mathbf{Z}_0 = (\mathbf{H})^+ \mathbf{Y} = (\mathbf{H})^+ \mathbf{R}_{\dot{x}_{ref}, \ddot{x}} \quad (7.18)$$

where $(\mathbf{H})^+$ is the pseudo-inverse of \mathbf{H} . The equivalent initial acceleration can be obtained from

$$\ddot{\mathbf{z}}_0 = -\mathbf{M}^{-1}(\mathbf{K}\mathbf{z}_0 + \mathbf{C}\dot{\mathbf{z}}_0) \quad (7.19)$$

7.3 Decentralized Damage Detection with Correlation Functions

Assuming that the structural damage is in the form of a reduction in the structural stiffness, the stiffness matrix of the damaged structure can then be expressed as

$$\mathbf{K}^d = \sum_{i=1}^{ne} (1 - \alpha_i) \mathbf{K}_i \quad (7.20)$$

where \mathbf{K}_i is the stiffness matrix of the i -th element in the intact state, α_i ($0 \leq \alpha_i \leq 1$) is defined as the damage index of the i -th element, and ne is the total number of elements in the structure. $\alpha_i=1$ denotes that the element loses its stiffness completely, whereas $\alpha_i=0$ indicates that the element is intact.

The idea is to identify the damage indices $\boldsymbol{\theta} = [\alpha_1, \alpha_2, \dots, \alpha_{ne}]$ from the correlation functions. In a large structure, the correlation function measured from the i -zone can be expressed as $\mathbf{Y}_{mea, i}$ and can be written as a function of the unknown structural

$$\begin{bmatrix} \boldsymbol{\theta}_1^{n+1} \\ \boldsymbol{\theta}_2^{n+1} \\ \vdots \\ \boldsymbol{\theta}_r^{n+1} \end{bmatrix} = \begin{bmatrix} \boldsymbol{\theta}_1^n \\ \boldsymbol{\theta}_2^n \\ \vdots \\ \boldsymbol{\theta}_r^n \end{bmatrix} - \begin{bmatrix} \frac{\partial \mathbf{g}_1}{\partial \boldsymbol{\theta}_1^n} & 0 & 0 & 0 \\ 0 & \frac{\partial \mathbf{g}_2}{\partial \boldsymbol{\theta}_2^n} & 0 & 0 \\ 0 & 0 & \ddots & 0 \\ 0 & 0 & 0 & \frac{\partial \mathbf{g}_r}{\partial \boldsymbol{\theta}_r^n} \end{bmatrix}^{-1} \begin{bmatrix} \mathbf{g}_1(\boldsymbol{\theta}^n, \mathbf{Z}_0) - \mathbf{Y}_{mea,1} \\ \mathbf{g}_2(\boldsymbol{\theta}^n, \mathbf{Z}_0) - \mathbf{Y}_{mea,2} \\ \vdots \\ \mathbf{g}_r(\boldsymbol{\theta}^n, \mathbf{Z}_0) - \mathbf{Y}_{mea,r} \end{bmatrix} \quad (7.26)$$

or

$$\boldsymbol{\theta}_i^{n+1} = \boldsymbol{\theta}_i^n - \left[\frac{\partial \mathbf{g}_i}{\partial \boldsymbol{\theta}_i^n} \right]^{-1} \left[\mathbf{g}_i(\boldsymbol{\theta}^n, \mathbf{Z}_0) - \mathbf{Y}_{mea,i} \right], \quad (i=1, 2, \dots, r) \quad (7.27)$$

The Tikhonov regularization technique (Tikhonov et al., 1995) is applied to Eq. (7.27), and the solution is obtained as

$$\boldsymbol{\theta}_i^{n+1} = \boldsymbol{\theta}_i^n - \left[\left(\frac{\partial \mathbf{g}_i}{\partial \boldsymbol{\theta}_i^n} \right)^T \left(\frac{\partial \mathbf{g}_i}{\partial \boldsymbol{\theta}_i^n} \right) + \lambda_i \right]^{-1} \left(\frac{\partial \mathbf{g}_i}{\partial \boldsymbol{\theta}_i^n} \right)^T \left[\mathbf{g}_i(\boldsymbol{\theta}^n, \mathbf{Z}_0) - \mathbf{Y}_{mea,i} \right], \quad (i=1, 2, \dots, r) \quad (7.28)$$

After each subset parameter $\boldsymbol{\theta}_i^{n+1}$ is calculated from Eq. (7.28), the global structural parameters are obtained, and the sensitivity matrix $\mathbf{G}'(\boldsymbol{\theta}^{n+1})$ is re-calculated. The correlation function (equivalent free vibration responses) in each zone are then computed.

The proposed approach is implemented as follows.

Step 1: Divide the structure into r small zones according to its finite element model. The correlation functions in each zone can be obtained from Eq. (7.6) using the measured acceleration.

Step 2: Divide the unknown structural parameters into r subset and set the initial values

$$\boldsymbol{\theta}^0 = [\boldsymbol{\theta}_1^0, \boldsymbol{\theta}_2^0, \dots, \boldsymbol{\theta}_r^0].$$

Step 3: The initial values of correlation functions \mathbf{Z}_0 can be identified from Eq. (7.18).

Step 4: Compute $\mathbf{g}_i(\boldsymbol{\theta}^n, \mathbf{Z}_0)$ from Eq. (7.7) and the sensitivity matrix of responses with respect to the structural parameters.

Step 5: Update each subset of the structural parameters $\boldsymbol{\theta}_i^{n+1}$ from Eq. (7.28).

Step 6: Repeat Steps 3 to 5 until the following convergence criterion is satisfied.

$$\frac{\|\boldsymbol{\theta}^{n+1} - \boldsymbol{\theta}^n\|}{\|\boldsymbol{\theta}^{n+1}\|} \times 100\% \leq Tol \quad (7.29)$$

The convergence criterion is set as $Tol = 1.0 \times 10^{-6}$.

The details of the damage identification process is given in Figure 7.1.

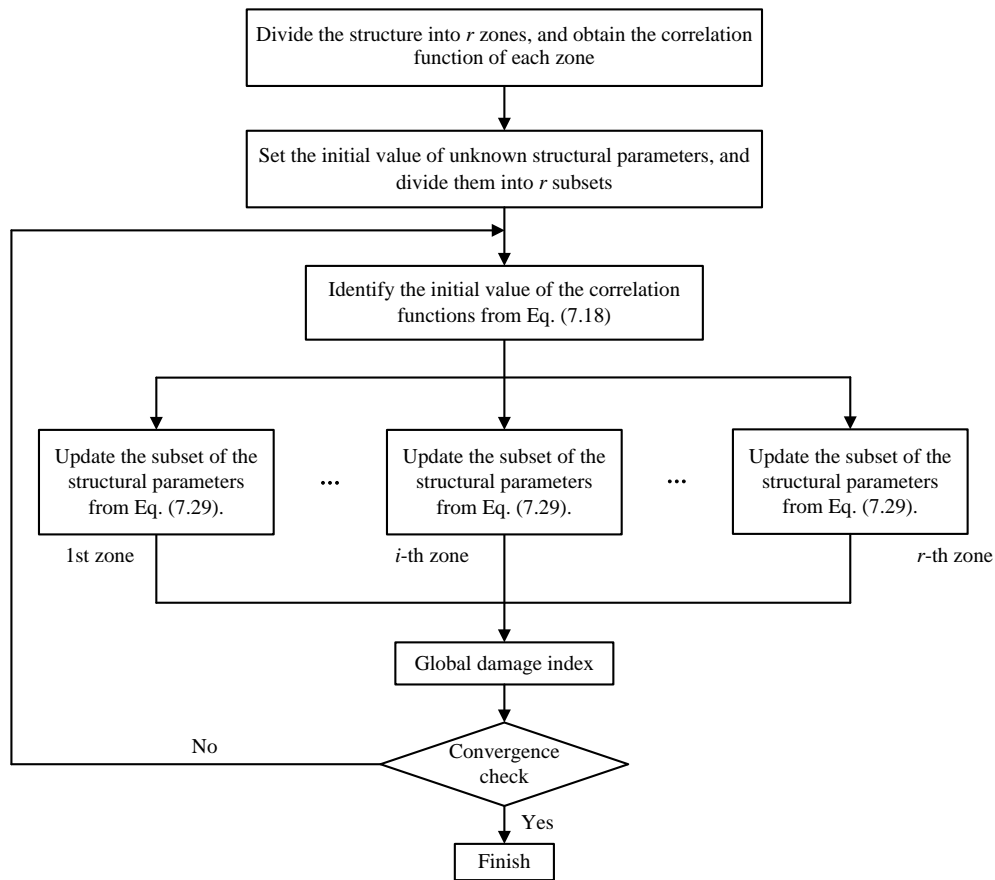
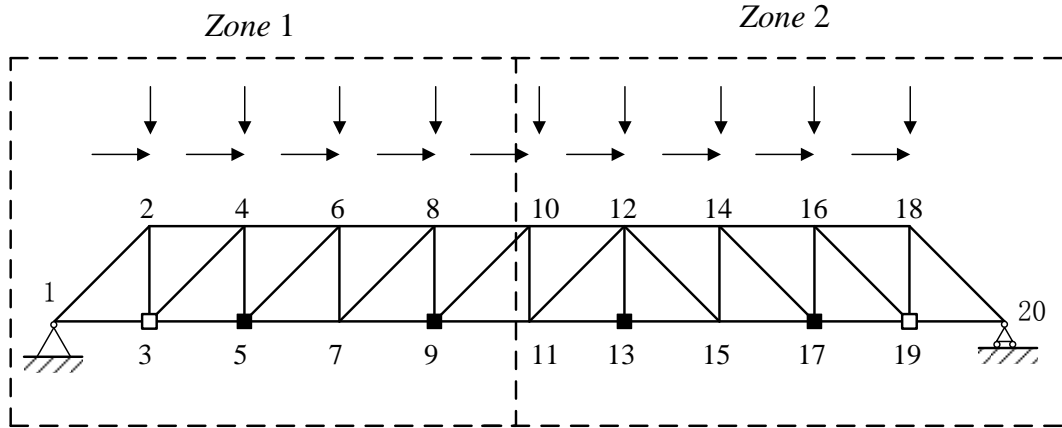


Figure 7.1 Flow chart of proposed damage detection method

7.4 Numerical Study

A two-dimensional truss structure, as shown in Figure 7.2, is adopted for the numerical study. The truss has a pin support at Node 1 and a roller support at Node 20. The finite element model consists of 37 planar truss elements with 37 DOFs. The cross-sectional area of each element is 0.0016 m^2 . Rayleigh damping is adopted for the system with



Note: (1): ■ denotes horizontal and vertical measurement.
(2): □ denotes vertical measurement.

Figure 7.3 Sensor and force locations

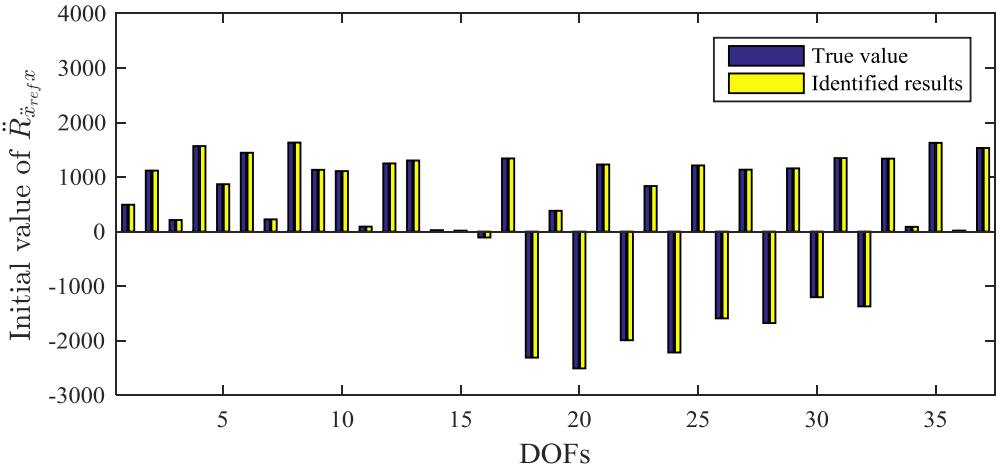
7.4.1 Initial value identification

An important assumption in this chapter is that the correlation function of the acceleration responses can be treated as free vibration responses of the same structure when the structure is under ambient white noise excitations. The correlation function of the measured acceleration responses can be obtained from Eq. (7.6).

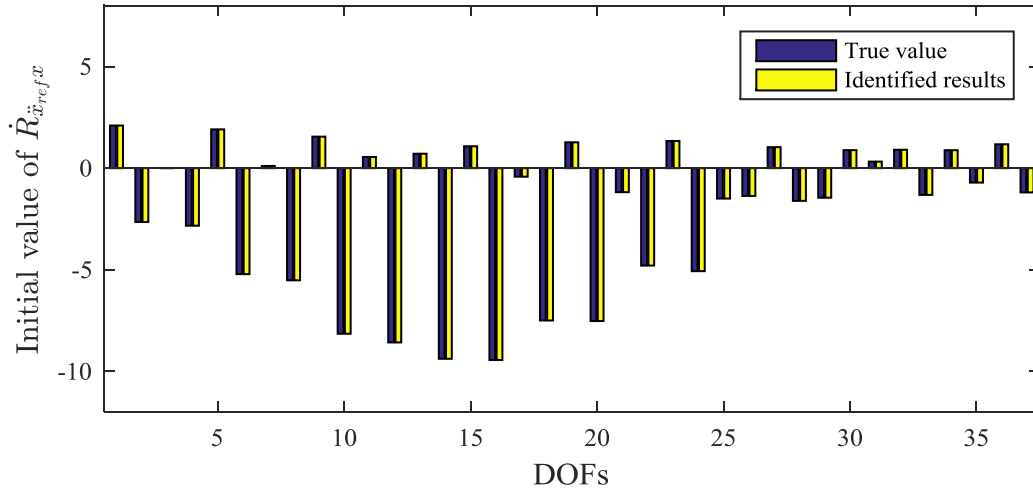
The correlation functions from the acceleration responses are used for initial value identification. In this study, the structural parameters are known. The true initial values of the correlation functions $\ddot{\mathbf{R}}_{\dot{x}_{ref}x}(0)$, $\dot{\mathbf{R}}_{\dot{x}_{ref}x}(0)$, and $\mathbf{R}_{\dot{x}_{ref}x}(0)$ in Eq. (7.5) can be obtained from $\mathbf{R}_{\dot{x}_{ref}\ddot{x}}$, $\mathbf{R}_{\dot{x}_{ref}\dot{x}}$, and $\mathbf{R}_{\dot{x}_{ref}x}$ with $\tau = 0$. The initial values of the correlation

functions are identified from the measurement correlation function with Eqs. (7.7) to (7.18)

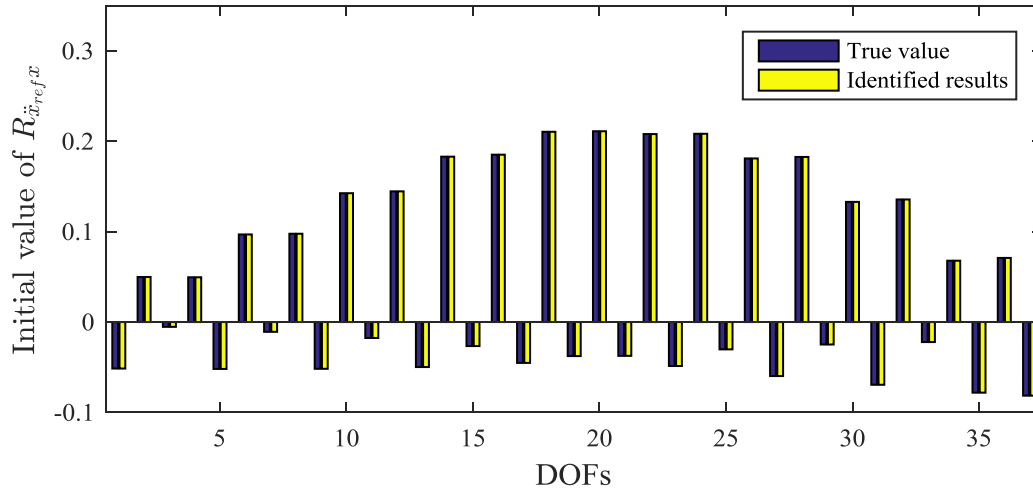
The identified initial values are shown in Figure 7.3. In this example, 20 min vibration responses are used for the calculation of the correlation functions, and the first 300 data points of the correlation functions are used for the initial value identification. The identified initial values from the measured correlation function match their true values well. These results can verify the accuracy of initial value identification and the above assumption.



(a) Initial value of $\ddot{\mathbf{R}}_{\dot{x}_{ref},x}$



(b) Initial value of $R_{\dot{x}_{ref}x}$



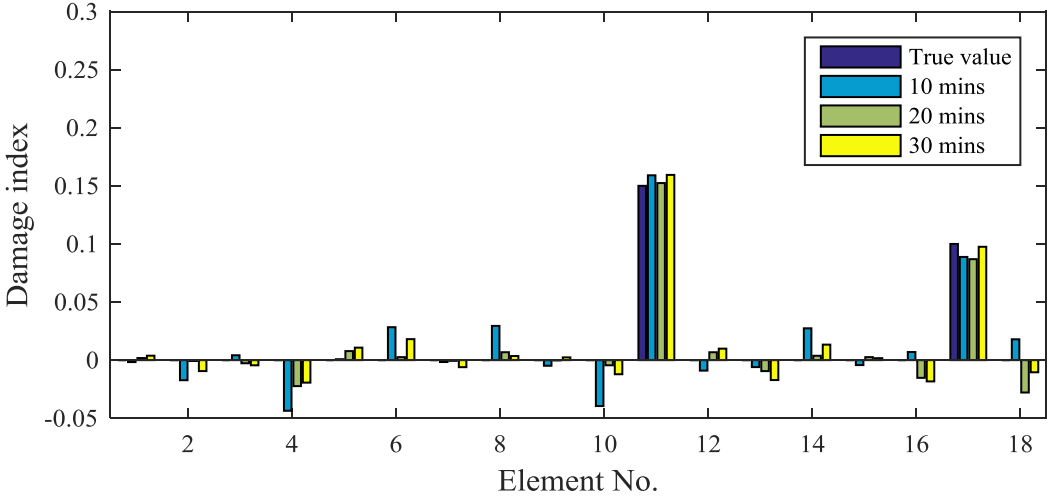
(c) Initial value of $R_{\ddot{x}_{ref}x}$

Figure 7.4 Initial values of correlation function

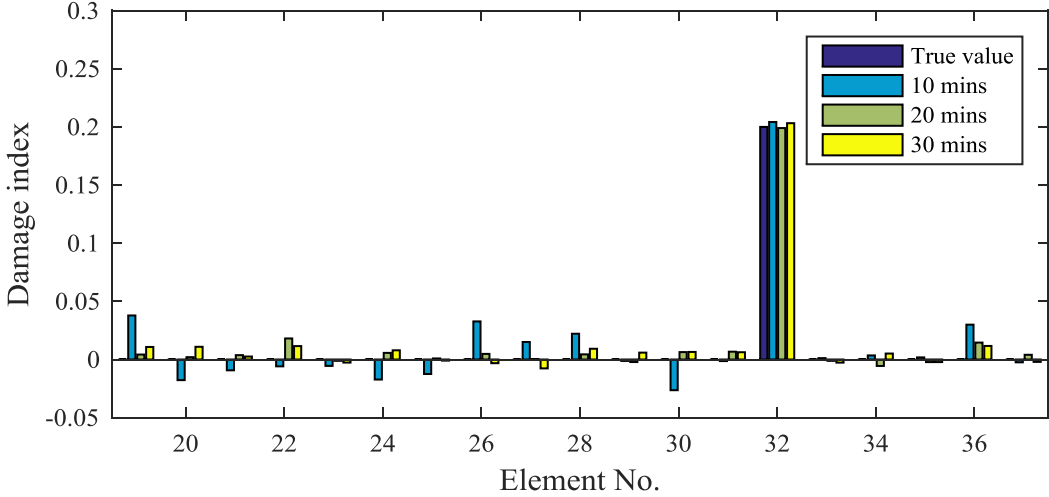
7.4.2 Damage detection without noise

The structure is assumed to suffer a reduction of 15% in the elastic modulus of the material in Element 11, 10% in Element 17, and 20% in Element 32 due to an adverse event. Different durations of vibration responses, say 10, 20, and 30 min of vibration

data are respectively used to calculate the correlation functions. They are divided into two subsets according to their locations and used to update the structural parameters of each subset.



(a) Subset 1



(b) Subset 2

Figure 7.5 Identified structural parameters with different durations of measurement data

The final identified results are shown in Figure 7.5. All of the damage locations and severities are correctly identified without significant false alarms in other elements. A longer vibration responses may lead to better identification results. The maximum errors in the results from 10 min vibration responses are 4.36% at Element 4, 3.95% at Element 10, and 3.79% at Element 19. The errors from 20 and 30 min vibration responses are less than 3%. These results can verify the accuracy of the proposed method in the identification of structural damage.

7.4.3 Damage detection with noise

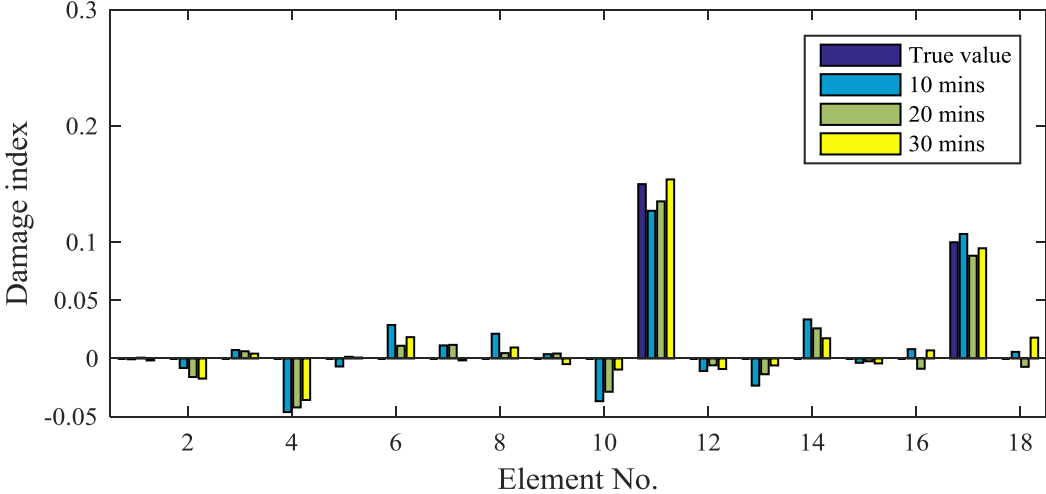
The measurement noise is then considered by adding a random component to the actual responses as

$$\ddot{\mathbf{x}}_{mea} = \ddot{\mathbf{x}} + E_p N_{noise} \sigma(\ddot{\mathbf{x}}) \quad (7.30)$$

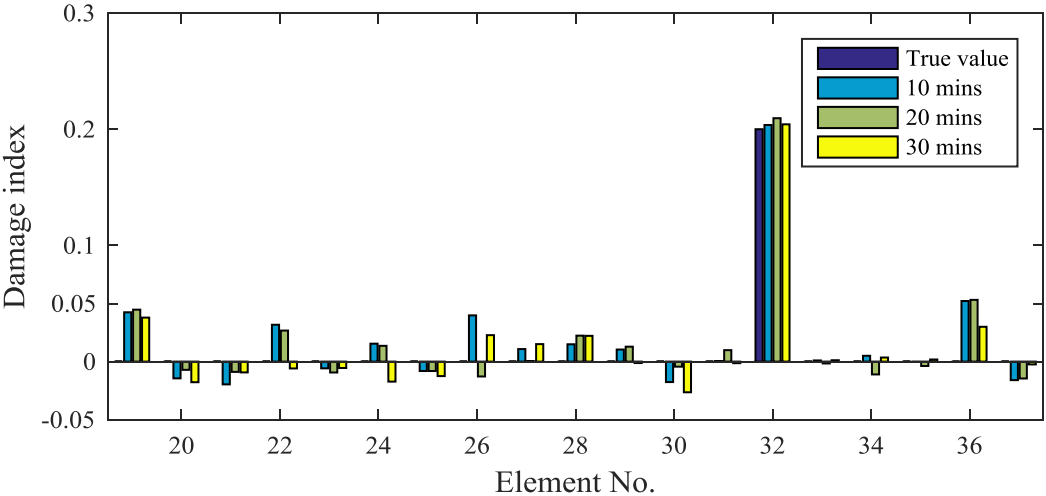
where E_p is the percentage noise level, N_{noise} is a standard normal distribution vector with zero mean and unit standard deviation, and $\sigma(\ddot{\mathbf{x}})$ is the standard deviation of the acceleration response.

The correlation function is insensitive to the measurement noise, as proved in Chapter 6. Here 20% of measurement noise is added. The correlation functions are calculated from the noisy responses and used for damage detection. The identified results using the different durations of the responses (10, 20, and 30 minutes) are shown in Figure 7.6. Damage location and severity are correctly identified in all cases with small identification errors in Elements 4, 19, and 36. A longer measurement of vibration

responses may improve the results slightly. These results verify that the proposed method is insensitive to the measurement noise.



(a) Subset 1



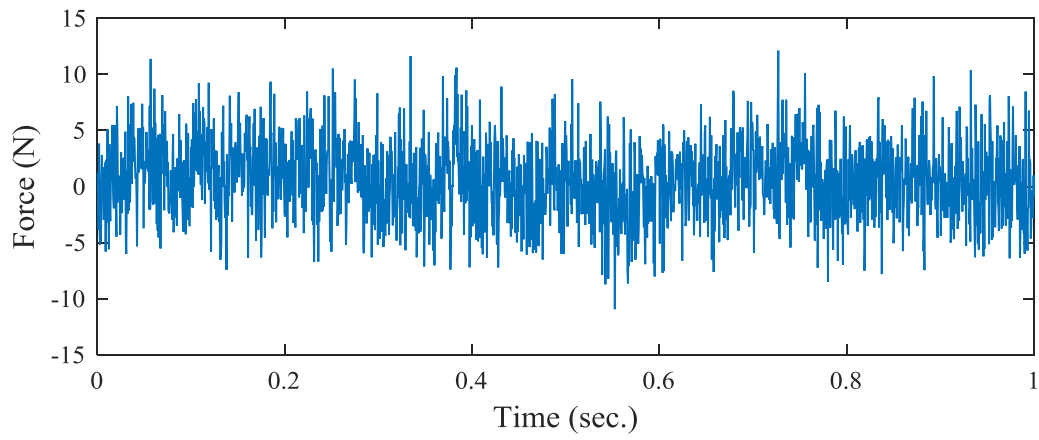
(b) Subset 2

Figure 7.6 Final identified results with measurement noise

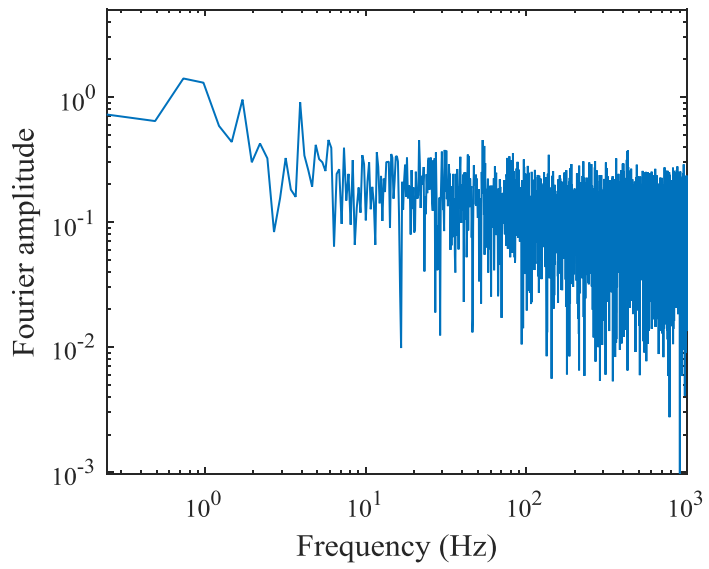
7.4.4 Damage detection under non-standard white noise excitation

In practice, excitations such as traffic loading and wind loading, may not be white noise. Non-standard white noise excitations are considered in this section. The excitation force is simulated with a combination of three times of standard white noise and one time of standard pink noise. The pink noise excitation force has a 3 dB attenuation with increasing frequency (Li, 2005). The forces locations are the same as the previous studies (Figure 7.3). The first second time history of the simulated excitation force and the spectrum are shown in Figure 7.7. The sampling rate is 2000 Hz. The measurement and the reference point are the same as those in previous studies. The first 30 and 60 min acceleration responses under the non-standard white noise force are computed from the structure, from which the correlation functions are calculated. The first 300 data points of the correlation functions are used for damage detection.

The damage identified results are shown in Figure 7.8. Generally, results with 30 min of vibration data have relatively large errors (e.g., 7.03%, 7.53%, 8.37%, and 7.58% in Elements 10, 18, 24, and 27, respectively). A longer duration of measurement (60 mins) improves the identification results (all elements less than 5%).

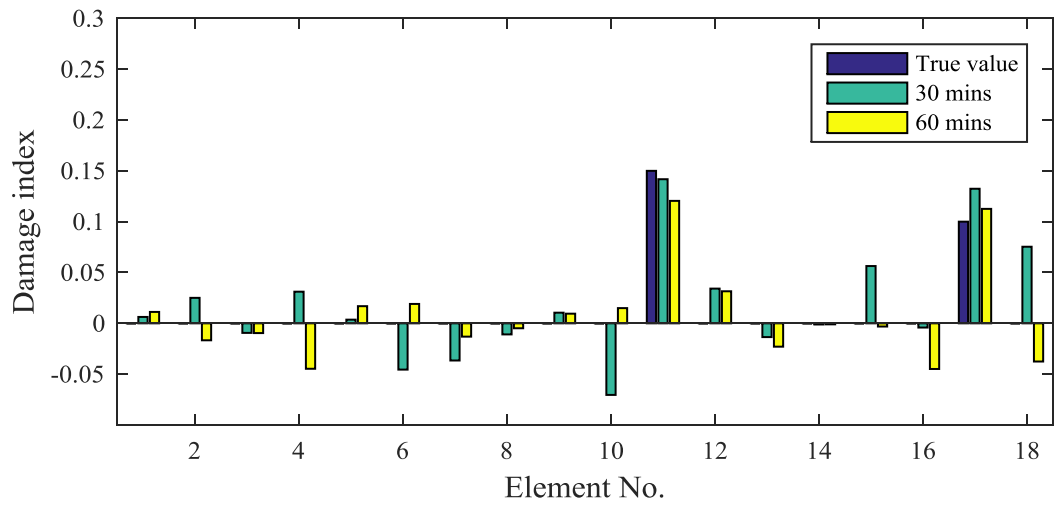


(a) Time history of the input force

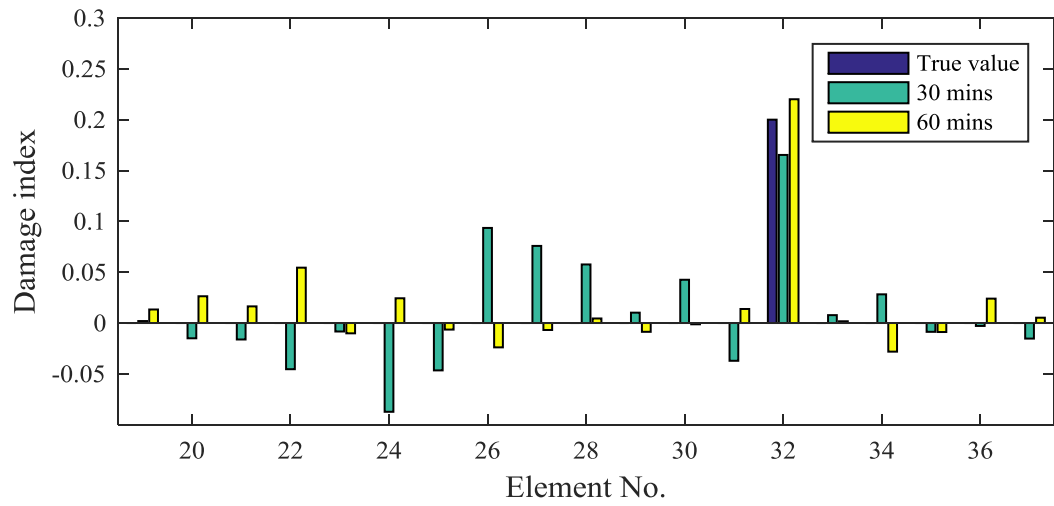


(b) Fourier amplitude spectrum

Figure 7.7 Non-standard white noise excitation



(a) Subset 1

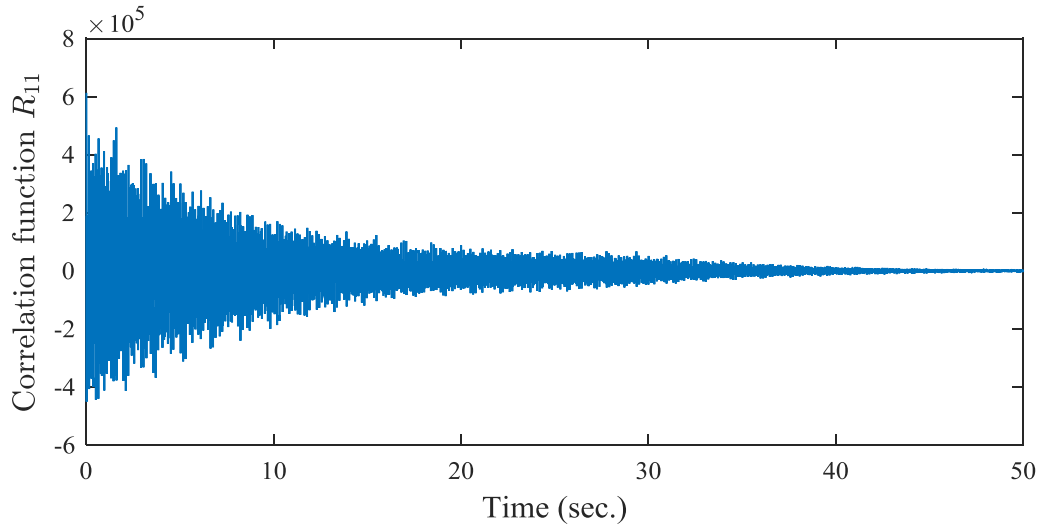


(b) Subset 2

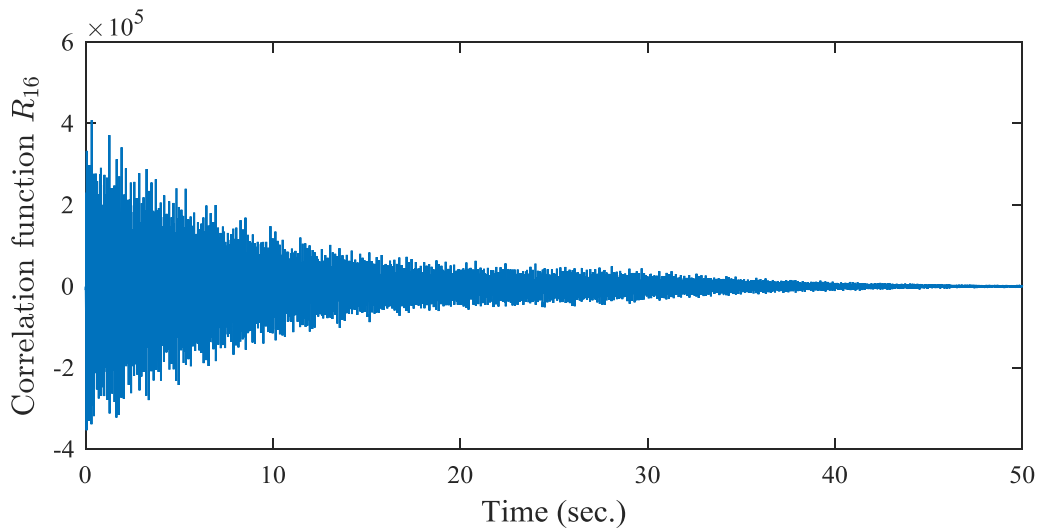
Figure 7.8 Identified results under non-standard white noise excitations

7.5 Experimental Study

The vibration response data in the experimental study in Chapter 4 are used here to validate the proposed decentralized damage detection method. The impact force is in broadband in the frequency domain. Therefore, the correlation function of vibration responses can also be treated as free vibration response (Ewins, 2003). After the initial finite element model was updated, the correlation functions from the experimental data of damage Cases 1 and 2 are used to identify the stiffness parameters of the eight-floor frame structure. The eight acceleration responses are used for damage detection, and the acceleration responses of the first floor is selected as the reference signal for the calculation of the correlation functions. The impact force was applied on the third floor. However, the force location and time history are not used in the damage detection. The correlation functions ($\mathbf{R}_{11} \sim \mathbf{R}_{18}$) are divided into two subsets. The first subset includes $\mathbf{R}_{11} \sim \mathbf{R}_{14}$, and the second subset includes $\mathbf{R}_{15} \sim \mathbf{R}_{18}$. The former subset of correlation functions are used to update the stiffness parameters of 1st to 4th floors and the second for 5th to 8th floors. Figure 7.9 shows the correlation functions of \mathbf{R}_{11} and \mathbf{R}_{16} . Only the first 300 data points of the correlation function are used.



(a) Correlation function R_{11}



(b) Correlation function R_{16}

Figure 7.9 Time history of correlation function in damage Case 1

The identified results are shown in Figure 7.10. In Case 1, 20% of stiffness reduction in Element 2 is successfully identified. In Case 2, 20% stiffness reduction in Element 2 and 10% in Element 7 are also identified, correctly. The results match their true values well.

The modal assurance criterion (MAC) is a statistical indicator of the difference between two mode shapes, which is calculated from the following equation:

$$MAC = \frac{\left(\{\Phi_{A,i}^T\}\{\Phi_{E,i}\}\right)^2}{\left(\{\Phi_{A,i}^T\}\{\Phi_{A,i}\}\right)\left(\{\Phi_{E,i}^T\}\{\Phi_{E,i}\}\right)} \quad (7.31)$$

where $\Phi_{A,i}$ and $\Phi_{E,i}$ are the i -th mode shape from the analytical and experimental models, respectively. The MAC indicator has a value between 0 and 1, 0 indicating the two vectors are perpendicular and 1 indicating they are the same but differ by a scalar only. The mode shapes from the updated numerical model should be consistent with those from the experimental model. Table 7.1 shows the MAC values of damage Cases 1 and 2. The results, which are all near 1, show that the updated numerical model is remarkably close to the experimental model. Thus, the accuracy of the damage detection method was verified.

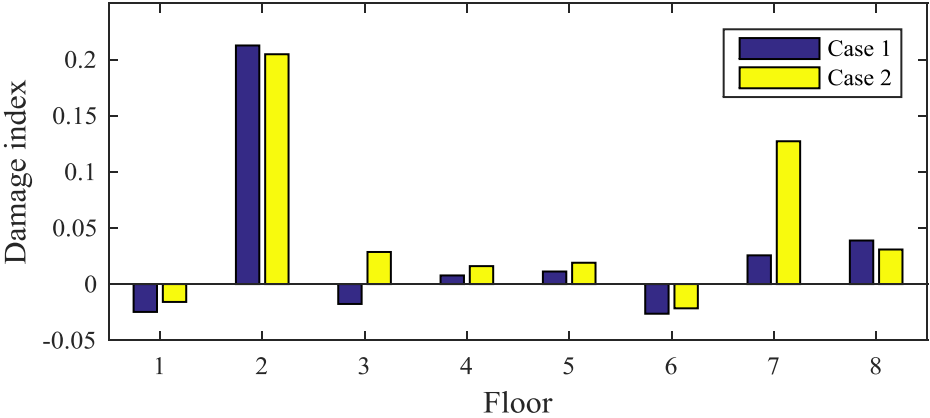


Figure 7.10 Damage identification results

Table 7.1 Modal data of the structure in damage Cases 1 and 2

Mode NO.	Case 1			Case 2		
	Tested (Hz)	Analytical (Hz)	MAC	Tested (Hz)	Analytical (Hz)	MAC
1	4.57	4.57	0.9998	4.54	4.54	0.9999
2	13.56	13.44	0.9991	13.38	13.24	0.9974
3	22.73	22.69	0.9992	22.34	22.26	0.9961
4	30.43	30.44	0.9954	30.14	30.17	0.9922
5	37.18	36.98	0.9807	37.19	36.95	0.9869
6	42.66	42.70	0.9793	42.29	41.8	0.9722
7	47.65	47.50	0.9652	46.69	45.98	0.9843
8	51.03	50.17	0.9701	50.54	51.40	0.9900

7.6 Summary

A decentralized damage detection method is proposed in this chapter for civil structures under multiple ambient white noise excitations. The correlation function of acceleration responses is treated as a free vibration response of the same structure on the basis of NExT theory (James *et al.*, 1995). The initial values of the correlation function can be identified from the system Markov parameters by using the state space method. A decentralized technique is used to identify the structural damage parameters of each subset using the correlation function of the subset. A simply-supported two-dimensional

numerical truss structure and a laboratory tested eight-floor steel frame structure are studied. The accuracy of the proposed method and the effect of measurement noise and non-standard white excitation forces are investigated. The results show that the proposed method in Chapter 7 can identify the structural damage with unknown input force location and the number of sensors can be less than the number of unknown input force. Both numerical and experimental studies are conducted to verify the advantages of the proposed method.

CHAPTER 8

CONCLUSIONS AND FUTURE RESEARCH

8.1 Conclusions

Structural damage detection using the time domain vibration responses has been receiving more and more attention in the past decades. This dissertation focused on the development of a decentralized damage detection framework for civil structures under earthquake and ambient loadings. The main contributions and conclusions of this dissertation are summarized as follows:

- 1) A decentralized damage detection method is proposed for large-scale civil structures. The structure can be divided into several zones for short term field test. The dynamic test in each zone is performed in sequence with its own set of sensors. After all the response sets are obtained, the external excitations in each test are

identified in the wavelet domain. The structural parameters of the whole structure are divided into several subsets according to their locations. Each subset of structural parameters is updated with the corresponding measurement subset with the Newton-SOR method. The unknown excitations and the physical structural parameters can be identified with iterations until a prescribed convergence condition is satisfied. The accuracy of the proposed decentralized method for structural damage detection is verified with numerical study of a truss structure. The decentralized method is implemented in a multi-core central processing unit with parallel processing and a reduction of approximately 37% of computation time can be achieved, compared with those results from computation in sequence.

- 2) The Kalman filter technique can be used to identify the unknown input force of the linear and nonlinear structures. An improved approach is proposed by using the Kalman filter technique for force identification and the decentralized method for unknown structural parameter identification. The unknown external excitations and the structural parameters are updated iteratively. Numerical studies on a six-floor nonlinear system and a linear planar truss structure demonstrate that the proposed approach is effective for output-only structural identification with a few sensors, even at the presence of 10% noise included in the measured data.

- 3) A structure may behave nonlinearly under earthquake excitation. The nonlinear dynamic behavior of a structure is simulated with the distributed plastic model. The nonlinear finite element model is updated with the proposed decentralized technique. In the process of model updating, the dynamic response sensitivity with

respect to the material parameters can be obtained from the direct difference method. Two numerical structures subjected to seismic input are employed to verify the accuracy of the proposed method. One is a three-floor reinforcement concrete structure, and the other is a six-floor steel frame structure. Results show that the parameters in the constitutive models can be identified, even with 10% of measurement noise. Also, proposed decentralized method takes less computational time than the global model updating method.

- 4) Correlation functions are used for structural damage identification under multiple unknown excitations. The correlation function is represented by two parts. One is obtained from the UIR function and the other is a constant part that depends on the energy of the excitation force. The correlation function is insensitive to the measurement noise and the correlation function based method can identify the structural damage even with high noise measurement condition. Moreover, the correlation function based damage detection method does not require the number of sensor larger than the number of excitations, as required in other methods.
- 5) The correlation function of acceleration responses are treated as the free vibration response of the same structure. The initial values of the correlation function are identified from the system Markov parameters by using the state space method. The proposed decentralized technique are combined with the correlation function for structural damage detection. The new proposed method can identify structural damage with unknown force location. Also, the number of sensor can be less than the number of unknown excitations. Numerical studies on a simply-supported two-

dimensional truss structure and experimental studies on a eight-floor steel frame structure are performed to demonstrate the accuracy and effectiveness of the proposed method. The results show that structural damage can be successfully identified with the proposed decentralized correlation function based damage detection, even with 20% noise.

8.2 Recommendations for Further Research

Although progress has been made in this thesis for the condition assessment of large civil structures, the proposed decentralized damage detection methods are still preliminary. Several important issues are suggested to be investigated in the future

- 1) Environmental variations have significant influences on the dynamic characteristics of the structure. For example, the temperature variation of a bridge during a year can be 50°C. Accordingly, the dynamic characteristics of the bridge may change, because the Young's modulus decreases with increasing temperature. The boundary conditions are also temperature-dependent. Environmental effects may cause false alarms and reduce the effectiveness of damage detection methods. Eliminating environmental impact in damage detection should be considered.

- 2) In the proposed decentralized damage detection method, a large-scale structure is divided into several zones and the structural damage is identified by the measurement data in the same zone. If the structure is divided into a smaller number of zones, each consisting of a large number of unknown structural parameters and

the computation is inefficient. On the other hand, if the structure is divided into a larger number of zones, the measurements and unknown structural parameters have to be divided into a larger number of subsets. The proposed method may fail to converge. An addition, the number of unknown in each subset should be similar to avoid one CPU waiting others. Therefore, the structure should be divided into several zones with the same size. However, the algorithm to divide the structure into several smaller zones and how to arrange the sensor placement in each zone are not touched in this thesis and worth further studying. Experimental verification of the proposed method in Chapter 3 is worth further study

- 3) In this thesis, the structural damage is identified by using the acceleration responses only. Usually, different types of sensors are installed in an SHM system (e.g. Fiber Bragg grating strain sensor, displacement meters and accelerometers). Utilizing different types of sensors and the multi-sensor data fusion technique for structural damage detection are worth exploring.
- 4) Nonlinear finite element model updating is a challenging job and has gained much attention in recent years. Nonlinear finite element model updating is time consuming since nonlinear dynamic analysis should be considered in each time step. When the ground acceleration input is given, the computational time for the reinforcement concrete structure and the steel structure is 3 and 4 hours, respectively. When the ground motion input is unknown and more unknown need to be identified, the computational time may five or six times longer than that case with known input. Due to the large computational workload, the output only method

has not been investigated in this thesis. Also, the experimental validation of the nonlinear finite element model updating technique needs further investigations.

- 5) To investigate the proposed decentralized method for operational condition assessment, the ambient loading is assumed to be broadband white noise excitation force. However, in many cases, the loading of a structure is non-white noise. For example, the sea wave loading of offshore structures is represented by Joint North Sea Wave Project spectrum. Damage detection with multiple unknown non-white noise excitation forces merits further study.

- 6) The measurement noise in vibration responses may lead to false positive identification results. It is essential to find out the influence of the uncertainties in the identified structural parameters. The probability-based model updating procedure (e. g. Bayesian methods) may be further introduced to investigate the measurement noise effect.

REFERENCES

- Alvin, K. and Park, K. (1999). Extraction of Substructural Flexibility from Global Frequencies and Mode Shapes. *AIAA Journal* 37(11): 1444-1451.
- Amani, M.G., Riera, J.D. and Curadelli, R.O. (2007). Identification of Changes in the Stiffness and Damping Matrices of Linear Structures through Ambient Vibrations. *Structural Control and Health Monitoring* 14(8): 1155-1169.
- Arruda, J. and Santos, J. (1993). Mechanical Joint Parameter Estimation Using Frequency Response Functions and Component Mode Synthesis. *Mechanical Systems and Signal Processing* 7(6): 493-508.
- Asgarieh, E., Moaveni, B. and Stavridis, A. (2014). Nonlinear Finite Element Model Updating of an Infilled Frame Based on Identified Time-Varying Modal Parameters During an Earthquake. *Journal of Sound and Vibration* 333(23): 6057-6073.
- Astroza, R., Ebrahimian, H. and Conte, J.P. (2014). Material Parameter Identification in Distributed Plasticity Fe Models of Frame-Type Structures Using Nonlinear Stochastic Filtering. *Journal of Engineering Mechanics* 141(5): 04014149.
- Astroza, R., Ebrahimian, H., Li, Y. and Conte, J.P. (2017). Bayesian Nonlinear Structural Fe Model and Seismic Input Identification for Damage Assessment of Civil Structures. *Mechanical Systems and Signal Processing* 93: 661-687.
- Azam, S.E., Chatzi, E. and Papadimitriou, C. (2015). A Dual Kalman Filter Approach for State Estimation Via Output-Only Acceleration Measurements. *Mechanical Systems and Signal Processing* 60: 866-886.

- Baber, T.T. and Wen, Y.-K. (1981). Random Vibration Hysteretic, Degrading Systems. *Journal of the engineering mechanics division* 107(6): 1069-1087.
- Bahlous, S.E.-O., Smaoui, H. and El-Borgi, S. (2009). Experimental Validation of an Ambient Vibration-Based Multiple Damage Identification Method Using Statistical Modal Filtering. *Journal of Sound and Vibration* 325(1-2): 49-68.
- Bakir, P.G., Reynders, E. and De Roeck, G. (2007). Sensitivity-Based Finite Element Model Updating Using Constrained Optimization with a Trust Region Algorithm. *Journal of Sound and Vibration* 305(1-2): 211-225.
- Barbato, M. and Conte, J.P. (2006). Finite Element Structural Response Sensitivity and Reliability Analyses Using Smooth Versus Non-Smooth Material Constitutive Models. *International Journal of Reliability and Safety* 1(1-2): 3-39.
- Barbato, M., Zona, A. and Conte, J.P. (2013). Probabilistic Nonlinear Response Analysis of Steel-Concrete Composite Beams. *Journal of Structural Engineering* 140(1): 04013034.
- Belytschko, T., Liu, W.K., Moran, B. and Elkhodary, K. (2013). *Nonlinear Finite Elements for Continua and Structures*, John Wiley & Sons.
- Bendat, J.S. and Piersol, A.G. (1980). *Engineering Applications of Correlation and Spectral Analysis*. New York, Wiley-Interscience, 1980. 315 p.
- Bendat, J.S. and Piersol, A.G. (2011). *Random Data: Analysis and Measurement Procedures*, John Wiley & Sons.

- Benedettini, F., Capecchi, D. and Vestroni, F. (1995). Identification of Hysteretic Oscillators under Earthquake Loading by Nonparametric Models. *Journal of Engineering Mechanics* 121(5): 606-612.
- Bi, K. and Hao, H. (2013). Numerical Simulation of Pounding Damage to Bridge Structures under Spatially Varying Ground Motions. *Engineering Structures* 46: 62-76.
- Brownjohn, J.M. (2003). Ambient Vibration Studies for System Identification of Tall Buildings. *Earthquake Engineering & Structural Dynamics* 32(1): 71-95.
- Caicedo, J.M., Dyke, S.J. and Johnson, E.A. (2004). Natural Excitation Technique and Eigensystem Realization Algorithm for Phase I of the Iasc-Asce Benchmark Problem: Simulated Data. *Journal of Engineering Mechanics* 130(1): 49-60.
- Carden, E.P. and Fanning, P. (2004). Vibration Based Condition Monitoring: A Review. *Structural Health Monitoring* 3(4): 355-377.
- Carey, G. and Krishnan, R. (1982). On a Nonlinear Iterative Method in Applied Mechanics, Part II. *Computer Methods in Applied Mechanics and Engineering* 30(3): 323-333.
- Chatzi, E.N. and Smyth, A.W. (2009). The Unscented Kalman Filter and Particle Filter Methods for Nonlinear Structural System Identification with Non - Collocated Heterogeneous Sensing. *Structural Control and Health Monitoring* 16(1): 99-123.
- Chen, G., Yang, X., Ying, X. and Nanni, A. (2006). Damage Detection of Concrete Beams Using Nonlinear Features of Forced Vibration. *Structural Health Monitoring* 5(2): 125-141.

- Ching, J., Beck, J.L. and Porter, K.A. (2006). Bayesian State and Parameter Estimation of Uncertain Dynamical Systems. *Probabilistic Engineering Mechanics* 21(1): 81-96.
- Chou, J.-H. and Ghaboussi, J. (2001). Genetic Algorithm in Structural Damage Detection. *Computers & Structures* 79(14): 1335-1353.
- Clough, R.W. and Penzien, J. (1975). Dynamics of Structures. *New York: McGraw-Hill, 1975.*
- Conte, J., Vijalapura, P. and Meghella, M. (2003). Consistent Finite-Element Response Sensitivity Analysis. *Journal of Engineering Mechanics* 129(12): 1380-1393.
- Conte, J.P. (2001). Finite Element Response Sensitivity Analysis in Earthquake Engineering. *Earthquake engineering frontiers in the new millennium*: 395-401.
- Cooreman, S., Lecompte, D., Sol, H., Vantomme, J. and Debruyne, D. (2007). Elasto-Plastic Material Parameter Identification by Inverse Methods: Calculation of the Sensitivity Matrix. *International Journal of Solids and Structures* 44(13): 4329-4341.
- Coronelli, D. and Gambarova, P. (2004). Structural Assessment of Corroded Reinforced Concrete Beams: Modeling Guidelines. *Journal of Structural Engineering* 130(8): 1214-1224.
- Daubechies, I. (1992). Ten Lectures on Wavelets, SIAM.
- De Borst, R., Crisfield, M.A., Remmers, J.J. and Verhoosel, C.V. (2012). Nonlinear Finite Element Analysis of Solids and Structures, John Wiley & Sons.

- Deraemaeker, A., Reynders, E., De Roeck, G. and Kullaa, J. (2008). Vibration-Based Structural Health Monitoring Using Output-Only Measurements under Changing Environment. *Mechanical Systems and Signal Processing* 22(1): 34-56.
- Ding, Z., Yao, R., Li, J. and Lu, Z. (2018). Structural Damage Identification Based on Modified Artificial Bee Colony Algorithm Using Modal Data. *Inverse Problems in Science and Engineering* 26(3): 422-442.
- Doebling, S.W., Farrar, C.R. and Cornwell, P.J. (1997). Diamond: A Graphical Interface Toolbox for Comparative Modal Analysis and Damage Identification. *Proceedings of the 6th International Conference on Recent Advances in Structural Dynamics, Southampton, UK.*
- Doebling, S.W., Farrar, C.R. and Prime, M.B. (1998). A Summary Review of Vibration-Based Damage Identification Methods. *Shock and vibration digest* 30(2): 91-105.
- Ebrahimian, H. (2015). Nonlinear Finite Element Model Updating for Nonlinear System and Damage Identification of Civil Structures, University of California, San Diego.
- Ebrahimian, H., Astroza, R. and Conte, J.P. (2015). Extended Kalman Filter for Material Parameter Estimation in Nonlinear Structural Finite Element Models Using Direct Differentiation Method. *Earthquake Engineering & Structural Dynamics* 44(10): 1495-1522.
- Ebrahimian, H., Astroza, R., Conte, J.P. and de Callafon, R.A. (2017). Nonlinear Finite Element Model Updating for Damage Identification of Civil Structures Using Batch Bayesian Estimation. *Mechanical Systems and Signal Processing* 84: 194-222.

- Ebrahimian, H., Astroza, R., Conte, J.P. and Papadimitriou, C. (2018). Bayesian Optimal Estimation for Output - Only Nonlinear System and Damage Identification of Civil Structures. *Structural Control and Health Monitoring* 25(4): e2128.
- Ewins, D. (2003). Modal Testing: Theory, Practice and Application (Mechanical Engineering Research Studies: Engineering Dynamics Series).
- Farhat, C. and Geradin, M. (1994). On a Component Mode Synthesis Method and Its Application to Incompatible Substructures. *Computers & Structures* 51(5): 459-473.
- Farhat, C. and Hemez, F.M. (1993). Updating Finite Element Dynamic Models Using an Element-by-Element Sensitivity Methodology. *AIAA Journal* 31(9): 1702-1711.
- Foliente, G.C. (1995). Hysteresis Modeling of Wood Joints and Structural Systems. *Journal of Structural Engineering* 121(6): 1013-1022.
- Furukawa, T., Ito, M., Izawa, K. and Noori, M.N. (2005). System Identification of Base-Isolated Building Using Seismic Response Data. *Journal of Engineering Mechanics* 131(3): 268-275.
- Gao, Y., Spencer, B. and Ruiz - Sandoval, M. (2006). Distributed Computing Strategy for Structural Health Monitoring. *Structural Control and Health Monitoring* 13(1): 488-507.
- Ghorbani, E. and Cha, Y.-J. (2018). An Iterated Cubature Unscented Kalman Filter for Large-Dof Systems Identification with Noisy Data. *Journal of Sound and Vibration* 420: 21-34.

- Gul, M. and Catbas, F.N. (2008). Ambient Vibration Data Analysis for Structural Identification and Global Condition Assessment. *Journal of Engineering Mechanics* 134(8): 650-662.
- Guo, L., Ding, Y., Wang, Z., Xu, G. and Wu, B. (2018). A Dynamic Load Estimation Method for Nonlinear Structures with Unscented Kalman Filter. *Mechanical Systems and Signal Processing* 101: 254-273.
- Hao, H. and Xia, Y. (2002). Vibration-Based Damage Detection of Structures by Genetic Algorithm. *Journal of Computing in Civil Engineering* 16(3): 222-229.
- Haukaas, T. and Der Kiureghian, A. (2004). Finite Element Reliability and Sensitivity Methods for Performance-Based Earthquake Engineering, Pacific Earthquake Engineering Research Center, College of Engineering, University of California, Berkeley.
- He, J., Xu, B. and Masri, S.F. (2012). Restoring Force and Dynamic Loadings Identification for a Nonlinear Chain-Like Structure with Partially Unknown Excitations. *Nonlinear Dynamics* 69(1-2): 231-245.
- Hoshiya, M. and Saito, E. (1984). Structural Identification by Extended Kalman Filter. *Journal of Engineering Mechanics* 110(12): 1757-1770.
- Huang, H., Yang, J.N. and Zhou, L. (2010). Adaptive Quadratic Sum - Squares Error with Unknown Inputs for Damage Identification of Structures. *Structural Control and Health Monitoring* 17(4): 404-426.
- Inman, D.J. (2008). Engineering Vibration, Prentice Hall New Jersey.

- Jaishi, B. and Ren, W.-X. (2005). Structural Finite Element Model Updating Using Ambient Vibration Test Results. *Journal of Structural Engineering* 131(4): 617-628.
- James, G., Carne, T.G. and Lauffer, J.P. (1995). The Natural Excitation Technique (Next) for Modal Parameter Extraction from Operating Structures. *Modal Analysis-the International Journal of Analytical and Experimental Modal Analysis* 10(4): 260.
- Jayawardhana, M., Zhu, X. and Liyanapathirana, R. (2013). An Experimental Study on Damage Detection of Concrete Structures Using Decentralized Algorithms. *Advances in Structural Engineering* 16(1): 33-50.
- Jo, H., Sim, S.-H., Nagayama, T. and Spencer Jr, B. (2011). Development and Application of High-Sensitivity Wireless Smart Sensors for Decentralized Stochastic Modal Identification. *Journal of Engineering Mechanics* 138(6): 683-694.
- Kang, F., Li, J.-J. and Xu, Q. (2012). Damage Detection Based on Improved Particle Swarm Optimization Using Vibration Data. *Applied Soft Computing* 12(8): 2329-2335.
- Kang, F., Li, J. and Xu, Q. (2009). Structural Inverse Analysis by Hybrid Simplex Artificial Bee Colony Algorithms. *Computers & Structures* 87(13-14): 861-870.
- Kim, J. and Lynch, J.P. (2011). Autonomous Decentralized System Identification by Markov Parameter Estimation Using Distributed Smart Wireless Sensor Networks. *Journal of Engineering Mechanics* 138(5): 478-490.

- Kleiber, M., Tran, D.H., Antùnez, H. and Kowalczyk, P. (1997). Parameter Sensitivity in Nonlinear Mechanics: Theory and Finite Element Computations. Chichester, England, John Wiley,.
- Ko, J. and Ni, Y. (2005). Technology Developments in Structural Health Monitoring of Large-Scale Bridges. *Engineering Structures* 27(12): 1715-1725.
- Koh, C. and Shankar, K. (2003). Substructural Identification Method without Interface Measurement. *Journal of Engineering Mechanics* 129(7): 769-776.
- Koh, C.G., Hong, B. and Liaw, C.Y. (2003). Substructural and Progressive Structural Identification Methods. *Engineering Structures* 25(12): 1551-1563.
- Koh, C.G., See, L.M. and Balendra, T. (1991). Estimation of Structural Parameters in Time Domain: A Substructure Approach. *Earthquake Engineering & Structural Dynamics* 20(8): 787-801.
- Kunnath, S.K., Mander, J.B. and Fang, L. (1997). Parameter Identification for Degrading and Pinched Hysteretic Structural Concrete Systems. *Engineering Structures* 19(3): 224-232.
- Law, S. and Li, X. (2007). Wavelet-Based Sensitivity Analysis of the Impulse Response Function for Damage Detection. *Journal of Applied Mechanics* 74(2): 375-377.
- Law, S. and Yong, D. (2011). Substructure Methods for Structural Condition Assessment. *Journal of Sound and Vibration* 330(15): 3606-3619.
- Law, S.S., Lin, J.F. and Li, X.Y. (2012). Structural Condition Assessment from White Noise Excitation and Covariance of Covariance Matrix. *AIAA Journal* 50(7): 1503-1512.

- Law, S.S., Ni, P.H. and Li, J. (2014). Parallel Decentralized Damage Detection of a Structure with Subsets of Parameters. *AIAA Journal* 52(3): 650-656.
- Law, S.S., Zhang, K. and Duan, Z.D. (2010). Structural Damage Detection from Coupling Forces between Substructures under Support Excitation. *Engineering Structures* 32(8): 2221-2228.
- Lee, J.J. and Yun, C.B. (2006). Damage Diagnosis of Steel Girder Bridges Using Ambient Vibration Data. *Engineering Structures* 28(6): 912-925.
- Lei, Y., Jiang, Y. and Xu, Z. (2012a). Structural Damage Detection with Limited Input and Output Measurement Signals. *Mechanical Systems and Signal Processing* 28: 229-243.
- Lei, Y., Liu, C., Jiang, Y. and Mao, Y. (2013). Substructure Based Structural Damage Detection with Limited Input and Output Measurements. *Smart Structures and Systems* 12(6): 619-640.
- Lei, Y. and Wu, Y. (2011). Non-Parametric Identification of Structural Nonlinearity with Limited Input and Output Measurements. *Advanced Materials Research*, Trans Tech Publications.
- Lei, Y., Wu, Y. and Li, T. (2012b). Identification of Non-Linear Structural Parameters under Limited Input and Output Measurements. *International Journal of Non-Linear Mechanics* 47(10): 1141-1146.
- Lei, Y., Xia, D., Chen, F. and Deng, Y. (2017). Synthesis of Cross-Correlation Functions of Partial Responses and the Extended Kalman Filter Approach for Structural Damage Detection under Ambient Excitations. *International Journal of Structural Stability and Dynamics*: 1840003.

- Li, J. and Chen, J. (2003). A Statistical Average Algorithm for the Dynamic Compound Inverse Problem. *Computational Mechanics* 30(2): 88-95.
- Li, J. and Hao, H. (2014). Substructure Damage Identification Based on Wavelet-Domain Response Reconstruction. *Structural Health Monitoring* 13(4): 389-405.
- Li, J. and Law, S. (2011). Substructural Response Reconstruction in Wavelet Domain. *Journal of Applied Mechanics* 78(4): 041010.
- Li, J. and Law, S. (2012a). Damage Identification of a Target Substructure with Moving Load Excitation. *Mechanical Systems and Signal Processing* 30: 78-90.
- Li, J. and Law, S. (2012b). Substructural Damage Detection with Incomplete Information of the Structure. *Journal of Applied Mechanics* 79(4): 041003.
- Li, J., Law, S. and Ding, Y. (2012). Substructure Damage Identification Based on Response Reconstruction in Frequency Domain and Model Updating. *Engineering Structures* 41: 270-284.
- Li, J., Law, S. and Hao, H. (2013). Improved Damage Identification in Bridge Structures Subject to Moving Loads: Numerical and Experimental Studies. *International Journal of Mechanical Sciences* 74: 99-111.
- Li, S.J., Suzuki, Y. and Noori, M. (2004). Identification of Hysteretic Systems with Slip Using Bootstrap Filter. *Mechanical Systems and Signal Processing* 18(4): 781-795.
- Li, X., Wang, L., Law, S. and Nie, Z. (2017a). Covariance of Dynamic Strain Responses for Structural Damage Detection. *Mechanical Systems and Signal Processing* 95: 90-105.

- Li, X.Y. and Law, S.S. (2008). Condition Assessment of Structures under Ambient White Noise Excitation. *AIAA Journal* 46(6): 1395-1404.
- Li, X.Y. and Law, S.S. (2010). Matrix of the Covariance of Covariance of Acceleration Responses for Damage Detection from Ambient Vibration Measurements. *Mechanical Systems and Signal Processing* 24(4): 945-956.
- Li, Y. (2005). Predictive Control for Dynamic Systems to Track Unknown Input in the Presence of Time Delay.
- Li, Y., Astroza, R., Conte, J.P. and Soto, P. (2017b). Nonlinear Fe Model Updating and Reconstruction of the Response of an Instrumented Seismic Isolated Bridge to the 2010 Maule Chile Earthquake. *Earthquake Engineering & Structural Dynamics* 46(15): 2699-2716.
- Lin, J.W., Betti, R., Smyth, A.W. and Longman, R.W. (2001). On - Line Identification of Non - Linear Hysteretic Structural Systems Using a Variable Trace Approach. *Earthquake Engineering & Structural Dynamics* 30(9): 1279-1303.
- Lin, T., Hung, S. and Huang, C. (2012). Detection of Damage Location Using a Novel Substructure-Based Frequency Response Function Approach with a Wireless Sensing System. *International Journal of Structural Stability and Dynamics* 12(04): 1250029.
- Liu, Y., Li, Y., Wang, D. and Zhang, S. (2014). Model Updating of Complex Structures Using the Combination of Component Mode Synthesis and Kriging Predictor. *The Scientific World Journal* 2014.

- Lu, X., Xie, L., Guan, H., Huang, Y. and Lu, X. (2015). A Shear Wall Element for Nonlinear Seismic Analysis of Super-Tall Buildings Using Opensees. *Finite Elements in Analysis and Design* 98: 14-25.
- Lu, X., Ye, L., Teng, J. and Jiang, J. (2005). Meso-Scale Finite Element Model for Frp Sheets/Plates Bonded to Concrete. *Engineering Structures* 27(4): 564-575.
- Lu, Z.R. and Law, S.S. (2007a). Features of Dynamic Response Sensitivity and Its Application in Damage Detection. *Journal of Sound and Vibration* 303(1-2): 305-329.
- Lu, Z.R. and Law, S.S. (2007b). Identification of System Parameters and Input Force from Output Only. *Mechanical Systems and Signal Processing* 21(5): 2099-2111.
- Lu, Z.R. and Wang, L. (2017). An Enhanced Response Sensitivity Approach for Structural Damage Identification: Convergence and Performance. *International Journal for Numerical Methods in Engineering* 111(13): 1231-1251.
- Ma, F., Ng, C. and Ajavakom, N. (2006). On System Identification and Response Prediction of Degrading Structures. *Structural Control and Health Monitoring* 13(1): 347-364.
- McKenna, F. (2011). Opensees: A Framework for Earthquake Engineering Simulation. *Computing in Science & Engineering* 13(4): 58-66.
- Michel, C., Guéguen, P. and Bard, P.-Y. (2008). Dynamic Parameters of Structures Extracted from Ambient Vibration Measurements: An Aid for the Seismic Vulnerability Assessment of Existing Buildings in Moderate Seismic Hazard Regions. *Soil Dynamics and Earthquake Engineering* 28(8): 593-604.

- Miguel, L.F.F., Miguel, L.F.F., Kaminski Jr, J. and Riera, J.D. (2012). Damage Detection under Ambient Vibration by Harmony Search Algorithm. *Expert Systems with Applications* 39(10): 9704-9714.
- Moës, N., Dolbow, J. and Belytschko, T. (1999). A Finite Element Method for Crack Growth without Remeshing. *International Journal for Numerical Methods in Engineering* 46(1): 131-150.
- Morton, K.W. and Mayers, D.F. (2005). Numerical Solution of Partial Differential Equations: An Introduction, Cambridge university press.
- Naaman, A.E. and Najm, H. (1991). Bond-Slip Mechanisms of Steel Fibers in Concrete. *Materials Journal* 88(2): 135-145.
- Nagayama, T., Spencer, B. and Rice, J.A. (2009). Autonomous Decentralized Structural Health Monitoring Using Smart Sensors. *Structural Control and Health Monitoring* 16(7 - 8): 842-859.
- Ni, P., Xia, Y., Law, S.-S. and Zhu, S. (2014). Structural Damage Detection Using Auto/Cross-Correlation Functions under Multiple Unknown Excitations. *International Journal of Structural Stability and Dynamics* 14(05): 1440006.
- Ni, Y.Q., Xia, Y., Liao, W.Y. and Ko, J.M. (2009). Technology Innovation in Developing the Structural Health Monitoring System for Guangzhou New Tv Tower. *Structural Control & Health Monitoring* 16(1): 73-98.
- Ortega, J.M. and Rheinboldt, W.C. (1970). Iterative Solution of Nonlinear Equations in Several Variables, Siam.

- Pandey, A. and Biswas, M. (1994). Damage Detection in Structures Using Changes in Flexibility. *Journal of Sound and Vibration* 169(1): 3-17.
- Pandey, A., Biswas, M. and Samman, M. (1991). Damage Detection from Changes in Curvature Mode Shapes. *Journal of Sound and Vibration* 145(2): 321-332.
- Papadimitriou, C. and Papadioti, D.-C. (2013). Component Mode Synthesis Techniques for Finite Element Model Updating. *Computers & Structures* 126: 15-28.
- Park, N.-G. and Park, Y.-S. (2005). Identification of Damage on a Substructure with Measured Frequency Response Functions. *Journal of Mechanical Science and Technology* 19(10): 1891.
- Peeters, B. and De Roeck, G. (2001). Stochastic System Identification for Operational Modal Analysis: A Review. *Journal of Dynamic Systems, Measurement, and Control* 123(4): 659-667.
- Penrose, R. (1955). A Generalized Inverse for Matrices. *Mathematical Proceedings of the Cambridge Philosophical Society*, Cambridge University Press.
- Peppin, R.J. (1994). An Introduction to Random Vibrations, Spectral and Wavelet Analysis, Hindawi Publishing Corporation.
- Perry, M., Koh, C. and Choo, Y. (2006). Modified Genetic Algorithm Strategy for Structural Identification. *Computers & Structures* 84(8): 529-540.
- Quek, S.T., Wang, W. and Koh, C.G. (1999). System Identification of Linear M dof Structures under Ambient Excitation. *Earthquake Engineering & Structural Dynamics* 28(1): 61-77.

- Ren, W.-X. and Peng, X.-L. (2005). Baseline Finite Element Modeling of a Large Span Cable-Stayed Bridge through Field Ambient Vibration Tests. *Computers & Structures* 83(8-9): 536-550.
- Reynders, E., Teughels, A. and De Roeck, G. (2010). Finite Element Model Updating and Structural Damage Identification Using Omax Data. *Mechanical Systems and Signal Processing* 24(5): 1306-1323.
- Rossi, M. and Pierron, F. (2012). Identification of Plastic Constitutive Parameters at Large Deformations from Three Dimensional Displacement Fields. *Computational Mechanics* 49(1): 53-71.
- Salawu, O. (1997). Detection of Structural Damage through Changes in Frequency: A Review. *Engineering Structures* 19(9): 718-723.
- Seyedpoor, S. (2012). A Two Stage Method for Structural Damage Detection Using a Modal Strain Energy Based Index and Particle Swarm Optimization. *International Journal of Non-Linear Mechanics* 47(1): 1-8.
- Shayanfar, M., Abbasnia, R. and Khodam, A. (2014). Development of a Ga-Based Method for Reliability-Based Optimization of Structures with Discrete and Continuous Design Variables Using Opensees and Tcl. *Finite Elements in Analysis and Design* 90: 61-73.
- Shinozuka, M., Vaicaitis, R. and Asada, H. (1976). Digital Generation of Random Forces for Large-Scale Experiments. *Journal of Aircraft* 13(6): 425-431.
- Sim, S.-H., Carbonell-Márquez, J.F., Spencer, B. and Jo, H. (2011). Decentralized Random Decrement Technique for Efficient Data Aggregation and System

- Identification in Wireless Smart Sensor Networks. *Probabilistic Engineering Mechanics* 26(1): 81-91.
- Sireteanu, T., Giuclea, M. and Mitu, A. (2010). Identification of an Extended Bouc–Wen Model with Application to Seismic Protection through Hysteretic Devices. *Computational Mechanics* 45(5): 431-441.
- Siringoringo, D.M. and Fujino, Y. (2006). Observed Dynamic Performance of the Yokohama - Bay Bridge from System Identification Using Seismic Records. *Structural Control and Health Monitoring* 13(1): 226-244.
- Siringoringo, D.M. and Fujino, Y. (2008). System Identification of Suspension Bridge from Ambient Vibration Response. *Engineering Structures* 30(2): 462-477.
- Sjövall, P. and Abrahamsson, T. (2008). Substructure System Identification from Coupled System Test Data. *Mechanical Systems and Signal Processing* 22(1): 15-33.
- Sohn, H. and Law, K.H. (1997). A Bayesian Probabilistic Approach for Structure Damage Detection. *Earthquake Engineering & Structural Dynamics* 26(12): 1259-1281.
- Su, J.-Z., Xia, Y., Chen, L., Zhao, X., Zhang, Q.-L., Xu, Y.-L., Ding, J.-M., Xiong, H.-B., Ma, R.-J. and Lv, X.-L. (2013). Long-Term Structural Performance Monitoring System for the Shanghai Tower. *Journal of civil structural health monitoring* 3(1): 49-61.
- Sun, H., Luş, H. and Betti, R. (2013). Identification of Structural Models Using a Modified Artificial Bee Colony Algorithm. *Computers & Structures* 116: 59-74.

- Sun, H., Mordret, A., Prieto, G.A., Toksöz, M.N. and Büyüköztürk, O. (2017). Bayesian Characterization of Buildings Using Seismic Interferometry on Ambient Vibrations. *Mechanical Systems and Signal Processing* 85: 468-486.
- Taucer, F., Spacone, E. and Filippou, F.C. (1991). A Fiber Beam-Column Element for Seismic Response Analysis of Reinforced Concrete Structures, Earthquake Engineering Research Center, College of Engineering, University of California Berkeley, California.
- Teughels, A. and De Roeck, G. (2004). Structural Damage Identification of the Highway Bridge Z24 by Fe Model Updating. *Journal of Sound and Vibration* 278(3): 589-610.
- Tikhonov, A.N., Goncharsky, A., Stepanov, V. and Yagola, A.G. (1995). Numerical Methods for the Solution of Ill-Posed Problems, Springer Science & Business Media.
- Toussi, S. and Yao, J.T. (1983). Hysteresis Identification of Existing Structures. *Journal of Engineering Mechanics* 109(5): 1189-1202.
- Trinh, T.N. and Koh, C.G. (2012). An Improved Substructural Identification Strategy for Large Structural Systems. *Structural Control and Health Monitoring* 19(8): 686-700.
- Val, D., Bljucer, F. and Yankelevsky, D. (1997). Reliability Evaluation in Nonlinear Analysis of Reinforced Concrete Structures. *Structural Safety* 19(2): 203-217.
- Wang, D. and Haldar, A. (1994). Element-Level System Identification with Unknown Input. *Journal of Engineering Mechanics* 120(1): 159-176.
- Wang, D. and Haldar, A. (1997). System Identification with Limited Observations and without Input. *Journal of Engineering Mechanics* 123(5): 504-511.

- Wang, L., Yang, Z. and Waters, T. (2010). Structural Damage Detection Using Cross Correlation Functions of Vibration Response. *Journal of Sound and Vibration* 329(24): 5070-5086.
- Wei, Z., Liu, J. and Lu, Z. (2018). Structural Damage Detection Using Improved Particle Swarm Optimization. *Inverse Problems in Science and Engineering* 26(6): 792-810.
- Weng, S., Xia, Y., Xu, Y.L., Zhou, X.Q. and Zhu, H.P. (2009). Improved Substructuring Method for Eigensolutions of Large-Scale Structures. *Journal of Sound and Vibration* 323(3-5): 718-736.
- Weng, S., Zhu, H.P., Xia, Y. and Mao, L. (2013). Damage Detection Using the Eigenparameter Decomposition of Substructural Flexibility Matrix. *Mechanical Systems and Signal Processing* 34(1-2): 19-38.
- Worden, K. and Hensman, J. (2012). Parameter Estimation and Model Selection for a Class of Hysteretic Systems Using Bayesian Inference. *Mechanical Systems and Signal Processing* 32: 153-169.
- Wu, A.-L., Yang, J.N. and Loh, C.-H. (2012). A Damage Detection Technique for Reinforced Concrete Structures. *Sensors and Smart Structures Technologies for Civil, Mechanical, and Aerospace Systems 2012*, International Society for Optics and Photonics.
- Wu, M. and Smyth, A.W. (2007a). Application of the Unscented Kalman Filter for Real-Time Nonlinear Structural System Identification. *Structural Control and Health Monitoring* 14(7): 971-990.

- Wu, M. and Smyth, A.W. (2007b). Application of the Unscented Kalman Filter for Real - Time Nonlinear Structural System Identification. *Structural Control and Health Monitoring* 14(7): 971-990.
- Wu, Z., Xu, B. and Yokoyama, K. (2002). Decentralized Parametric Damage Detection Based on Neural Networks. *Computer - Aided Civil and Infrastructure Engineering* 17(3): 175-184.
- Xia, Y. (2011). System Identification and Damage Detection of Nonlinear Structures.
- Xia, Y., Hao, H., Deeks, A.J. and Zhu, X.Q. (2008). Condition Assessment of Shear Connectors in Slab-Girder Bridges Via Vibration Measurements. *Journal of Bridge Engineering* 13(1): 43-54.
- Xie, Z. and Feng, J. (2012). Real-Time Nonlinear Structural System Identification Via Iterated Unscented Kalman Filter. *Mechanical Systems and Signal Processing* 28: 309-322.
- Xu, B., He, J. and Masri, S.F. (2012). Data-Based Identification of Nonlinear Restoring Force under Spatially Incomplete Excitations with Power Series Polynomial Model. *Nonlinear Dynamics* 67(3): 2063-2080.
- Xu, Y., Zhang, J., Li, J. and Xia, Y. (2009). Experimental Investigation on Statistical Moment-Based Structural Damage Detection Method. *Structural Health Monitoring* 8(6): 555-571.
- Yang, J.N. and Huang, H. (2007). Sequential Non-Linear Least-Square Estimation for Damage Identification of Structures with Unknown Inputs and Unknown Outputs. *International Journal of Non-Linear Mechanics* 42(5): 789-801.

- Yang, J.N., Huang, H. and Lin, S. (2006a). Sequential Non-Linear Least-Square Estimation for Damage Identification of Structures. *International Journal of Non-Linear Mechanics* 41(1): 124-140.
- Yang, J.N., Huang, H. and Pan, S. (2009a). Adaptive Quadratic Sum-Squares Error for Structural Damage Identification. *Journal of Engineering Mechanics* 135(2): 67-77.
- Yang, J.N. and Lin, S. (2004). On-Line Identification of Non-Linear Hysteretic Structures Using an Adaptive Tracking Technique. *International Journal of Non-Linear Mechanics* 39(9): 1481-1491.
- Yang, J.N., Lin, S., Huang, H. and Zhou, L. (2006b). An Adaptive Extended Kalman Filter for Structural Damage Identification. *Structural Control and Health Monitoring* 13(4): 849-867.
- Yang, J.N., Pan, S. and Huang, H. (2007a). An Adaptive Extended Kalman Filter for Structural Damage Identifications Ii: Unknown Inputs. *Structural Control and Health Monitoring* 14(3): 497-521.
- Yang, J.N., Pan, S. and Lin, S. (2007b). Least-Squares Estimation with Unknown Excitations for Damage Identification of Structures. *Journal of Engineering Mechanics* 133(1): 12-21.
- Yang, J.N., Xia, Y. and Loh, C.-H. (2014). Damage Detection of Hysteretic Structures with a Pinching Effect. *Journal of Engineering Mechanics* 140(3): 462-472.
- Yang, Z., Wang, L., Wang, H., Ding, Y. and Dang, X. (2009b). Damage Detection in Composite Structures Using Vibration Response under Stochastic Excitation. *Journal of Sound and Vibration* 325(4): 755-768.

- Yang, Z., Yu, Z. and Sun, H. (2007c). On the Cross Correlation Function Amplitude Vector and Its Application to Structural Damage Detection. *Mechanical Systems and Signal Processing* 21(7): 2918-2932.
- Yin, T., Lam, H.F., Chow, H.M. and Zhu, H. (2009). Dynamic Reduction-Based Structural Damage Detection of Transmission Tower Utilizing Ambient Vibration Data. *Engineering Structures* 31(9).
- Yu, J.-x., Xia, Y., Lin, W. and Zhou, X.-q. (2016). Element-by-Element Model Updating of Large-Scale Structures Based on Component Mode Synthesis Method. *Journal of Sound and Vibration* 362: 72-84.
- Yuen, K.-V., Au, S.K. and Beck, J.L. (2004). Two-Stage Structural Health Monitoring Approach for Phase I Benchmark Studies. *Journal of Engineering Mechanics* 130(1): 16-33.
- Yuen, K.-V. and Beck, J.L. (2003). Updating Properties of Nonlinear Dynamical Systems with Uncertain Input. *Journal of Engineering Mechanics* 129(1): 9-20.
- Yuen, K.-V. and Kuok, S.-C. (2010). Ambient Interference in Long-Term Monitoring of Buildings. *Engineering Structures* 32(8): 2379-2386.
- Yun, G.J., Lee, S.-G., Carletta, J. and Nagayama, T. (2011). Decentralized Damage Identification Using Wavelet Signal Analysis Embedded on Wireless Smart Sensors. *Engineering Structures* 33(7): 2162-2172.
- Zhang, K., Law, S.S. and Duan, Z.D. (2009). Condition Assessment of Structures under Unknown Support Excitation. *Earthquake Engineering and Engineering Vibration* 8(1): 103-114.

- Zhang, M. and Schmidt, R. (2014). Sensitivity Analysis of an Auto-Correlation-Function-Based Damage Index and Its Application in Structural Damage Detection. *Journal of Sound and Vibration* 333(26): 7352-7363.
- Zhang, M. and Schmidt, R. (2015). Study on an Auto-Correlation-Function-Based Damage Index: Sensitivity Analysis and Structural Damage Detection. *Journal of Sound and Vibration* 359: 195-214.
- Zhang, Y. and Der Kiureghian, A. (1993). Dynamic Response Sensitivity of Inelastic Structures. *Computer Methods in Applied Mechanics and Engineering* 108(1): 23-36.
- Zhou, L., Wu, S. and Yang, J.N. (2008). Experimental Study of an Adaptive Extended Kalman Filter for Structural Damage Identification. *Journal of Infrastructure Systems* 14(1): 42-51.
- Zhu, H.-P., Mao, L. and Weng, S. (2014). A Sensitivity-Based Structural Damage Identification Method with Unknown Input Excitation Using Transmissibility Concept. *Journal of Sound and Vibration* 333(26): 7135-7150.
- Zona, A., Barbato, M. and Conte, J.P. (2005). Finite Element Response Sensitivity Analysis of Steel-Concrete Composite Beams with Deformable Shear Connection. *Journal of Engineering Mechanics* 131(11): 1126-1139.